THESIS REPORT
Master's Degree

S Y S T E M S
R E S E A R C H
C E N T E R

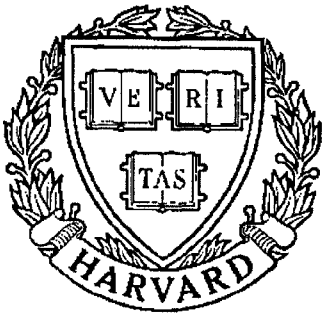

Supported by the National Science Foundation Engineering Research Center Program (NSFD CD 8803012), the University of Maryland, Harvard University, and Industry

Mathematical Modeling and Analysis of the Surface Topography Generated During End Milling Processes

by C.C. Chang
Advisor: G.M. Zhang

M.S. 92-13

ABSTRACT

Title of Thesis:	Mathematical Modeling and Analysis of the Surface Topography Generated During End Milling Processes
Degree Candidate:	Chongcherng Chang
Degree and Year:	Master of Science, 1992
Thesis Directed By:	Dr. Guangming Zhang, Assistant Professor Department of Mechanical Engineering and Systems Research Center

Computer integrated manufacturing systems have emerged in response to the requirements for greater flexibility, productivity, high precision and quality of the product. As the computer technology advances, the manufacturing industry is now seeking a higher degree of production automation. Numerical Control (NC) machining stands out in this regard. There is a pressing need for computer-based simulation models that can be used for the purpose of analyzing the machining performance during the programming stage.

Research has been done in this thesis to develop a system model which can describe the generation of machined surfaces during an end milling process. In the first step, an ideal surface topography is constructed based on the kinematics of a vertical milling machine tool. Building on the ideal surface topography, factors such as the parallel axial offset of an end mill (runout), tool static deflection and vibration are taken into consideration in the surface texture generation. Consequently, the developed mathematical model represents a realistic picture on how the machined surface is produced during an end milling process.

In order to gain a comprehensive understanding of the dynamic nature of surface generation during an end milling process, the method of design of experimentation is employed to investigate three system parameters, namely, the feedrate, helix angle, and

runout, and their effects on the surface topography generation. Computer simulations based on a 2^3 factorial design are conducted in this thesis work to obtain the predicted values of indices such as roughness average (R_a) and Peak-to-Valley (PTV) that characterize the finish quality of machined surfaces.

Experimental verification has been done in this thesis work. Samples are made on a Matsuura 510 Machining Center. These samples are inspected and data are recorded at the National Institute of Standards and Technology at Gaithersburg, Maryland. For a similar machining condition, the results predicted through computer simulation are compared with the results obtained from the direct measurements taken on the samples, showing good agreements.

Mathematical Modeling and Analysis of the Surface Topography Generated During End Milling Processes

by

Chongcherng Chang

Thesis submitted to the Faculty of the Graduate School
of The University of Maryland in partial fulfillment
of the requirements for the degree of
Master of Science
1992

Advisory Committee:

Assistant Professor Guangming Zhang, Chairman/Advisor
Professor James Dally
Professor Andre Tits

ACKNOWLEDGEMENTS

The first acknowledgement is due the Taiwan Government for granting me scholarship to pursue my graduate studies in the United States.

I wish to express my gratitude to my advisor, Dr. Guangming Zhang, who always provided enthusiastic guidance, encouragement, and support throughout this work. I would like to thank Professor James Dally and Professor Andre Tits for serving on my thesis committee.

I thank my fellow students in Dr. Zhang's research group. I particularly want to thank Tsuwei, who helped me with the thesis editing on weekends or even overnight, Don DeVoe, who helped me with the experimental data processing, and Raju, Farukh, Jayant, Shuvanker. I also thank my good friends in Robotic lab for their help when the research was in difficulty.

Finally, I want to express my great respect to my parents for their patient concern and invaluable support. Without their love, I would have not been able to complete this thesis work.

TABLE OF CONTENTS

LIST OF TABLES

LIST OF FIGURES

NOMENCLATURE

a	Width of workpiece
$c, c_{1,2,...10}$	Damping factor
da,Z	Axial depth of cut
E	Modules of elasticity
fr	Feed per cutter revolution
ft	Feedrate
I	Moment of inertia
$k, k_{1,2,...10}$	Stiffness
k_a	Unit cutting force
k_c	Cutting stiffness
L	Effective length of the end mill
m	Tool mass
N	Spindle speed
Nt	Number of the flutes
PTV	Peak to valley value
q_1, q_2	Principle mode
R	Cutter radius
Ra	Roughness average
S^2PTV	Variance of PTV values
S^2Ra	Variance of Ra values
u_o	Depth of cut
y(t)	Tool motion in the direction normal to the machined surface
αhx	Helix angle
$\alpha(Z)$	Angle shift associated with a particular axial position along the cutter axis
ρ	Parallel axis offset runout

λ	Locating angle for the runout
$\psi(I)$	Angle between flute 1 and flute I
ζ	Damping ratio

CHAPTER 1 INTRODUCTION

1.1 Background

The end milling process is widely used in industry because of its versatility and efficiency. Applications of the end milling process can be found in almost every industry ranging from large aerospace industry to small tool and die makers. One reason for the popularity of the end milling process is that it can be used for both rough and finish machining of components. An end milling operation may be used to generate the following features in a workpiece: slot , pockets/cavities and faces of thin parts. The aerospace industry makes wide use of the end milling process. The process is used in the production of a variety of components including missile housings and aircraft wing sections. Many of these parts can be characterized as thin walled sections with tight design specifications which required high machining accuracy.

One principal problem which may result from the end milling process is the generation of a finished part surface which does not satisfy product design specifications. A finished part surface might violate product texture (the finish of the surface is too rough) or poor surface accuracy (the location of the surface differs from that desired). An undesirable part surface may necessitate additional machining, thus lowering productivity and increasing the cost of the part . Otherwise in the worst case,the workpiece/part might have to be scrapped.

In order to produce parts which conform to design specifications, proper machining conditions (tool geometry and material, fixtures, feedrate, spindle speed, cutter diameter, number of cutting flutes and runout) must be selected. Traditionally, very conservative settings result in lower productivity and hence, higher cost.

When a manufacturing process is used to produce a newly designed component, it is not uncommon to examine different combinations of the aforementioned process parameters. It may happen that the newly design component doesn't satisfy the design

specifications. This is largely due to incomplete understanding of how the various inputs to the manufacturing process interact. In the aerospace/defence industry, where the production quantity of components is small and the dimensional accuracies are tight , a trial and error approach to manufacturing may generate ten to fifteen bad parts for every good one . This low yield from the manufacturing process results in low productivity and high costs.

In order to operate a manufacturing process at high productivity and low cost conditions and to produce high quality parts, the production of unacceptable part surfaces must be avoided. This problem is typically due to the selection of machining conditions for the process which results in one or more of the following : excessive deflection of thin-walled workpiece section, excessive deflection of the end mill and system instabilities/chatter. Chatter is a phenomenon indicative of an unstable system, where the displacement of the tool relative to workpiece increases until the tool moves away from the workpiece. The increased use in many industries of machine tools which are capable of operating at high spindle speeds and feedrates further complicates these problems, since the available informations about high speed machining is not yet sufficient for complete understanding of this new technology.

Historically, machining conditions have been selected based on empirical models, past experience or by trial and error as discussed above. Empirical models, typically based on experimental data, have two principal drawbacks:

1. Since an empirical model is only valid in the range over which the data have been collected, it is difficult to extrapolate result from one set of machining conditions to a new set of conditions. Consequently, experiments must be conducted for every combination of machining conditions. Such a comprehensive experimental program would be very expensive and time consuming to complete.

2. Although an empirically based mathematical model may adequately predict most of the trends and subtleties in the data, it does not lead to a complete understanding of the mechanics of the process.

Rather than using data based empirical models to select machining conditions it would be more desirable to perform the selection based on mathematical models that are derived from the mechanics of the end milling process. Such mechanistically based models are more difficult to develop than the empirical models because this requires the process modeler to understand the physics of the process and make appropriate assumptions when necessary. Once such model has been developed, based on which the effects of varying process variables can be examined without physically performing the machining experiments.

The main purpose of this thesis is to develop a model to predict the three-dimensional surface texture for an end milling process in presence of runout and cutter vibration. A series of surface simulation and case studies are presented in order to clearly understand the effects of parallel axis offset runout and cutter vibration.

Various surface characterization parameters are examined to provide quantitative measures of these effects. Experiments are frequently performed to measure the effects of one or more variables on a response. Factorial designs are extremely useful for this purpose, especially two-level factorial designs. These designs and the fractional factorial designs derived from them are economical and easy to use and can provide valuable informations. In this thesis, empirical modeling and the principles governing the construction and analysis of factorial designs are discussed. Actual problems are never so straightforward that they can easily be solved mechanically. Therefore it is necessary to think about the real nature of the scientific problem itself, to mull over data plots and other graphical displays as well as to understand potentially useful statistical principles and their practical consequences. The possible difficulties caused by the violation of the assumptions, such as the lack of independence of data, should also be pointed out .

Furthermore ways should be discussed to overcome such difficulties. Special emphasis is given on the design of experiments because this is the most valuable aspect of the statistical method. Frequently conclusions are easily drawn from a well-designed experiment, even when rather elementary methods of analysis are employed. Conversely, even the most sophisticated statistical analysis cannot salvage a badly designed experiment.

1.2 Outline of Thesis

There are six chapters in this thesis. Chapter 2 is a literature review of the end milling process covering the areas of basic process mechanics, process geometry, surface accuracy etc. In addition to that literature, focusing on the effect of system rigidity/dynamics on milling processes, is also explored.

Chapter 3 describes the basic methodology for simulation of surface topography in an end milling process. In this simulation a surface machined by the end milling process is modeled by considering parallel axis offset runout , static deflection and tool vibration. This model can be used to predict the surface accuracy for a flexible end milling system when operating at conventional spindle speeds. The model, describing the deflection of the end mill , is based on beam theory. The notion of a balanced force/deflection equilibrium position is established.

Chapter 4 describes the experiment for surface roughness measurement techniques In this chapter, the development of a sensor based measurement system and the experimental methodology used in this research on the end mill process are presented. In order to verify the simulation model for surface topography generation in an end milling process, experiments are performed on a CNC machining center in Advance Design and Manufacturing Laboratory in the Department of Mechanical Engineering, University of Maryland, College Park. After machining, the surface roughness measurements are carried out at NIST.

Chapter 5 describes the factorial design on simulation of the surface topography generated during end milling process. To perform a general factorial design, a fixed

number of " levels " (Or "versions") for each of the variables (factors) is selected and then experiments are carried out for all possible combinations. If there are l_1 levels for the first variable, l_2 for the second,..., and l_k for the kth variable, then the complete arrangement of $l_1 \times l_2 \times \ldots\ldots \times l_k$ experimental runs is called an $l_1 \times l_2 \times \ldots\ldots \times l_k$ factorial design. For example, a $2 \times 3 \times 5$ factorial design requires $2 \times 3 \times 5 = 30$ runs and $2 \times 2 \times 2 = 2^3$ factorial design requires 8 runs. The variables used in various factorial designs in this research work occur at only two levels.

Chapter 6 summarizes the thesis and provides a brief discussion for future work in this area.

CHAPTER 2 LITERATURE REVIEW

A review of the past research suggests that the analysis of the end milling process can be divided into two basic areas:

(1) analysis for the prediction of the surface topography and

(2) analysis devoted to examine the dynamic structure of the machining system of an end milling process.

The first area has been primarily devoted to develop models based on fundamental theories. These models can be used to predict a wide variety of performance measures of the process. These models, based on first principles, are generally referred as mechanistic models due to there limited dependence on experimentally obtained data. The second area of research has proven to be useful in predicting the dynamic characteristics of milling operation for a given set of input process parameters.

2.1 A Mechanistic Model for the End Milling Process

A model that describes in a mechanistic sense and simulates the performance of the end milling process for a given set of input process parameters, must have two components. The first component should deal with process geometry and the second should deal with surface generation. Work performed in each of these individual areas will be examined in this chapter and then a model that has incorporated these separate components into one computer-based simulation algorithm will be developed in this research work.

2.1.1 Geometric Models for the Milling Process

The pioneering work in analytical evaluation of cutter paths in a milling operation was done by Martellotti [11,12]. In these two fundamental papers, Matellotti showed that the paths followed by the cutter flutes are trochoidal and he formulated mathematical expressions describing the path followed by a given point on a flute I with respect to the spindle axis in a Cartesian coordinate (X, Y, Z,) . These mathematical expressions are :

$$X(I,Z,t) = \rho*\sin(\theta(t)+\lambda)+R*\sin(\theta(t)-\psi(I)-\alpha(Z))+fr/60*t \quad (1)$$

$$Y(I,Z,t) = -\rho*\cos(\theta(t)+\lambda)-R*\cos(\theta(t)-\psi(I)-\alpha(Z)) \quad (2)$$

Also,

relative position of cutter axis w. r. t. spindle axis, X1 and is given as

$X1=\rho*\sin(\theta(t)+\lambda)$ and $Y1=-\rho*\cos(\theta(t)+\lambda)$

relative position of flute I w. r. t. cutter axis, X2 and is given as

$X2=R*\sin(\theta(t)-\psi(I)-\alpha(Z))$ and $Y2=-R*\cos(\theta(t)-\psi(I)-\alpha(Z))$

relative position of spindle axis w. r. t. workpiece, X3 and is given as

$X3=fr/60*t$

where,

fr	the feedrate	(mm/min)
ρ	the parallel axis offset runout	(mm)
λ	the locating angle for the runout	(rad)
R	the cutter radius	(mm)
$\psi(I)$	the angle between flute1 and flute I	(rad)

$\alpha(Z)=(Z*\tan(\alpha hx))/R$

the angle shift associated with a particular axial position along the cutter axis (rad)

αhx	the helix angle	(rad.)

If the spindle speed N (rev./min) is constant, $\theta(t)$ is a linear function of time t, then

$\theta(t)=2*\pi*N/60*t$ (rad/min)

Obviously, when t=T (sec.), where T=60/N is the time period of a cutter revolution,

$\theta(T)=2*\pi$ (rad)

Also, X3 can be rewritten as

$$X3 = fr*\theta(t)/(2*\pi)$$

where

fr	the feed per cutter revolution	(mm/rev.)
fr = ft*Nt		
ft	the feed per flute	(mm/flu.)
Nt	the number of the flutes	

2.1.2 Surface Generation Models

End milling is a flexible process that is widely used in industries. Figure 2.1 shows the cut geometry and the coordinate system for an end milling process.

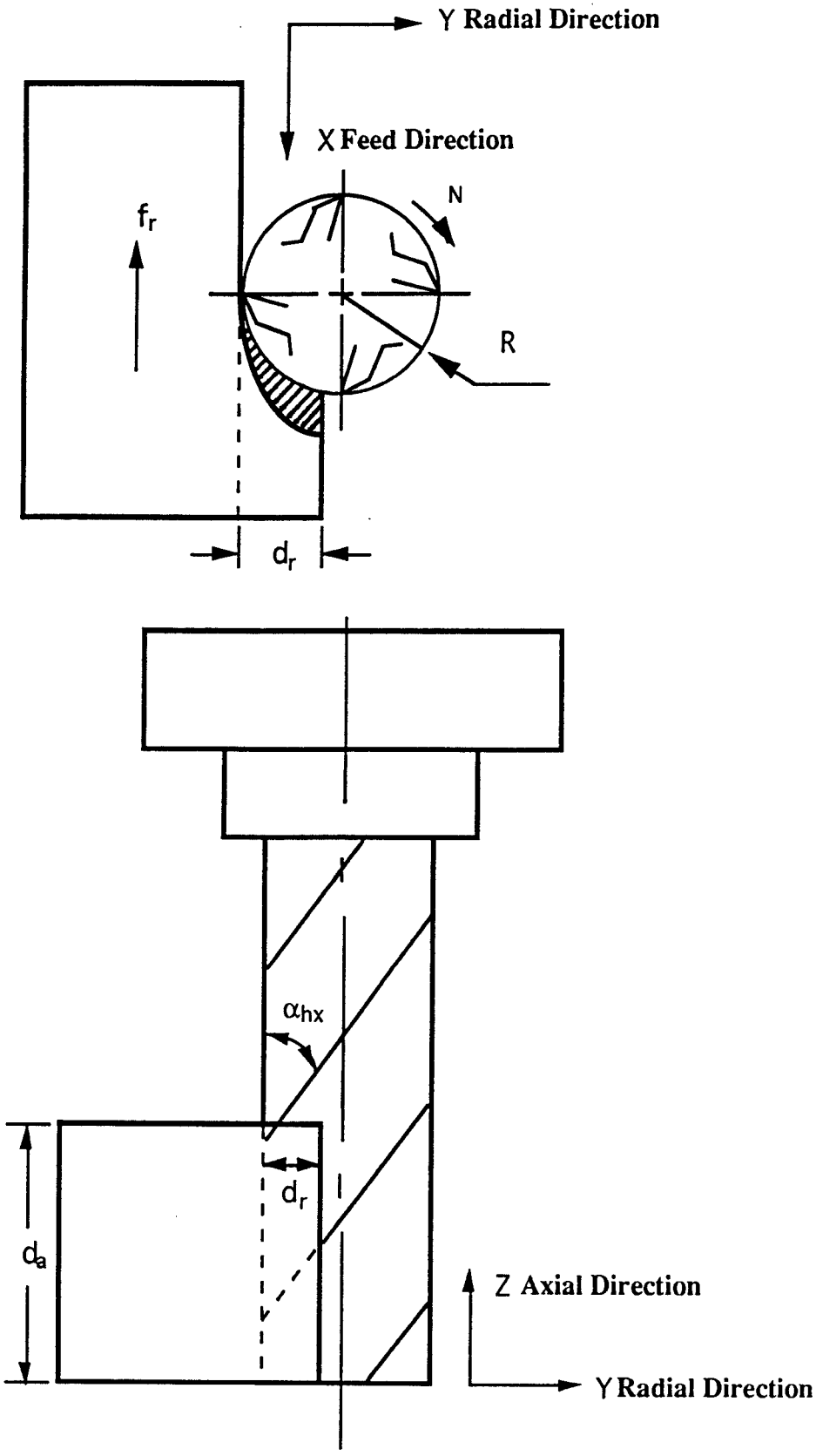

Fig. 2.1 Cut geometry and coordinate system for the end milling process

where

N is the rotational speed of the end mill (rev./min),

R is the radius of the end mill,

f_r is the table velocity or feedrate,

d_r is the radial depth of cut,

d_a is the axial depth of cut and

α_{hx} is the helix angle of the end mill.

One problem frequently encountered in using the end milling process is cutter runout. This phenomenon, which can be reduced but not eliminated entirely, causes the end mill axis to differ from that of the axis about which the cutter rotates. In general, set screwtype tool holders give rise to parallel axis offset runout and the collettype tool holders give rise to spindle tilt runout. Both of these forms of end mill runout were characterized by Kline and Devor[9] and are illustrated in Fig. 2.2 where

ρ is the amount of parallel axis offset runout,

λ is the locating angle for ρ,

τ is amount of spindle tilt runout,

ϕ is the locating angle for τ and,

L is the effective length of the end mill.

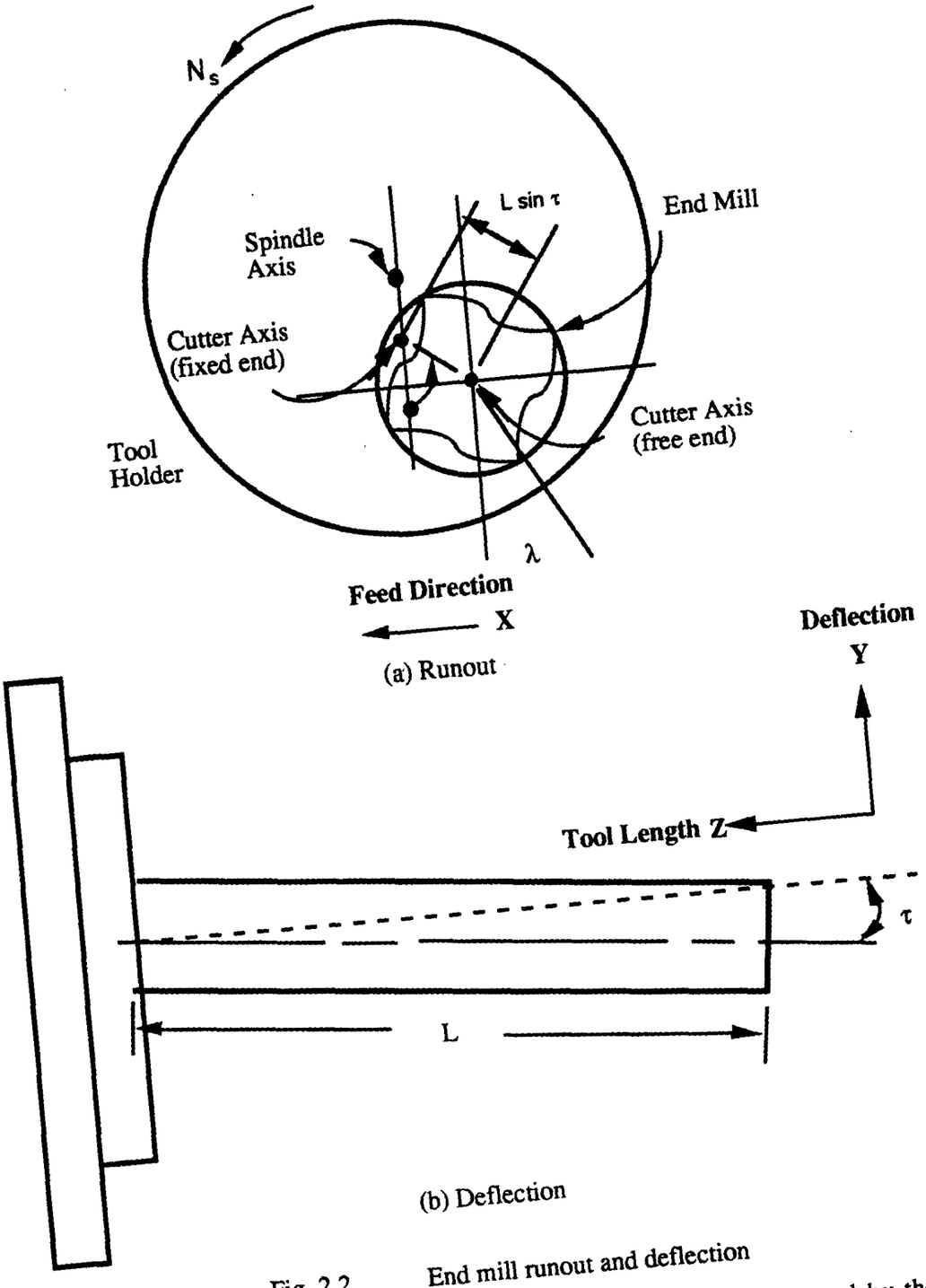

Fig. 2.2 End mill runout and deflection

Experimental investigations into the surface topography generated by the end milling process have been made at the National Twist Drill Company [1] and by Fujii, et

al. [6]. The National Twist Drill studies examined the effects of various cutter and cut geometry variables on the surface topography including milling type, cutter diameter, number of flutes and the cut geometry (radial depth of cut, axial depth of cut, and feedrate). These studies identified cutter runout as an important variable in the surface generation process. For down milling it was noted that the cutter always deflect away from the workpiece leaving a positive surface error. Surface error as it is used here and as used in this research, is defined to be the deviation of the surface from the surface that would be produced by a completely rigid machining system. A number of solutions are offered to reduce surface errors including using the most rigid cutter available and reducing feedrate for finishing cuts.

In the Fujii study, the surface generation process was viewed as being the projection of a helical flute moving across the work surface. A carefully instrumented set of experiments were conducted measuring cutting forces, cutter deflection and workpiece deflection over the rotation of the end mill. These data were then used to predict surface error at a particular point on the workpiece surface.

Further analytical investigations into the surface generation mechanism of the end milling process were undertaken by Kline, et al. [10], and Babin, et al. [2]. The Kline study centered on the prediction of surface errors for which models for the end mill and the workpiece deflections were developed. The results of this work indicated that relatively simple geometric and mechanistic models may be used to accurately predict the surface errors produced by the end milling process. A later investigation, which combined the surface error prediction model of Kline to a model for surface roughness, also showed close agreement between predicted and measured machined workpiece surface shapes.

2.2 Dynamic Analyses

The dynamic displacement of various parts of a machine tool structure (vibration) is a problem that is inherent in all metal cutting processes. The displacement of the

cutting tool relative to the workpiece may adversely affect surface finish, dimensional accuracy, tool life and machine life. Vibration in a process such as end milling may arise due to internal sources such as the movement of rotating parts, workpiece inhomogeneities, the feed mechanisms of the machine tool, the cutting process dynamics and the varying cutting forces produced by a varying chip load. External sources (for example, neighbouring vibrating machine tools) may excite the floor and induce vibration into the machine tool structure of interest. Milling processes are recognized for their characteristically large levels of vibration resulting form the cyclic nature of the chip loading mechanics and the cyclic nature of the cutting force system produced by a multi-tooth cutter . In general, the level of forced displacement present in the machining system depends on the characteristics of the exciting force system as well as the dynamic properties of the structure [13].

One form of vibration which is widely recognized for its deleterious effects is chatter. Chatter is an unstable form of forced vibration in which displacement amplitudes increase with time until they are large enough to cause the cutting tool to move away from the workpiece. At some point this vibration amplitude stabilizes and the cutter is not in contact with the workpiece for a part of the oscillatory cycle. This stabilization of the displacement amplitude to a finite level was described by Tlusty and Ismail [19] as a nonlinear phenomenon. In machining, the phenomenon of chatter is totally unacceptable because it indicates the presence of severe vibrations, degraded surface finish and large amounts of acoustical noise. Chatter is a phenomenon specific to metal cutting and mechanistically results from self-excited vibration due to regeneration. Regeneration refers to machining of a surface that has already been machined by a vibrating cutting tool. Regeneration produces chip load that varies with time [13].

Process decision makers seek cutting conditions that avoid large levels of forced vibration and chatter. This is not an easy task since machine tool structures usually have low damping which is partly responsible for large levels of forced vibrations in machine

tool structure. In order to aid the process of selecting satisfactory cutting conditions, much attention has been devoted to the development of dynamic models for different processes and also to the explanation and prediction of machine tool chatter and processes stability. Because of the complexity of the chatter phenomenon, most analytical approaches have examined geometrically simple processes such as single point turning. In addition, much of this analytical work has been performed only in the frequency domain and has been devoted only toward stability analysis.

A dynamic model for a metal cutting system may be represented as a closed loop model as illustrated in Fig 2.3. The model and its components shown in the figure are briefly described below.

1. Machine tool structure--characterizes the position of the cutting tool relative to the workpiece.
2. Cutting process--calcuates forces. A common way of accomplishing this is to equate force to the product of the chip thickness, width of cut, and the specific cutting pressure. A more elaborate approach includes the effects of penetration rate and cutting speed.
3. Chip thickness--the chip thickness is calculated based on past and present relative cutter positions.
4. Primary feedback path--used to feed back the current position of the cutting tool relative to the workpiece.
5. Regenerate feedback path-- used to feed back the past position of the cutting tool relative to the workpiece. In turning the length of the time delay is the time needed for one revolution of the wokpiece. In milling the length of the time delay is the time needed for one revolution of the cutter divided by the number of teeth on the cutter.

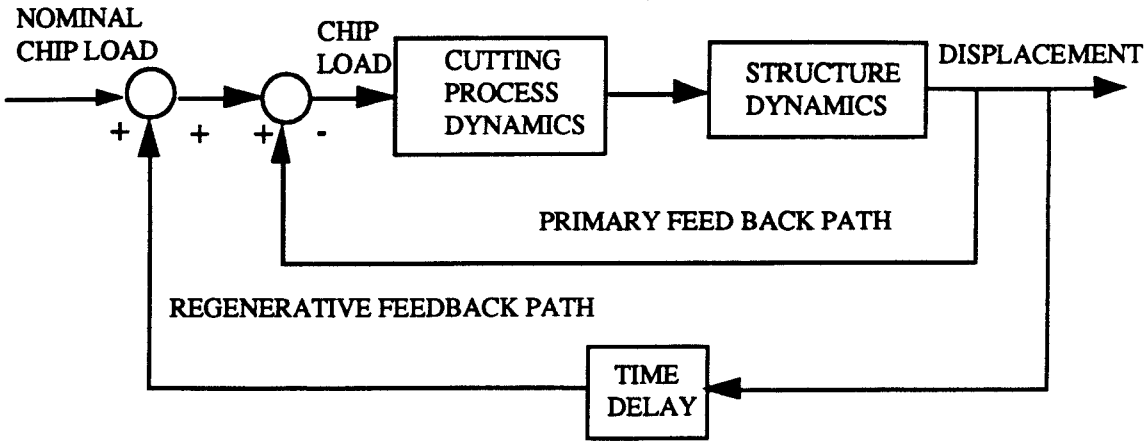

Fig. 2.3 Closed loop dynamical model for a metal cutting system

2.3 Summary

The model of Kline, et al. [10], very accurately predicts the force system and the resulting surface error for various sets of input condition for the end milling process. They included in their model the effects of cutter runout and the helix angle which were often neglected or ignored by others. In predicting the surface error, the model takes into account the flexibility of the end mill and the workpiece. However, for some cutting conditions, most notably those with small radial depth of cut and/or those with a long end mill, the predictions of the force system and surface errors are erroneous because flexibility is not considered during the calculation of the chip thickness. The fact that the system deflection is not considered in the determination of chip thickness results in overestimation of both the cutting force and the surface error.

The model of Kline, may be considered as static and as such cannot predict important characteristics like stability and dynamic displacement. Most of the work done by Tlusty and Tobias is based on a model proposed by Merritt. Merritt's model is a dynamic representation of a turning process. This formulation helps in developing decision-making tools such as stability charts and simple stability criteria that may be used to assess the suitability of a given set of cutting conditions prior to machining.

Sridhar,et al.[16] modified the dynamic model for turning to describe the dynamic behavior of the various milling processes. They accounted for various characteristics such

as intermittent cutting, multiple edges engaged in cutting and the varying direction of the cutting force as the mill rotates and the chip load changes. Sridhar describes the relative movement of the milling cutter for a set of forces and torques through a flexibility matrix, the elements of which were obtained experimentally. Tlusty also used experimentation to obtain the frequency response in the X- and Y- directions for the machine tool. He then simulated the end milling process based on a selected frequency from each direction. The stability charts or lobes for the end milling process were presented.

Several difficulties still exist in the dynamic models that have been developed for the milling process. First of all, most models of the milling processes do not acknowledge the existence of cutter runout, the only exception being the face milling model developed by Fu, et al.[7].Cutter runout drastically alters the frequency content of the forces which in turn will strongly affect the response of the end milling process and hence one must include the effects of cutter runout while developing dynamical models for a milling process.

Finally, most researchers have obtained information on the dynamics of various machine tool structures (table slides, spindle, fixtures, etc.)through experimentation. This approach requires various equipment in addition to the actual machine tool structure and may deter some of the smaller manufacturing industries which have limited amount of capital and techniques from studying the dynamic response of a machine tool. As computer technology improves, a computer based approach will be more commonplace and the models for the machine tool structure will become even more accurate. The structural dynamics for a machine tool structure is dependent, however, on the relative position of the various elements of the structure(for example, the position of the tool relative to the machine bed) which also provides a major hindrance in completely understanding the machine tool structural dynamics. Also, transfer functions developed for one machine tool structure are in general totally independent of those that describes another machine tool structure. In brief, the structural dynamics that have been used in

previous dynamic models for milling process are difficult to obtain and once obtained are valid only for a given orientation of the specific machine tool structure of interest. A simple model for dynamic response of the machine tool structure is needed that is valid for various machine orientations and milling machine types.

CHAPTER 3 BASIC METHODOLOGY

Simulation of topography of an end milling surface can be facilitated by considering several steps. First, we select the ideal surface topography without the parallel axis offset runout, static deflection, and tool vibration. In the Second step, we generate the surface topography with runout. The next step includes runout and static deflection. Finally, we generate the surface topography with runout, static deflection, and tool vibration.

There are two main steps in the process of surface topography prediction:

1. Select the parametric equations of the tool path (mathematic model) to describe the physical system.
2. Select a suitable procedure to generate the surface.

3.1 Parametric Equations of the Tool Path

In order to determine the flute trajectories, we must develop equations to describe the tooth path. Fig 3.1, 3.2, and 3.3 graphically depicts the variables and coordinate system employed during the model development. A point at flute I with respect to the spindle axis in a Cartesian coordinate (X, Y, Z) is represented by the following

$$X(I, Z, t) = X1+X2+X3 \tag{3.1}$$

$$Y(I, Z, t) = Y1+Y2 \tag{3.2}$$

where

the relative position of the cutter axis with respect to the spindle axis is given by

$$X1=\rho*\sin(\theta(t)+\lambda) \text{ and } Y1=-\rho*\cos(\theta(t)+\lambda)$$

the relative position of flute I with respect to the cutter axis is given by

$$X2=R*\sin(\theta(t)-\psi(I)-\alpha(Z)) \text{ and } Y2=-R*\cos(\theta(t)-\psi(I)-\alpha(Z))$$

and the relative position of spindle axis with respect to workpiece is given by

$X3=fr/60*t$

and

fr	the feedrate	(mm/min)
ρ	the parallel axis offset runout	(mm)
λ	the locating angle for the runout	(rad)
R	the cutter radius	(mm)
$\psi(I)$	the angle between flute1 and flute I	(rad)
$\alpha(Z)=(Z*\tan(\alpha hx))/R$	the angle shift associated with a particular axial position along the cutter axis	(rad)
α_{hx}	the helix angle	(rad)

If the spindle speed N (rev./min) is constant, $\theta(t)$ is a linear function time t:

$\theta(t)=2*\pi*(N/60)*t$ (rad/min)

Obviously, when t=T (sec.), where T=60/N is the period time of a cutter revolution,

$\theta(T)=2*\pi$ (rad)

Also, X3 can be rewritten as

$$X3 = fr*\theta(t)/(2*\pi)$$

where

fr is the feed per cutter revolution (mm/rev.)

$$fr = ft*Nt$$

where

ft	the feed per flute	(mm/flu.)
Nt	the number of the flutes	

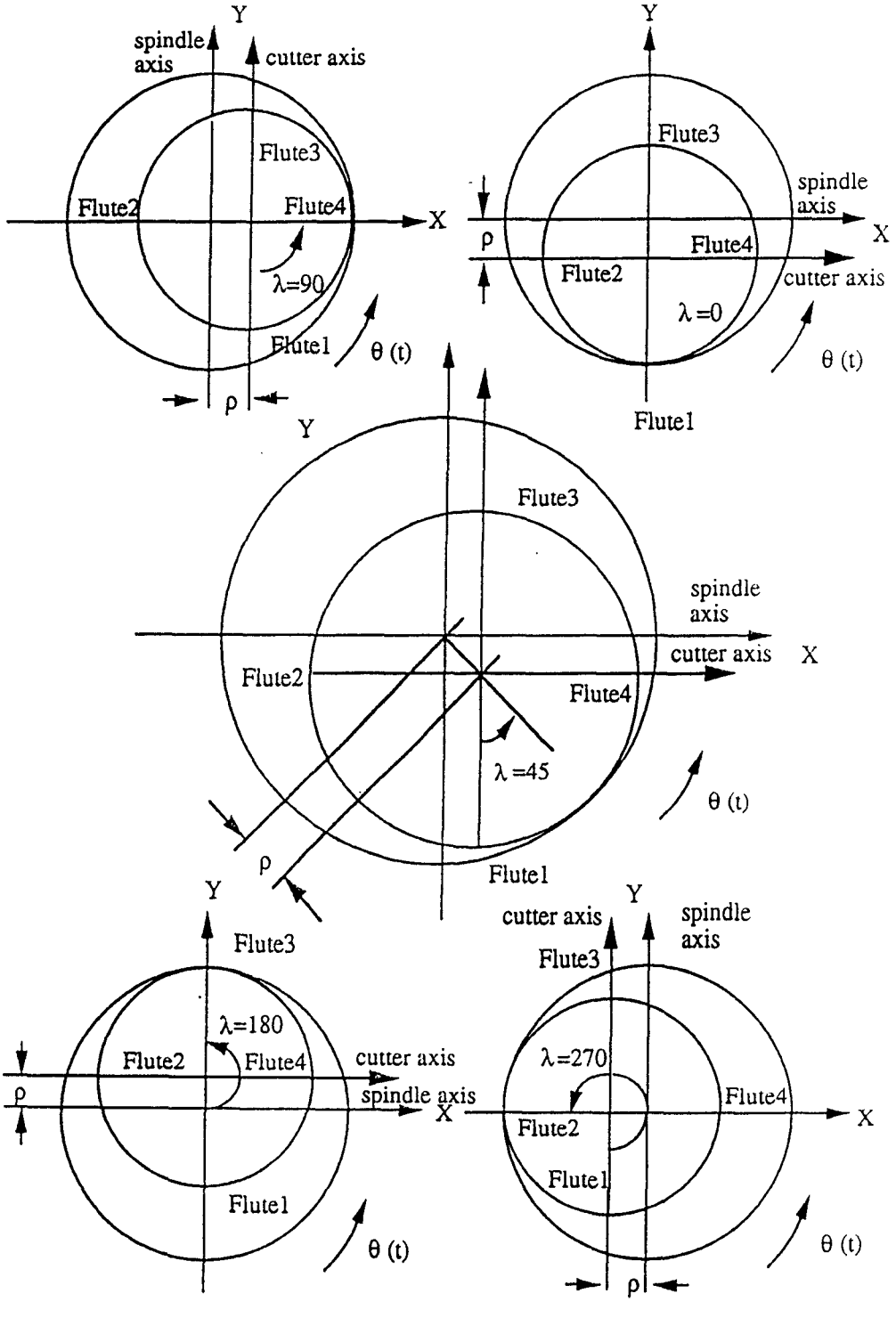

Fig3.1 Runout definition at λ=0,45,90,180,270 degrees

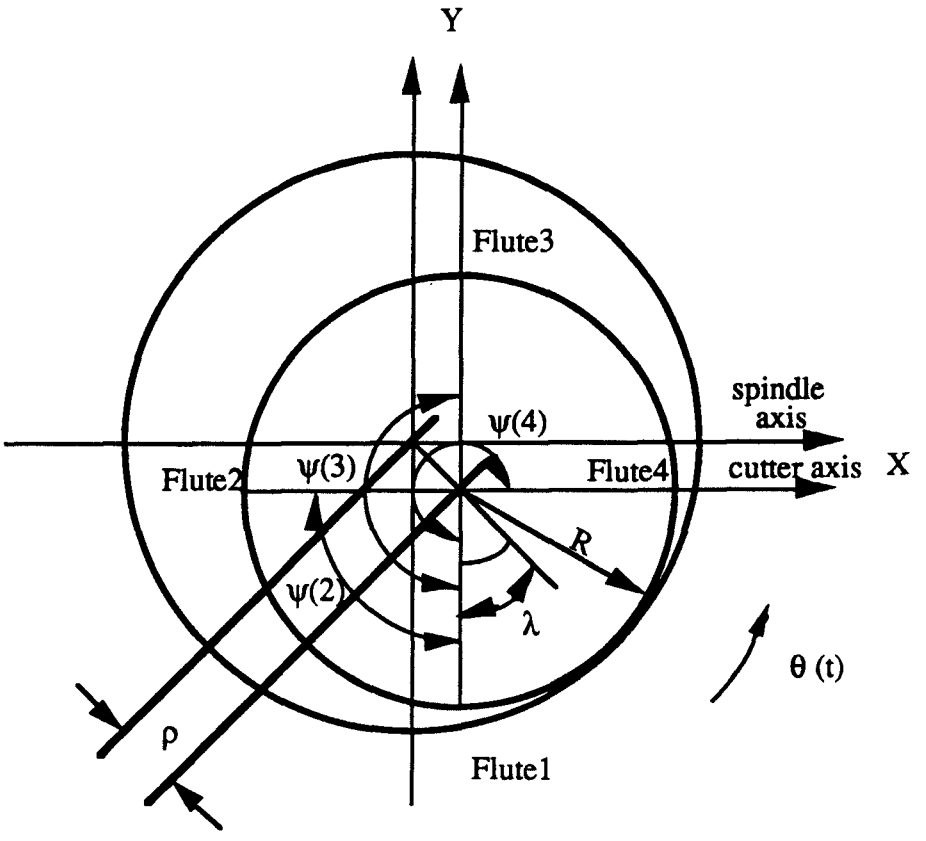

Fig3.2 Geometry and variable definitions for model development

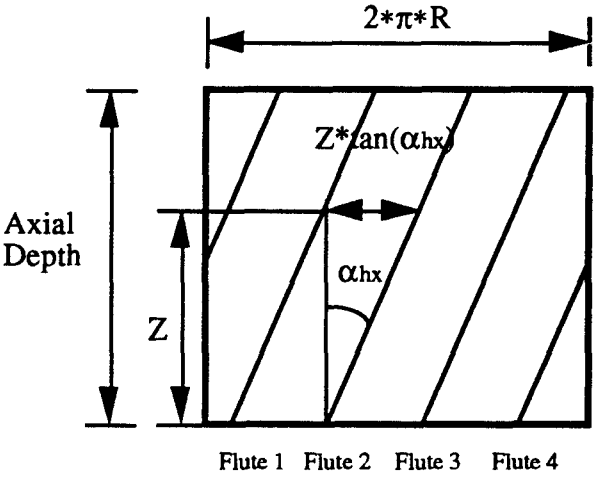

Fig3.3 Angle corresponding to a particular Z location

3.2 The Surface Generation

3.2.1 The Surface Generation Procedure

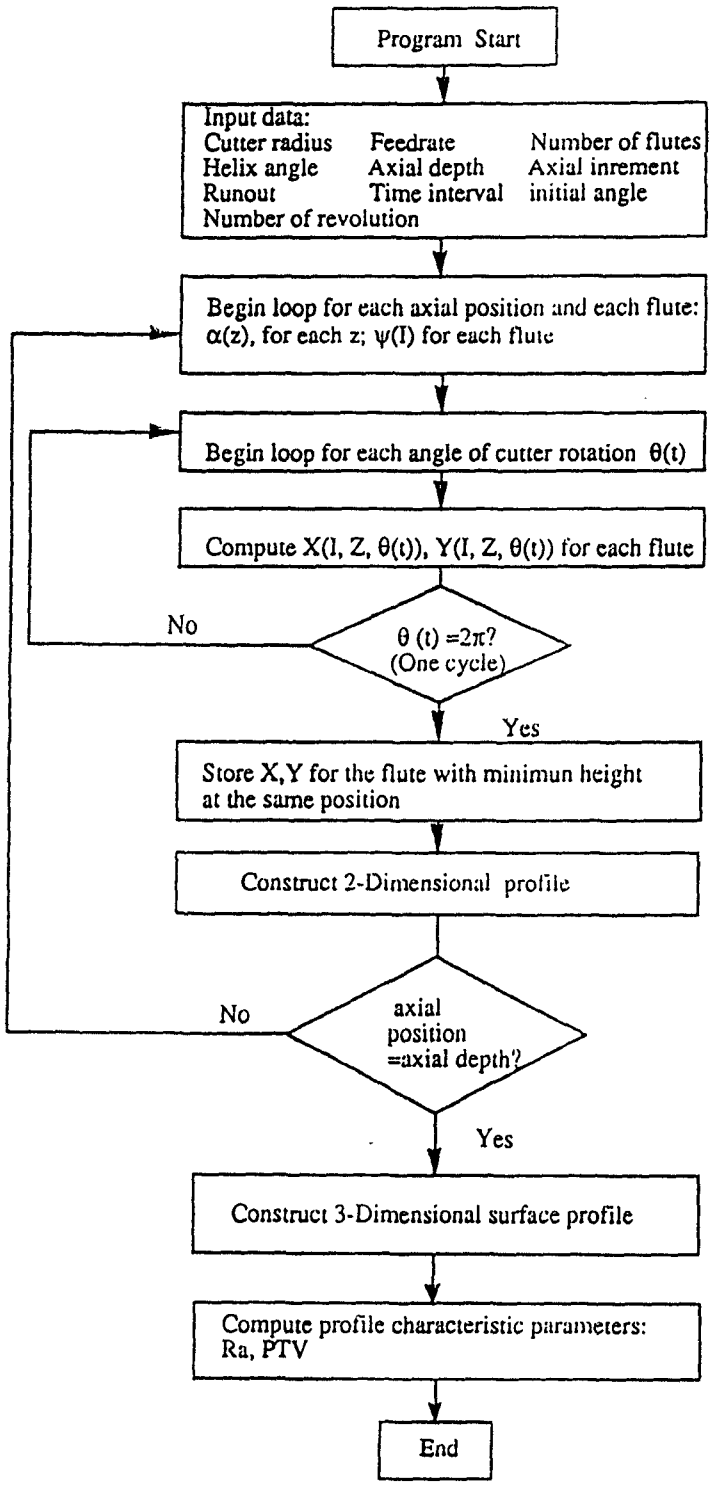

Fig3.4 The surface generation procedure

3.2.2 The Illustration of the Surface Generation Procedure

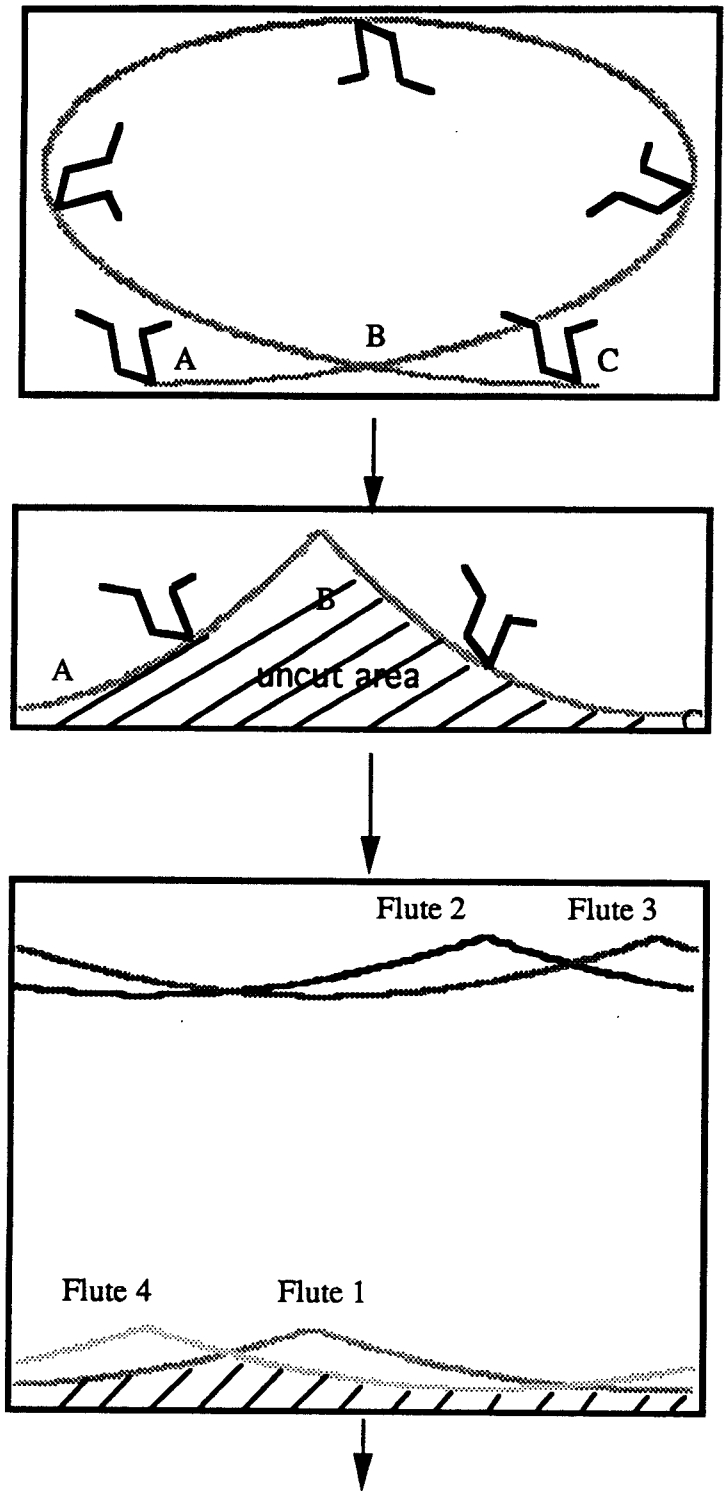

The trajectory of a flute in a cycle of motion by the equations of flute position

$X(I, Z, \theta)$, $Y(I, Z, \theta)$

$\theta: 0 - 2\pi$

(a) The trajectory of a flute in a cycle of motion

Taken from part of above profile ABC, corresponding to end milled surface

(b) Uncut area

Because of cutter runout, only flute 1 and flute 4 are involved in end milled surface generation

(c) The trajectory of each flute in a cutter revolution

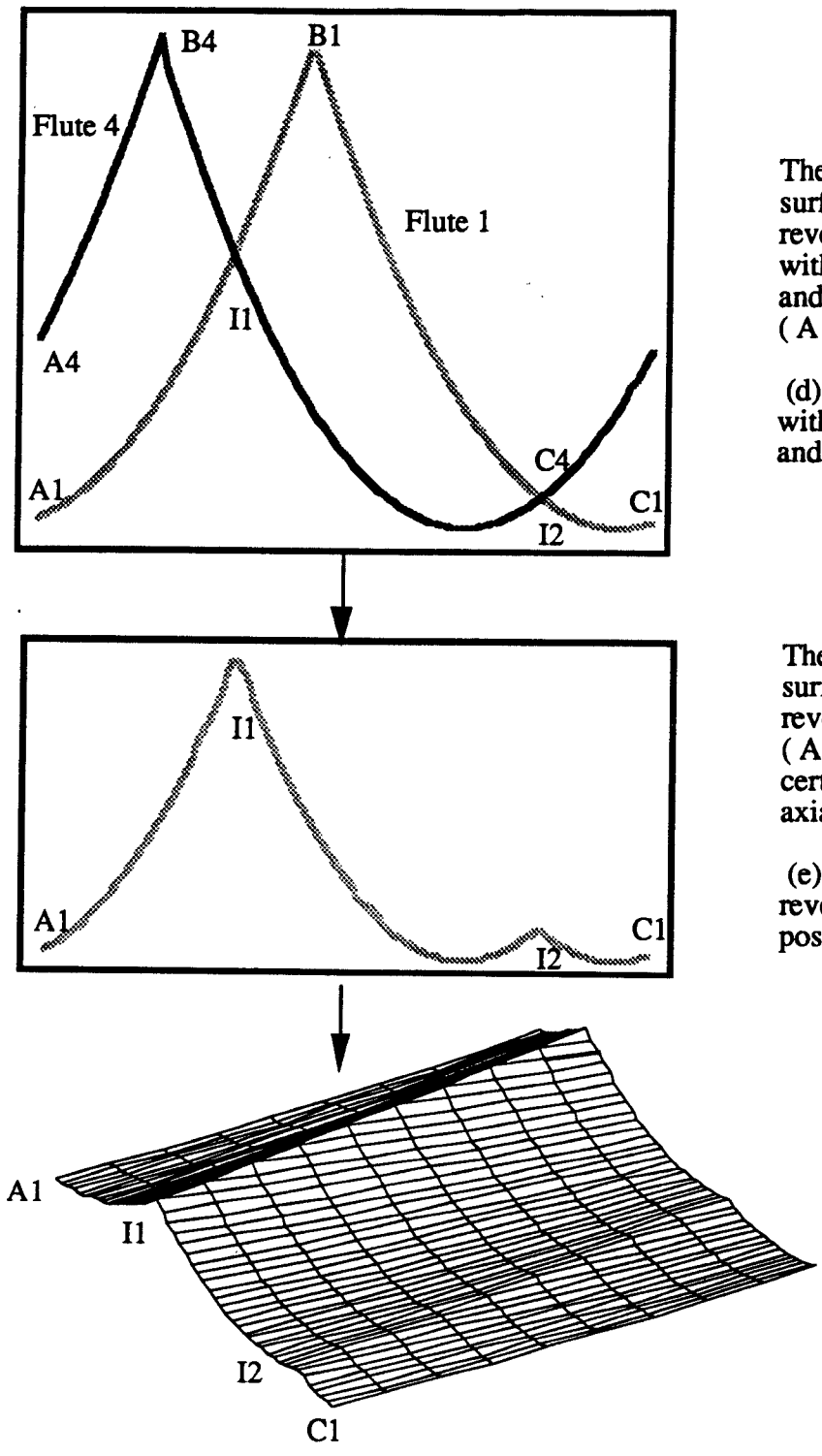

The profile of end milled surface in a cutter revolution is combined with trajectory of flute 1 and trajectory of flute4 (A1, I1,I2,C1)

(d) The profile combined with trajectory of flute1 and 4

The profile of end milled surface in a cutter revolution (A1,I1,I2,C1) and a certain axial position (Z)

(e) The profile in a cutter revolution with a axial position Z

Finally, the 3-D geometry of end milled surface be built in a cutter revolution and a certain range of axial distance

(f) The 3-D geometry of end milled surface

Fig. 3.5 The illustration of surface generation procedure

3.3 Ideal Surface Topography

The ideal surface topography is considered selecting the appropriate feedrate without runout, deflection, and tool vibration

The input data are:

Radius of Cutter	R	20 mm
Number of Flutes	Nt	4
Helix Angle	α_{hx}	10 degree
Feed Per Revolution	fr	0.5 mm/rev.
Axial Depth of Cut	Z	20 mm
Runout	ρ	0 mm

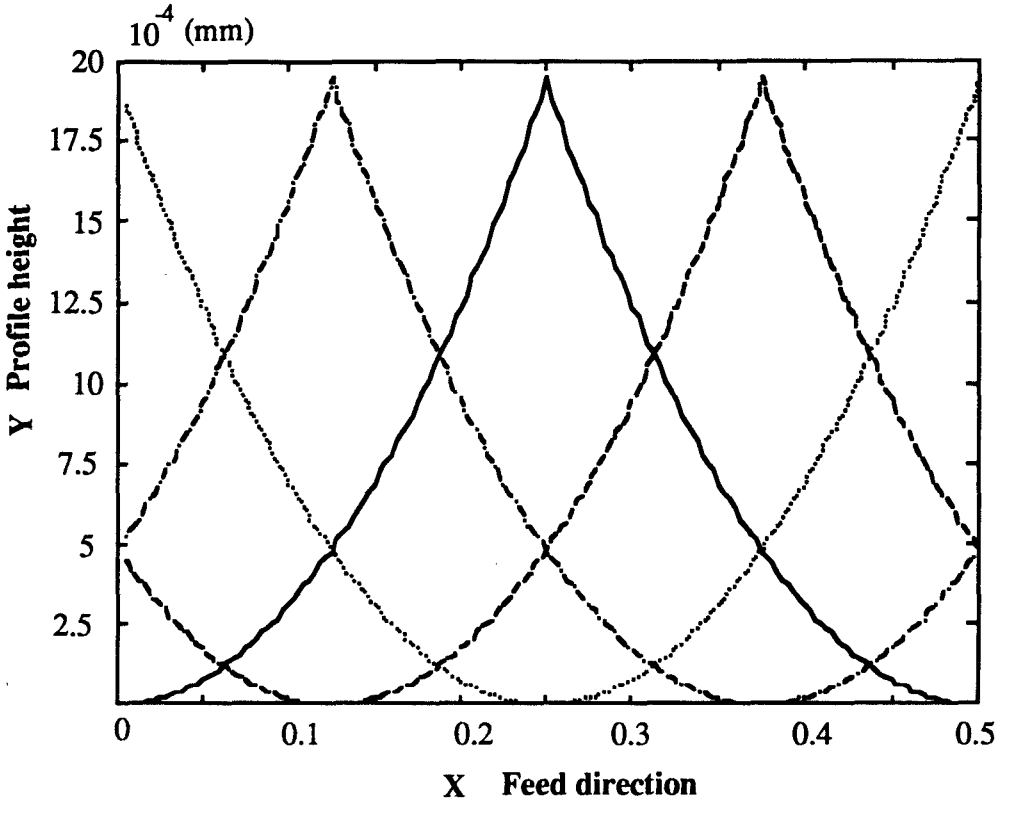

Fig.3.6 The trajectory of each flute in a cutter revolution

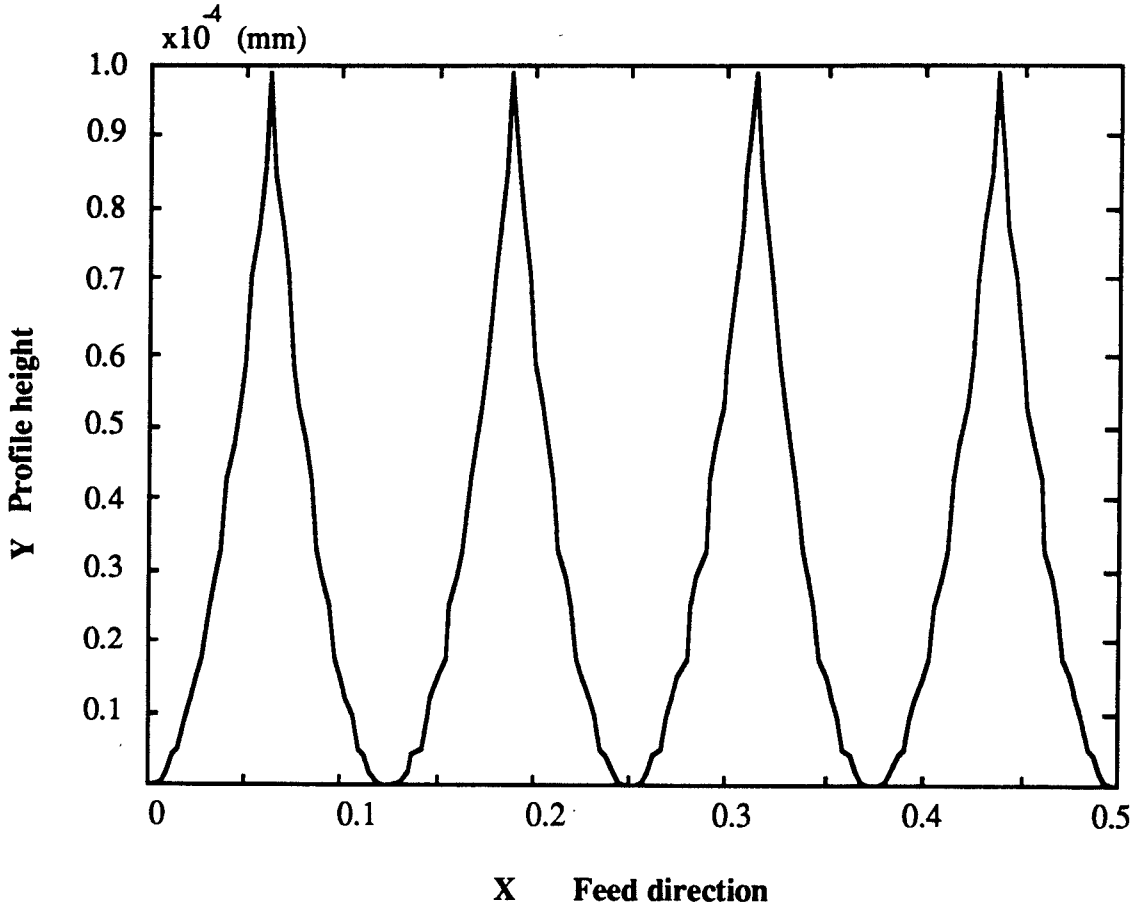

Fig.3.7 The profile of milling surface in a cutter revolution

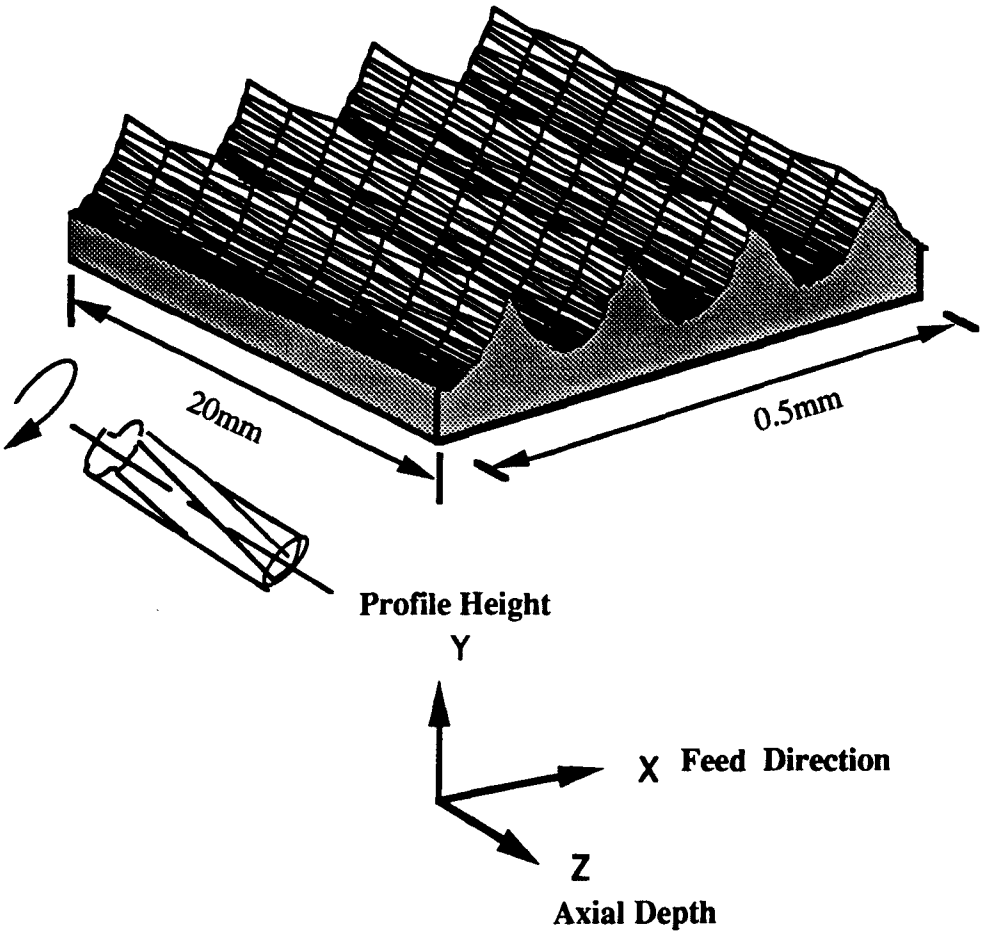

Fig. 3.8 The 3-D geometry of end milling surface for an ideal case

where

Ra = 0.025μm

PTV = 0.1μm

3.4. Surface Topography with Runout

The input data are:

Radius of Cutter	R	20 mm
Number of Flutes	Nt	4
Helix Angle	α_{hx}	10 degree
Feed Per Revolution	fr	0.5 mm/rev.
Axial Depth of Cut	Z	20 mm

Runout	ρ	0.05 mm
Locating Angle	λ	45 degree

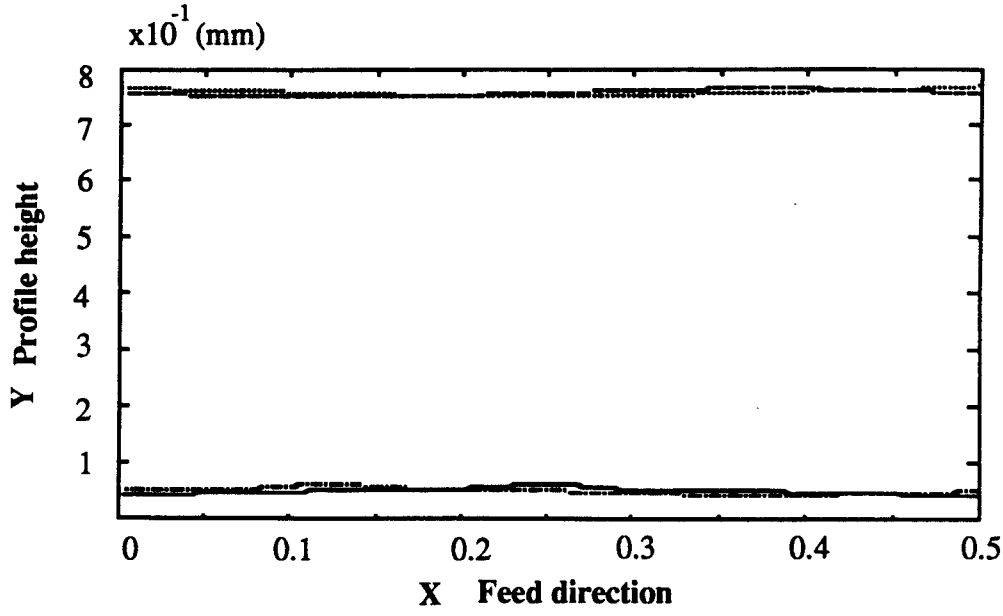

Fig.3.9 The trajectory of each flute in a cutter revolution

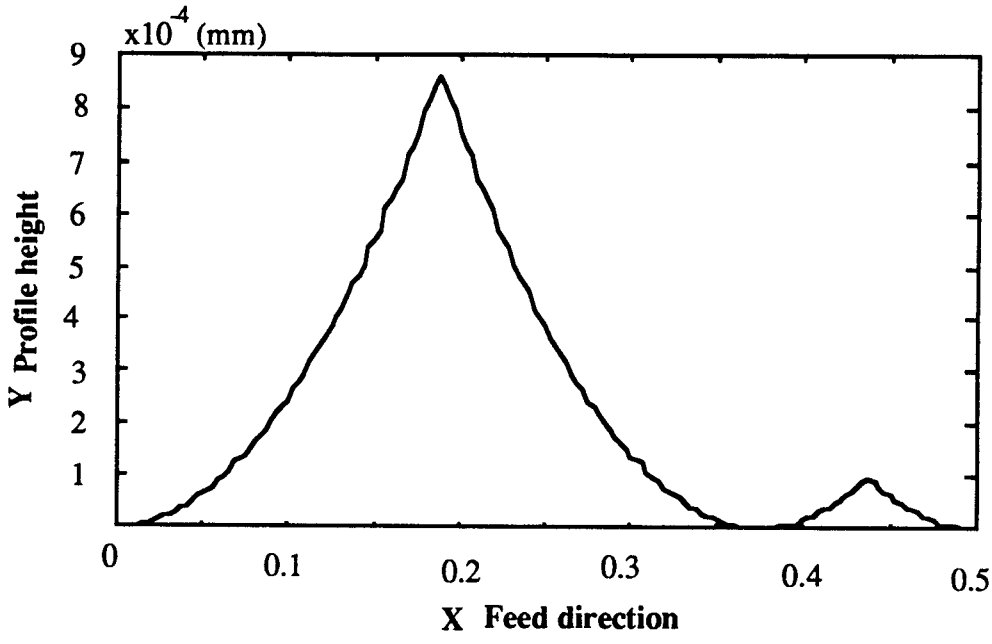

Fig.3.10 The profile of end milling surface in a cutter revolution at Z = 0

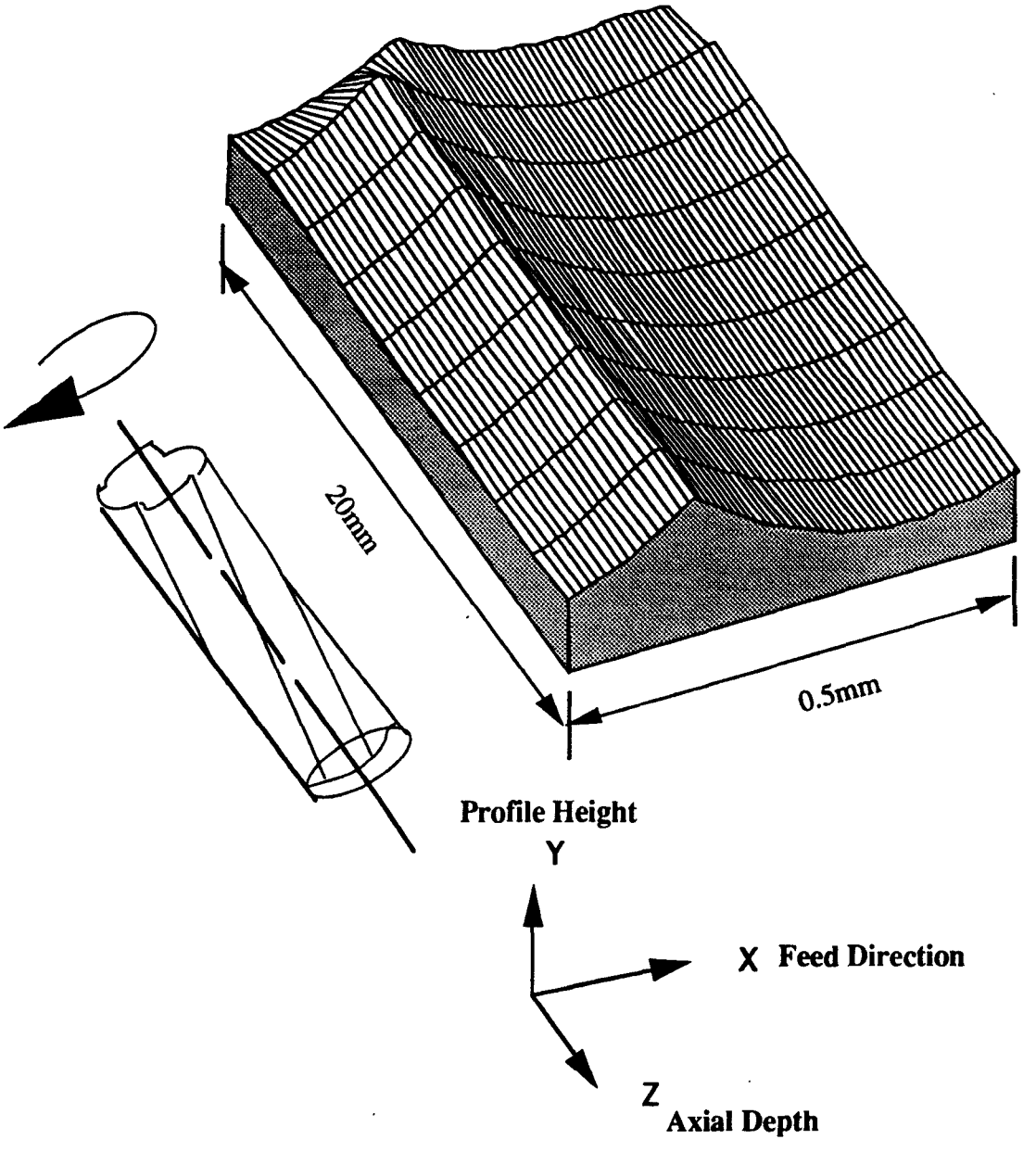

Fig. 3.11 The 3-D geometry of end milling surface for a runout case

where

Ra =0.374 μm
PTV =0.329 μm

3.5 Surface Topography with Runout and Static Deflection

In this thesis, a model has been developed to predict the force system for a flexible end milling system. For many end milling geometries, the cutter behaves like a cantilever beam. Since the chip load calculation algorithm requires deflections (in Y-direction) at many axial positions along the cutter length, The prediction of cutter displacements over the entire length of workpiece engagement is given by the following differential equation:

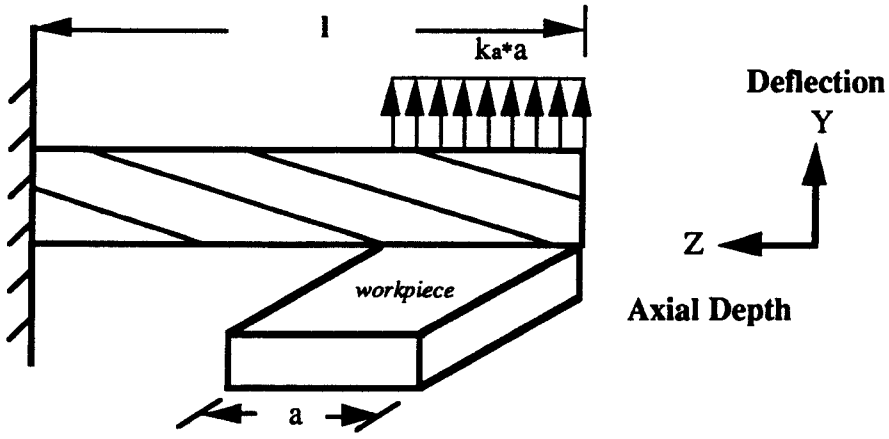

Fig. 3.12 The deflection of the cantilever beam

$$\text{Let} \quad [Z - a]^n = (Z - a)^n \quad \text{if } Z \leq a$$

$$= 0 \qquad \text{if } Z > a$$

The static deflection of a cantilever beam displayed in Fig 3.12 is given by the differential equation

$$EIY(Z)''''=k_a(Z)=k_a[Z - a]^0$$

where

Y(Z) the displacement in Y-direction of the beam at a distance Z from the free end of the beam,

E is the modules of elasticity for the beam,

I the moment of inertia for the beam, and

k_a is the loading force per unit length of the beam.

$$EIY'''=k_a[Z-a]^1 + C_1$$

$$EIY''=k_a[X-a]^2/2 + C_1Z + C_2$$

$$EIY'=k_a[Z-a]^3/6 + C_1Z^2/2 + C_2Z + C_3$$

$$EIY=k_a[Z-a]^4/24 + C_1Z^3/6 + C_2Z^2/2 + C_3Z + C_4$$

To complete the formulation of the boundary value problem, the boundary conditions must be specified. The boundary conditions at the free end of the beam are:

$$\frac{d^2Y(0)}{d^2Z} = 0 \quad , \quad \frac{d^3Y(0)}{dZ^3} = 0$$

The boundary conditions at the fixed/clamped end of the beam are:

$$Y(Z)_{Z=l} = 0 \quad , \quad \frac{dY(Z)}{dZ}_{Z=l} = 0$$

where C_1, C_2, C_3, and C_4, are constants of integration.Applying the boundary conditions get the value of C_1, C_2, C_3, and C_4, and yield the general solution (when $Z \leq a$) is:

$$Y=1/EI\{k_a(Z-a)^4/24 + ak_aZ^3/6 - k_aa^2Z^2/4 + (k_aa^2l-k_aal^2)Z/2 + (ak_al^3/3 - a^2k_al^2/4)\} \qquad (3.3)$$

The input data are:

Radius of Cutters	R	20 mm
Number of Flutes	Nt	4

Helix Angle	α_{hx}	10 degree
Feed Per Revolution	fr	0.5 mm/rev.
Axial Depth of Cut	Z	20 mm
Runout	ρ	0.05 mm
Locating Angle	λ	45 degree
EI		10e08 Nt/mm^2
Tool Length	l	70 mm
Width of Workpiece(cut)	a	20 mm
Loading Force Per Unit Length	k_a	$50Nt/mm^2$

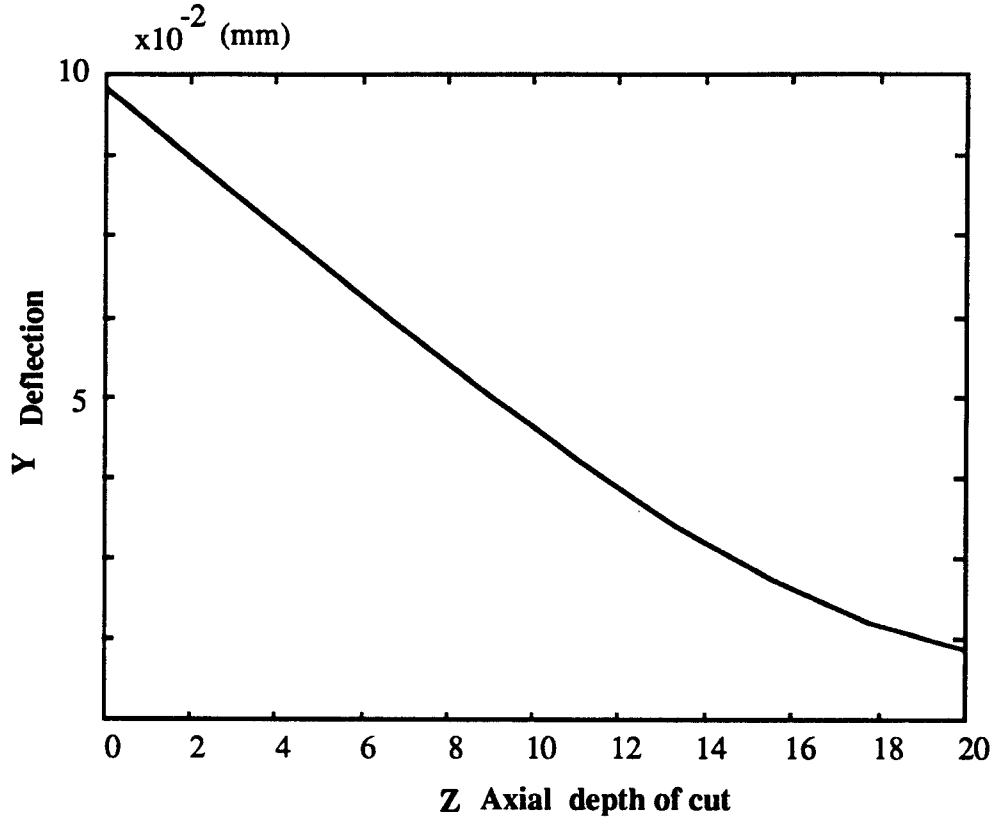

Fig.3.13 The deflection of the cutting tool along the depth of cut

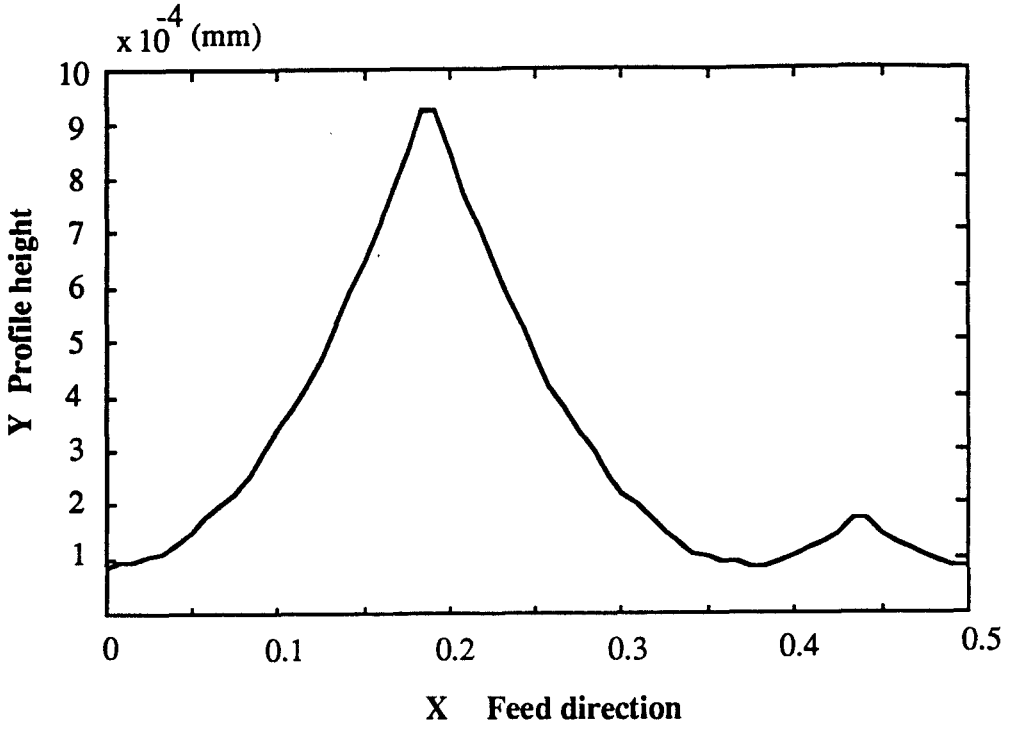

Fig.3.14 The profile of end milling surface in a cutter revolution at Z=0 mm

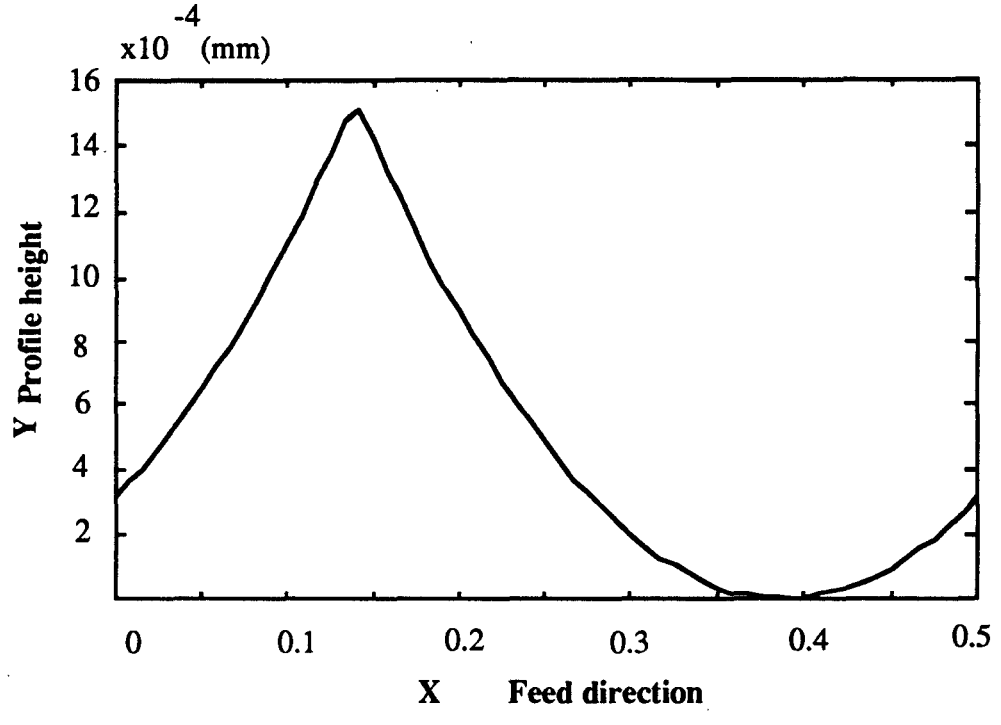

Fig.3.15 The profile of end milling surface in a cutter revolution at Z=20 mm

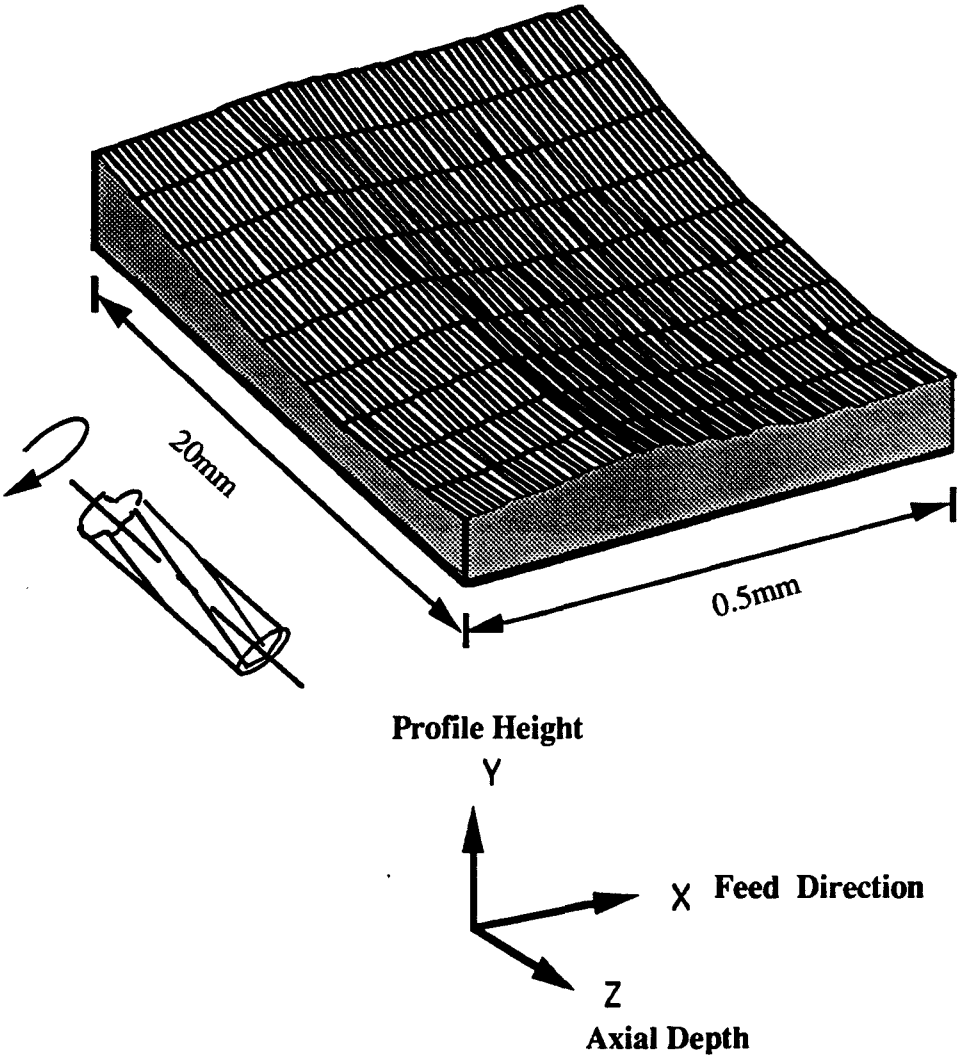

Fig.3.16 The 3-D geometry of end milling surface for a deflection case

where

Ra = 0.38 μm

PTV = 73.6 μm

3.6 Surface Topography with Runout, Static Deflection, and Tool Vibration

As a first step towards the development of a dynamic model for the end milling process, consider first the case where any dynamic effect due to the machine tool structure may be neglected. The dynamics of the machine tool structure may be neglected when the structure is acted on axially, as would be the case at conventional spindle speeds, i.e., when the flute passing frequency component of the cutting force is less then,

as an approximation, one-tenth of the system's lowest natural frequency. For a case such as this, the end milling process may be represented by essentially three component:

1. A model for the chip thickness, or chip load, that reflects dependence on cut geometry and static system deflection.
2. A relationship for cutting force as a function of chip load, and
3. A static model for the machine tool structure that, for a given force system, predicts the displacement of the end mill relative to the workpiece.

Under static loading conditions, i.e. at conventional spindle speeds, any cutting force applied to the end mill must produce deflection and in turn generate a chip load which agrees with the initial force/chip load. Thus, in a sense, the forces and system deflections are balanced. At conventional cutting speeds, a change in the cutting force causes the end mill to change its position, and it does so very quickly relative to the speed at which the spindle is rotating. Thus, since the time response of the machine tool structure is much faster than the rate at which the cutting forces are changing, shortly after the end mill has been directed to move, it reaches its steady-state position. In the time it takes for the end mill to reach its steady steady-state position, the end mill has rotated very little, i.e., the chip load remains constant,and the force being generated must match the new deflected cutter position. This balancing effect between the chip load, cutting forces, and deflection would not be present at higher spindle speeds since for those cases the force changes faster than the end mill responds.

3.6.1 Vibration Simulation Procedure

1. How to model the machining process

(1) Cutting force evaluation

Form static point of view, we have

$$\text{Force} = k_c \times u(t)$$

where $k_c = k_a \times a$, called cutting stiffness,

k_a is the unit cutting force and a is the width of cut .

The input of the machining system is the chip load. In general, the input is the nominal chip-uncut thickness, denoted by u(t) and $u(t)=u_0-y(t)$.

The output of the machining system is the tool motion, or the relative motion between the tool and workpiece. In general, the output is the tool motion in the direction normal to the machined surface, with respect to the workpiece, denoted by y(t). u_0 is the depth of cut. The equation can be rewritten as:

$$\text{Force} = k_c \times [u_0 - y(t)]$$

(2) Tool vibration evaluation

Let us make two assumptions here.

a. The rigidity of the workpiece is high. Its motion during machining is negligible.

b. We are only concerned about the tool motion in the direction normal to the machined surface.

Therefore, we use a one degree of freedom system to model the structural dynamics of the machine tool.

We consider a milling machining system as a second order system. Then we have

$$m\ddot{y} + c\dot{y} + ky = \text{Force}$$

where

m tool mass

c damping factor

k stiffness

combining all these considerations, we come up with

$$m\ddot{y} + c\dot{y} + ky = k_c \times [u_0 - y(t)]$$

2. Modeling of structural dynamics of machine tool

Consider a milling machine system as a two degree of freedom system as shown below.

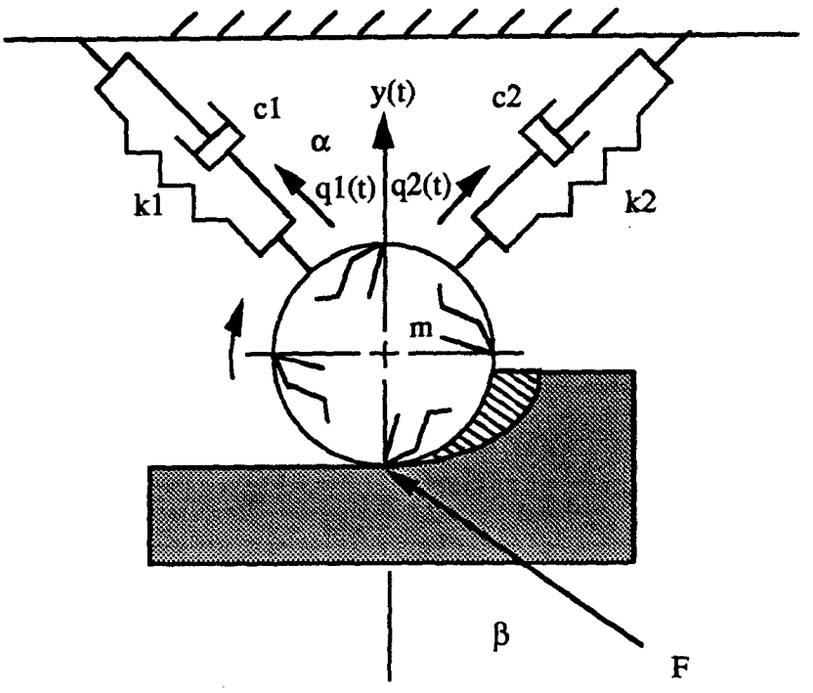

Fig. 3.17 Two degree of freedom system

The two principle modes are denoted as q1(t) and q2(t). The cutting forces should be decomposed into two components along the two principle modes.

$$m\ddot{q}_1(t) + c_1\dot{q}_1(t) + k_1q_1(t) = \left\{(k_cu_0 + A\cos wt + B\sin wt) - k_cy(t)\right\}\cos(\alpha - \beta) \quad (3.4)$$

$$m\ddot{q}_2(t) + c_2\dot{q}_2(t) + k_2q_2(t) = \left\{(k_cu_0 + A\cos wt + B\sin wt) - k_cy(t)\right\}\sin(\alpha - \beta) \quad (3.5)$$

$$y(t) = q_1(t)\cos\alpha + q_2(t)\sin\alpha \quad (3.6)$$

where

$\alpha=40^0$

$\beta=60^0$

From static point of view,we only interested in particular solution.

We rewrite Eq. (3.4), (3.5), (3.6),

$$m\ddot{q}_1(t)+c_1\dot{q}_1(t)+\left[k_1+k_c\cos(\alpha-\beta)\cos\alpha\right]q_1(t)+k_c\cos(\alpha-\beta)\sin\alpha q_2(t)=$$
$$k_c u_0+A\cos wt+B\sin wt \tag{3.7}$$

$$m\ddot{q}_2(t)+c_2\dot{q}_2(t)+\left[k_2+k_c\cos(\alpha-\beta)\cos\alpha\right]q_2(t)+k_c\cos(\alpha-\beta)\sin\alpha q_1(t)=$$
$$k_c u_0+A\cos wt+B\sin wt \tag{3.8}$$

from Eq. (3.7), (3.8)

$$m\ddot{q}_1(t)+c_1\dot{q}_1(t)+k_1'q_1(t)+Rq_2=k_c u_0+A\cos wt+B\sin wt \tag{3.9}$$

$$m\ddot{q}_2(t)+c_2\dot{q}_2(t)+k_2'q_2(t)+Rq_1=k_c u_0+A\cos wt+B\sin wt \tag{3.10}$$

where

$$k_1'=k_1+k_c\cos(\alpha-\beta)$$

$$k_2'=k_2+k_c\sin(\alpha-\beta)$$

$$R_1=k_c\cos(\alpha-\beta)$$

$$R_2=k_c\sin(\alpha-\beta)$$

Let

$$q_1=a_1\cos wt+b_1\sin wt+d_1 \tag{3.11}$$

$$q_2=a_2\cos wt+b_2\sin wt+d_2 \tag{3.12}$$

and integrating we have,

$$q_1'=-a_1w\sin wt+b_1w\cos wt \qquad q_1''=-a_1w^2\cos wt-b_1w^2\sin wt$$

$$q_2'=-a_2w\sin wt+b_2w\cos wt \qquad q_2''=-a_2w^2\cos wt-b_2w^2\sin wt$$

Solving Eq. (3.9), (3.10), we get

$$R_1d_2+k_1'd_1=k_cu_0 \tag{3.13}$$

$$R_2d_1+k_2'd_2=k_cu_0 \tag{3.14}$$

From the Eq. (3.13),(3.14), solve d_1,d_2, we get

$$d_1=\frac{R_1-k_2'}{R_1R_2-k_1'k_2'}k_cu_0 \tag{3.15}$$

$$d_2=\frac{R_2-k_1'}{R_1R_2-k_1'k_2'}k_cu_0 \tag{3.16}$$

also solving Eq.(3.13), (3.14), get

$$R_1a_2+(k_1'-mw^2)a_1+c_1wb_1=A$$

$$R_2b_2+(k_1'-mw^2)b_2-c_1wa_1=B$$

$$R_2a_1+(k_2'-mw^2)a_2+c_2wb_2=C$$

$$R_2b_1+(k_2'-mw^2)b_1-c_2wa_2=D$$

Let

$$\begin{bmatrix} A \\ B \\ C \\ D \end{bmatrix} = \begin{bmatrix} k_1'-mw^2 & c_1w & R_1 & 0 \\ c_1w & k_1'-mw^2 & 0 & R_1 \\ R_2 & 0 & k_2'-mw^2 & c_2w \\ 0 & R_2 & -c_2w & k_2'-mw^2 \end{bmatrix} \begin{bmatrix} a_1 \\ b_1 \\ a_2 \\ b_2 \end{bmatrix}$$

then,

$$\begin{bmatrix} a_1 \\ b_1 \\ a_2 \\ b_2 \end{bmatrix} = \begin{bmatrix} k_1'-mw^2 & c_1w & R_1 & 0 \\ c_1w & k_1'-mw^2 & 0 & R_1 \\ R_2 & 0 & k_2'-mw^2 & c_2w \\ 0 & R_2 & -c_2w & k_2'-mw^2 \end{bmatrix}^{-1} \begin{bmatrix} A \\ B \\ C \\ D \end{bmatrix}$$

From the above calculations we can get the system response y(t)

3. Simulation procedure

We divide axial depth of cut or width of cut (in Z direction) to 10 sections (Z from 1 to 10), as shown in Fig. 3.18.

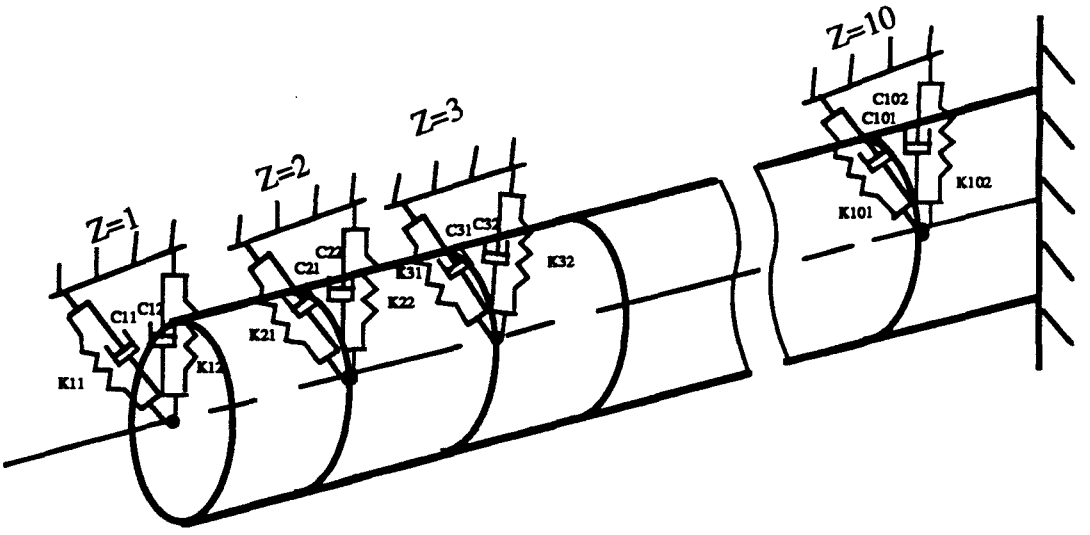

Fig. 3.18 Cutting tool divided by 10 sections from Z=1 to Z=10

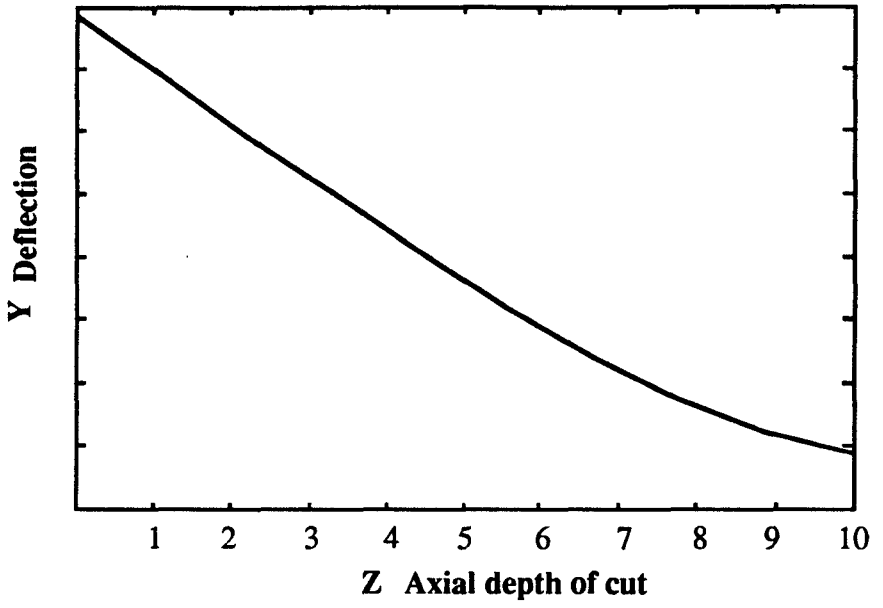

Fig. 3.19 Static deflection along the axial depth of cut Z by calculation

From the equations (3.11) and (3.12)

$$q_1=a_1\cos wt+b_1\sin wt+d_1$$

$$q_2=a_2\cos wt+b_2\sin wt+d_2$$

we know d_1 and d_2 determine the deflection, and from the equations (3.15) and (3.16) , d_1 and d_2 are determined by k_1, k_2,u_0, and k_c. k_c and u_0 which are given during the simulation. From the section 3.5 we can get the static deflection by the equation (3.3)

$Y=1/EI\{k_a(Z-a)^4/24 + ak_aZ^3/6 - k_aa^2Z^2/4 + (k_aa^2l-k_aal^2)Z/2 + (ak_al^3/3 - a^2k_al^2/4)\}$(see Fig. 3.19). Therefore, we can get the k value (from k_1, k_2, to k_{101}, k_{102}) for each section of Z direction from Z=1 to Z=10 (as shown in Fig.3.20) just by adjusting them to match the static deflection equation When k values are determined, we can get the c values from the damping ratio ζ, k, m ,and natural frequency ω using the equation $c_{eq} = 2m \times \omega \times \zeta$

where

ζ is the damping ratio, the value of damping ratio always be from 0.02 to 0.05. In this thesis we take 0.035

$\omega = \sqrt{\frac{k_{eq}}{m}}$, $k_{eq}y(t) = k_1y(t)\cos^2\alpha + k_2y(t)\sin^2\alpha$, according to the Fig.3.16, we get

$k_{eq} = k_1\cos^2\alpha + k_2\sin^2\alpha$, and $\alpha = 40^0$

Therefore, we finally can get $k_{eq} = 0.5868k_1 + 0.4232k_2$, (3.17)

according to equation (3.17), we can get the ω value, and also get c_{eq} from

$c_{eq} = 2m \times \omega \times \zeta$, and $c_{eq} = 0.5868c_1 + 0.4232c_2$ (3.18)

by equation (3.18),we can adjust and get c_1 and c_2 values according to the c_{eq} value.

After k, c. values are determined, we can get the y(t) response or vibration profile from Z=1 to Z=10 as shown in Fig.3.21.

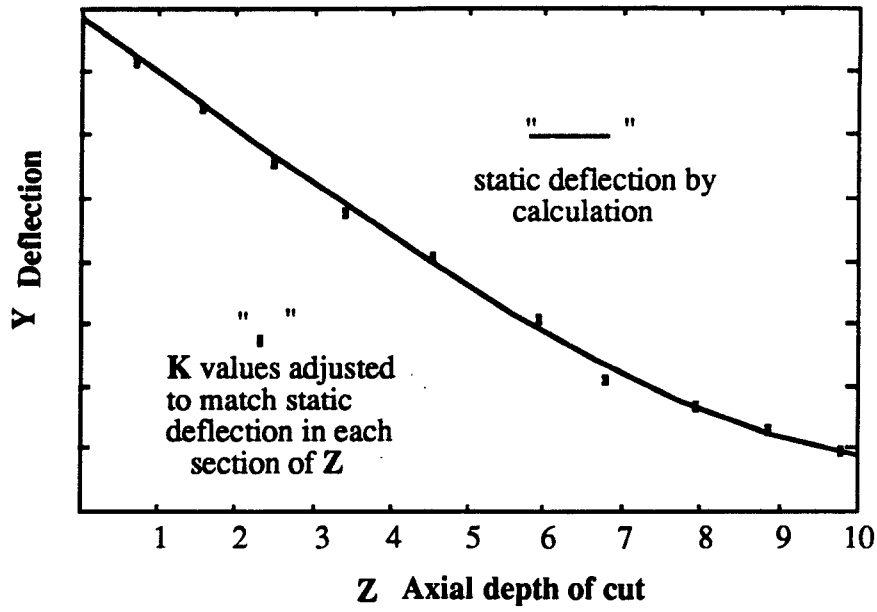

Fig. 3.20 Static deflection along the axial depth of cut Z

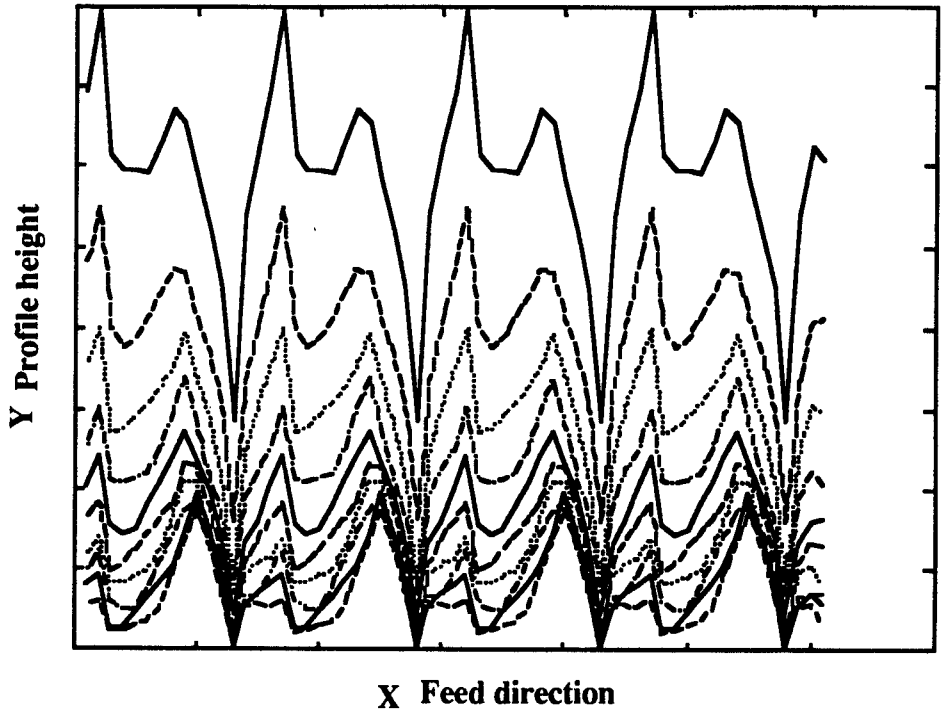

Fig. 3.21 The profiles of milling surface from Z=1 to Z=10 in one cutter revolution

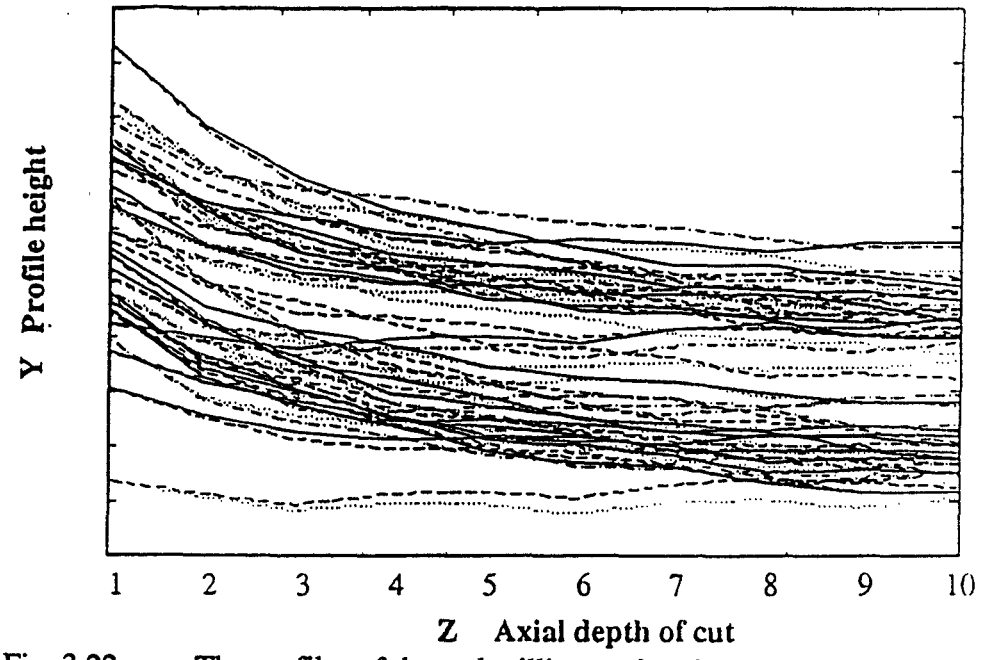

Fig. 3.22 The profiles of the end milling surface in a cutter revolution along axial depth of cut

Finally, we construct the 3-D geometry of end milling surface as follow:

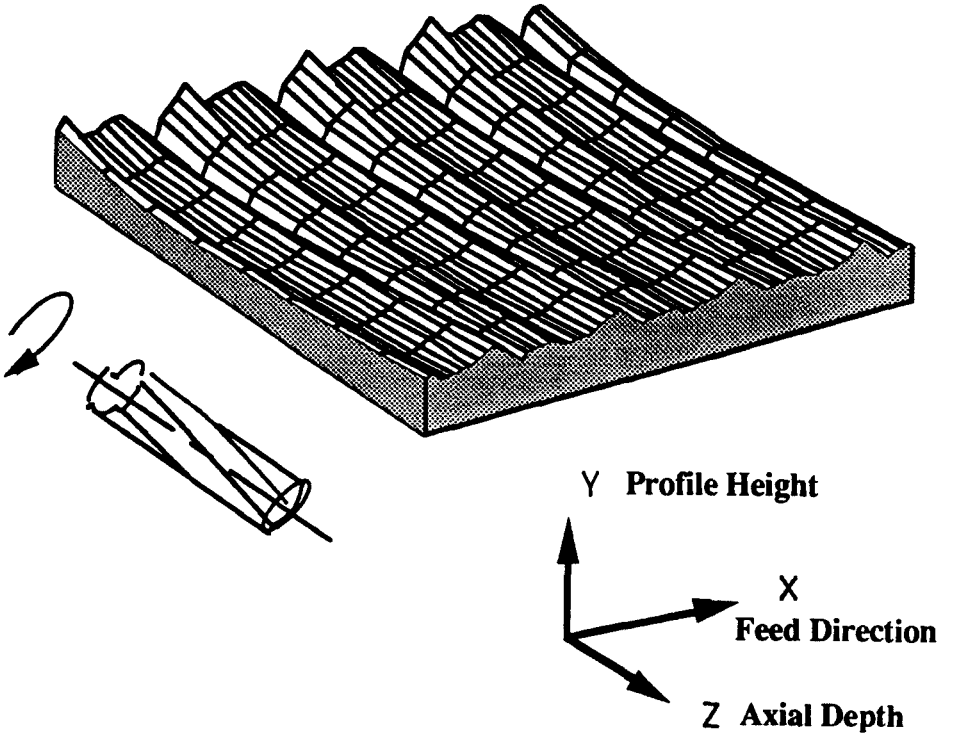

Fig.3.23 The 3-D geometry of end milled surface for vibration case in one cutter revolution

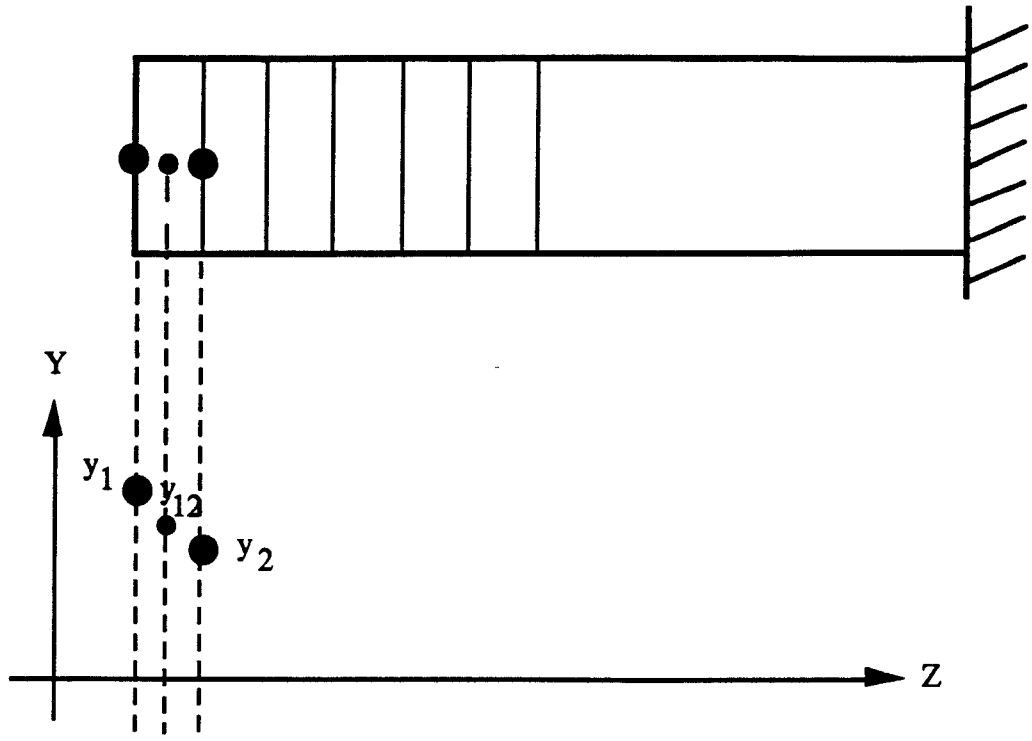

Fig 3.24 Finite element method

From the Finite Element Method (FEM) point of view, we can construct the 3-D surface from 10 profiles at each axial depth of cut (Z) in one cutter revolution to 20 profiles as shown in Fig.3.24 and Fig. 3.25. In Fig. 3.24, we assume y1 is the profile when Z=1, y2 is the profile when Z=2 and y12 is the profile between Z=1 and Z=2 section at the same feed direction. From Fig.3.24 as shown, we get the profile y12=(y1+y2)/2 using the FEM. Also, we can use this method to get the other profiles in each section of Z.

Fig.3.25 shown we use FEM to construct the 3-d geometry of end milling surface in one cutter revolution just according to the case of Fig. 3.23.

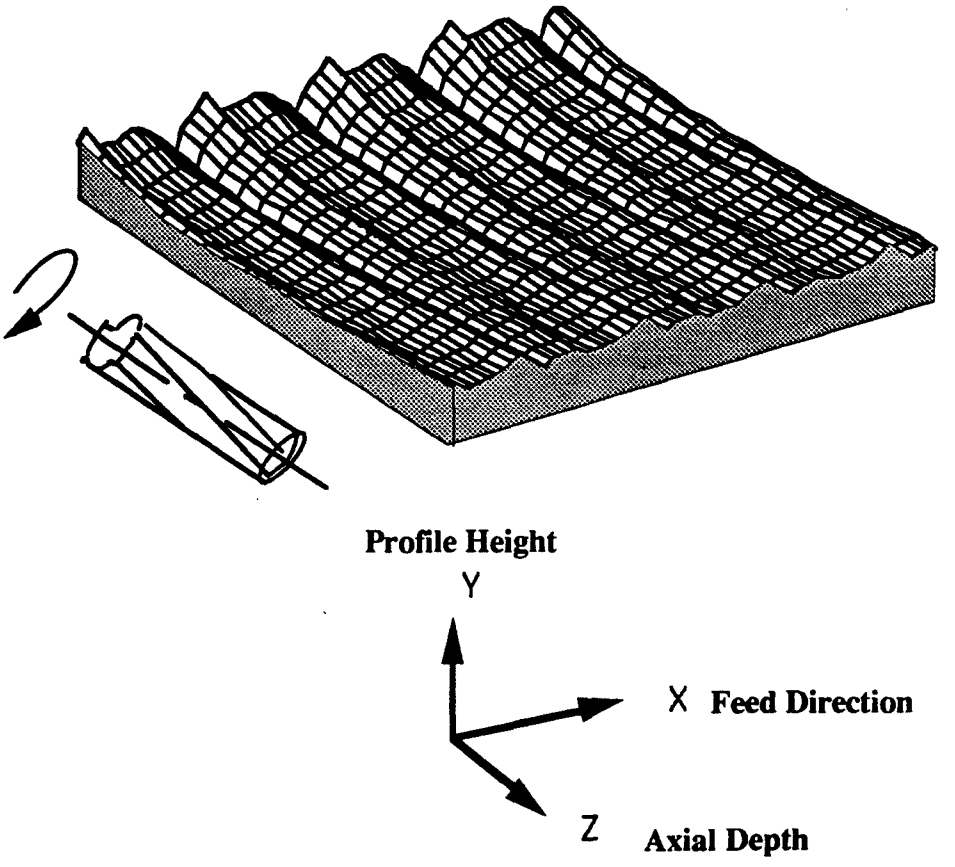

Fig.3.25 The 3-D geometry of end milled surface by using the FEM

3.6.2 Example of Vibration Simulation

The input data are:

Radius of Cutters	R	20 mm
Number of Flutes	Nt	4
Helix Angle	α_{hx}	10 degree
Feed Per Revolution	fr	0.5 mm/rev.
Axial Depth of Cut	Z	20 mm
Runout	ρ	0.05 mm
Locating Angle	λ	45 degree
EI		10e08Nt/mm^2
Tool Length	l	70 mm

Width of Workpiece	a	20 mm
Loading Force Per Unit Length	ka	$50Nt/mm^2$
Depth of Cut	u_0	0.2 mm
Tool Mass	m	5 kg

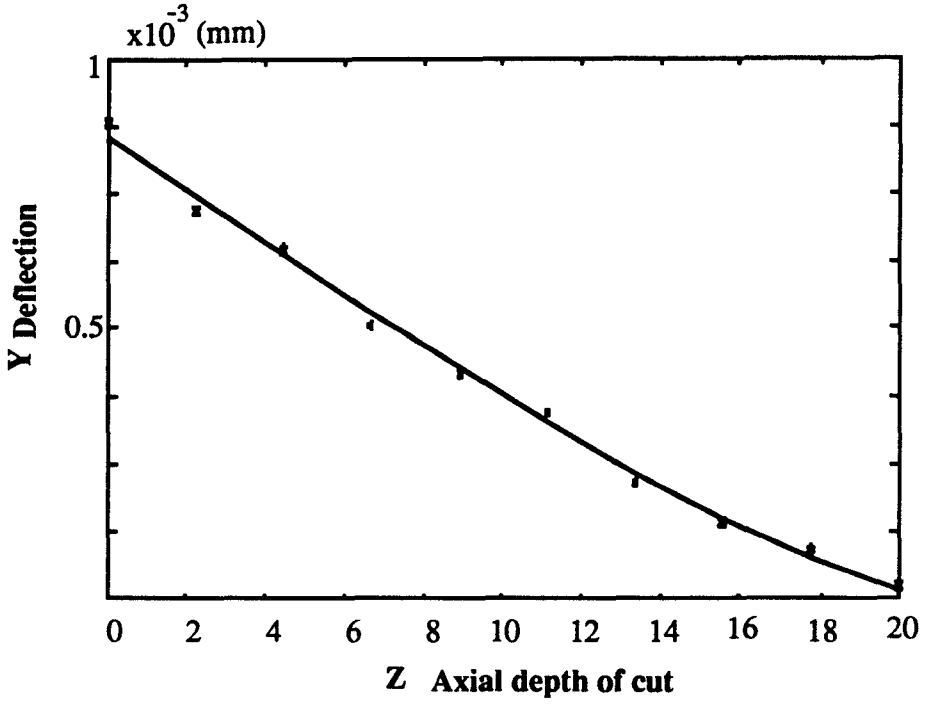

Fig. 3.26 Static deflection along the axial depth of cut Z

We adjust k values in each section of Z (from Z=1 to Z=10) according to the static deflection from the calculation (see Fig. 3.26) , and get:

k_{11}=1.3000e8(N/m), k_{21}=1.3100e8(N/m), k_{31}=1.3120e8(N/m), k_{41}=1.3150e8(N/m), k_{51}=1.3200e8(N/m), k_{61}=1.3220e8(N/m), k_{71}=1.3230e8(N/m), k_{81}=1.3240e8(N/m), k_{91}=1.3260e8(N/m), k_{101}=1.3280e8(N/m),

k_{12}=6,1000e7(N/m), k_{22}=6.1100e7(N/m), k_{32}=6.1200e7(N/m), k_{42}=6.1300e7(N/m), k_{52}=6.1400e7(N/m), k_{62}=6.1500e7(N/m), k_{72}=6.1800e7(N/m), k_{82}=6.1900e7(N/m), k_{92}=6.2100e7(N/m), k_{102}=6.2200e7(N/m),

According to the m, ζ, and k values, we can get the c values in each section of Z and vibration profiles are established (see Fig. 3.27). The c values in each section of Z are:

c_{11}=950(N-sec/m), c_{21}=970(N-sec/m), c_{31}=990(N-sec/m), c_{41}=1015(N-sec/m), c_{51}=1030(N-sec/m), c_{61}=1190(N-sec/m), c_{71}=1115(N-sec/m), c_{81}=1140(N-sec/m), c_{91}=1190(N-sec/m), c_{101}=1210(N-sec/m),

c_{12}=2467(N-sec/m), c_{22}=2450(N-sec/m), c_{32}=2423(N-sec/m), c_{42}=2389(N-sec/m), c_{52}=2379(N-sec/m), c_{62}=2294(N-sec/m), c_{72}=2250(N-sec/m), c_{82}=2215(N-sec/m), c_{92}=2135(N-sec/m), c_{102}=2107(N-sec/m),

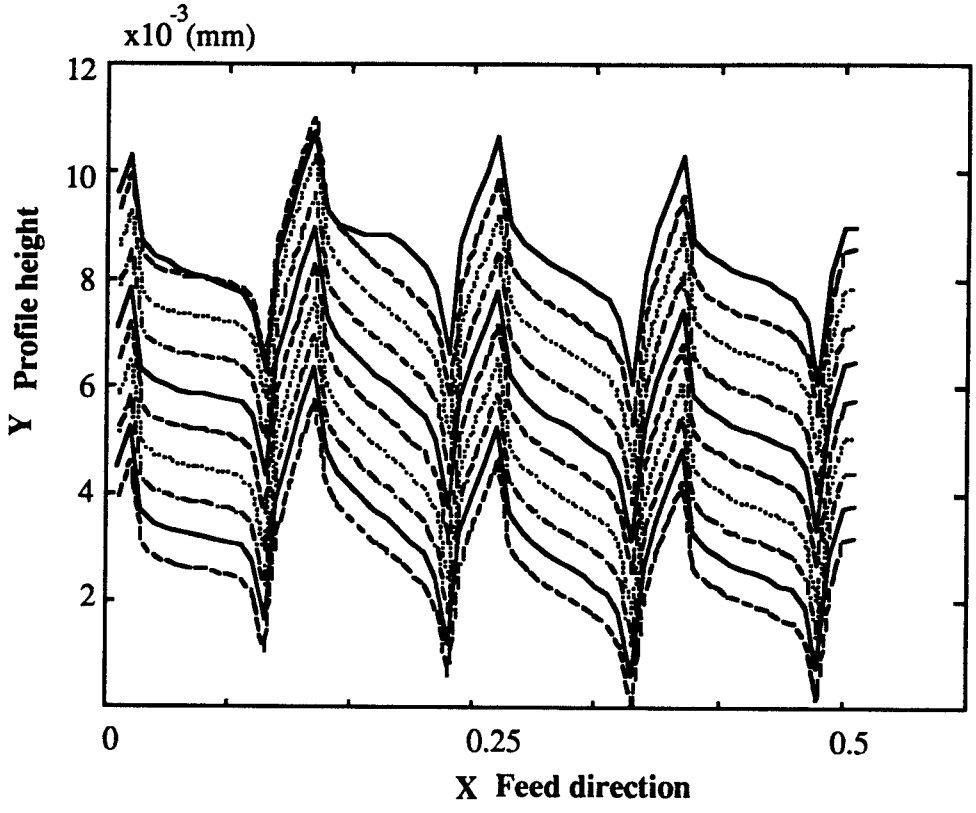

Fig. 3.27 The profiles of milling surface from Z=1 to Z=10 in one cutter revolution

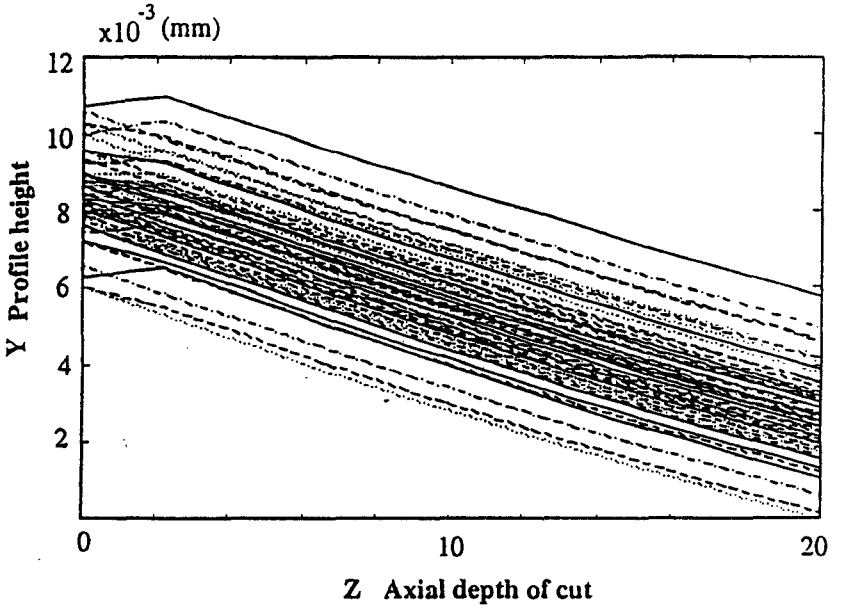

Fig. 3.28 The profiles of the end milling surface in a cutter revolution along axial depth of cut

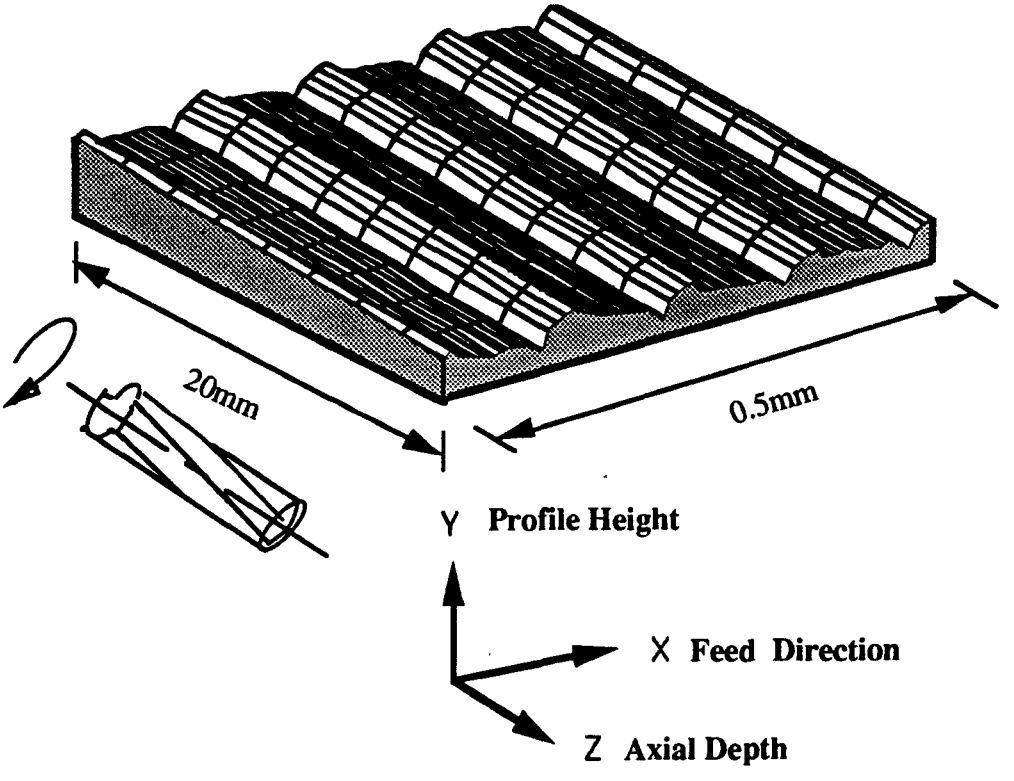

Fig.3.29 The 3-D geometry of end milling surface for a vibration case

CHAPTER 4 EXPERIMENTAL VERIFICATION

In this chapter, the development of a sensor measurement system and method of the end milling experiments are presented. To verify the simulation model on end milling surface, we performed experiments on many cases by considering several steps as discussed previously in chapter 3 involving ideal, runout, tool deflection, and vibration factors. To measure surface finish quality, particularly roughness, there are variety of techniques available, most of which must be performed off-line. In this experiment, we measure the surface roughness using TALYSURF 6 surface profiles matter at the National Institute of Standards & Technology (NIST). The method is explored with the goal of developing an on -line technique for maximum efficiency and quality. The stylus, a commonly used surface profile measurement instrument is used for these purposes. Various surface roughness conditions, generated by varying feedrate and cutting speed during the milling process of the aluminum metals, is used to illustrate the ranges of facility of each surface measurement method.

4.1 Surface Machining Process

Milling machines share with lathes the distinction of being the most useful and versatile machines in the shop. The lathe mainly deals with the production of cylindrical surfaces, whereas the milling machine can produce both cylindrical and flat surfaces; although both are capable of performing other operations. In milling, the cutter rotates, usually at fairly high speed, and the work is fed past it at a uniform rate. The position of the spindle and cutter remains fixed, and the table, carrying the work, moves right and left, up and down, or in and out . Most milling machines have mechanically operated feeds,although hydraulic operation has been incorporated in some models. Milling cutters consist generally of a cylindrical body with teeth on the periphery. The teeth may be straight--parallel to the axis--or arranged in a helix. The machining process and the type of cutter selected play a significant role in the final quality of the machined surface.

In this experiment, the sample material is aluminum.The material is machined on a CNC milling machine,at selected "slow" and"fast" cutting speeds in conjunction with "slow" and "fast" feedrates to reduce vibration in the ideal case and generate vibration in vibration case, also adjust the spindle position to make reasonable artificial runout for the runout case.

4.2 Surface Characterization

The *surface roughness* with its typical roughness height and roughness spacing represents the more closely spaced peaks and valleys. Roughness is usually produced by the basic surface forming process. The waviness consists of the more widely spaced irregularities and is often produced by vibration in the machine.*Lay* is the term used to indicate the direction of the dominant pattern of texture on the surface, as shown in figure 4.1. Surface produced by machining processes ordinarily have a strong lay pattern, that is they are unidirectional.

The term *surface finish* generally refers to the overall description of the surface including the texture, the flaws, the materials, and any coatings applied. The term *texture* and *roughness* are generally preferred to the term *finish* and are used almost exclusively in discussions of surface quality.

The stylus surface roughness measurement device provides extensive characterization of the traced surface, serving as a reference for other surface roughness methods applied to the material under study. The characterization can be described by a variety of indices which are generally applicable to the other techniques as well. Descriptions and derivations of these indices are presented below.

LT Length of trace The length of trace is the total horizontal distance traversed by the stylus, as shown in Figure 4.2

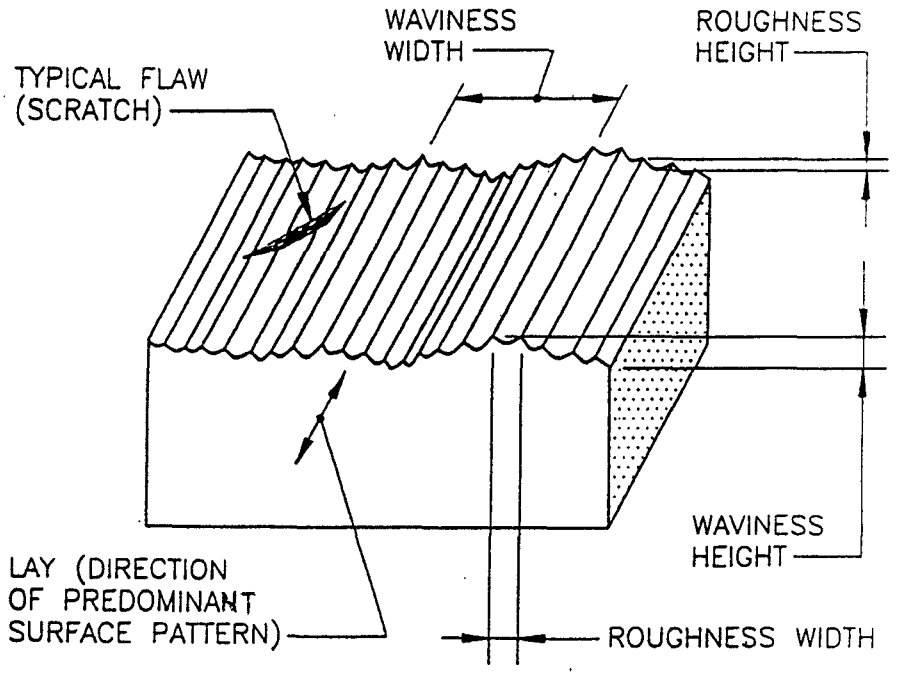

Fig 4.1 Surface roughness terms

Sampling Length The sampling length is a fraction of total length of trace.

Ra Average Roughness or Center-Line Average. The most commonly used index of surface roughness,Ra, as shown in Figure 4.3 is defined for a given length as

$$Ra = \frac{1}{L}\int^{L} Z\,dx$$

PTV or Rt Peak-to-Valley Height, or separation of the highest peak and the lowest valley encountered within a given sampling length, as shown in Figure 4.4

In this thesis we only provide the Ra, PTV characterization of the traced surface from the experiment, the other characterizations are illustrated in the Appendix.

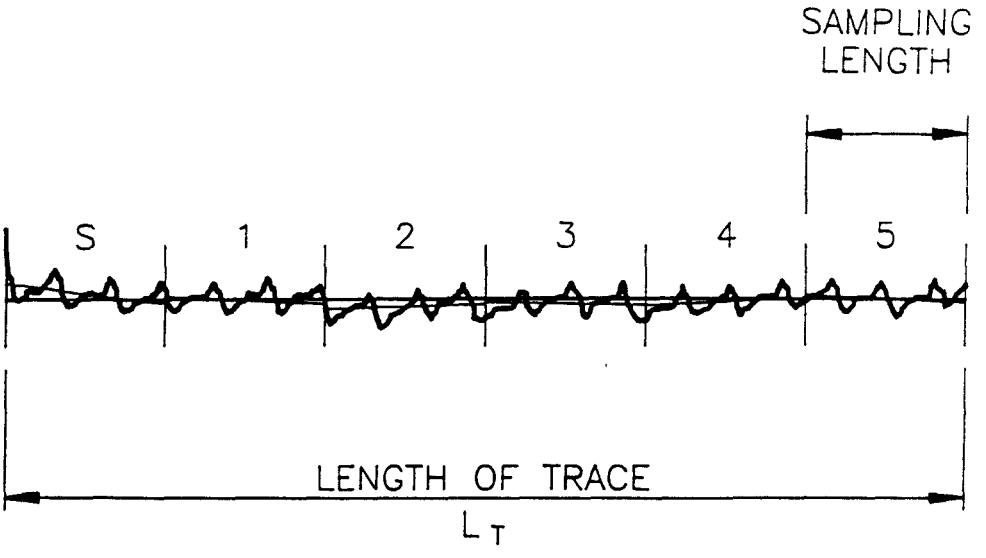

Fig 4.2 Surface profile divided into sampling lengths

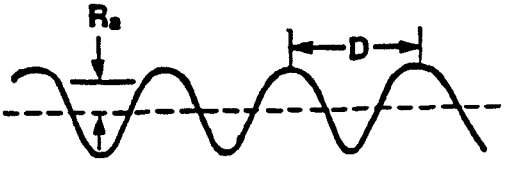

Fig.4.3 Ra parameters

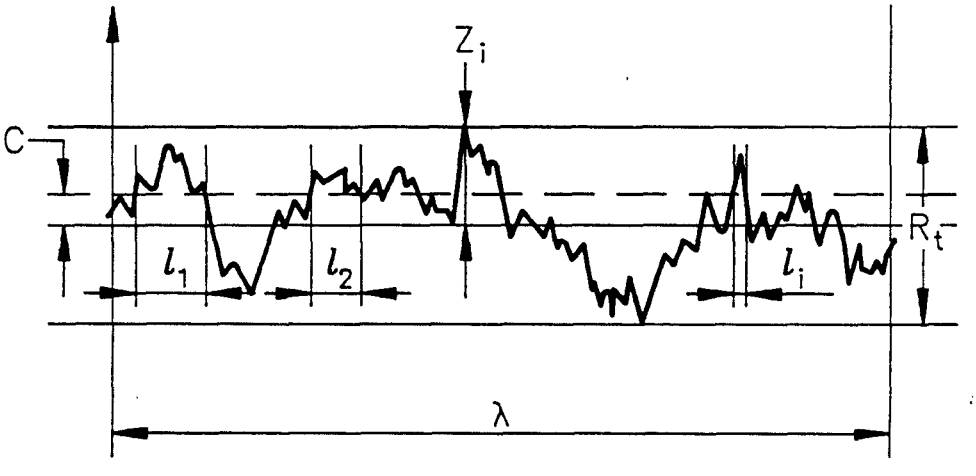

Fig 4.4 Peak and valley parameters

4.3 Surface Measurement

Surface roughness measurement is one of the essential quality control processes that are carried out during inspection to ensure that manufactured parts conform to specified standards. This kind of inspection is most often done through the use of mechanical stylus-type devices, such as the Talysurf 6 System (as shown in Figure 4.5) used in this investigation.

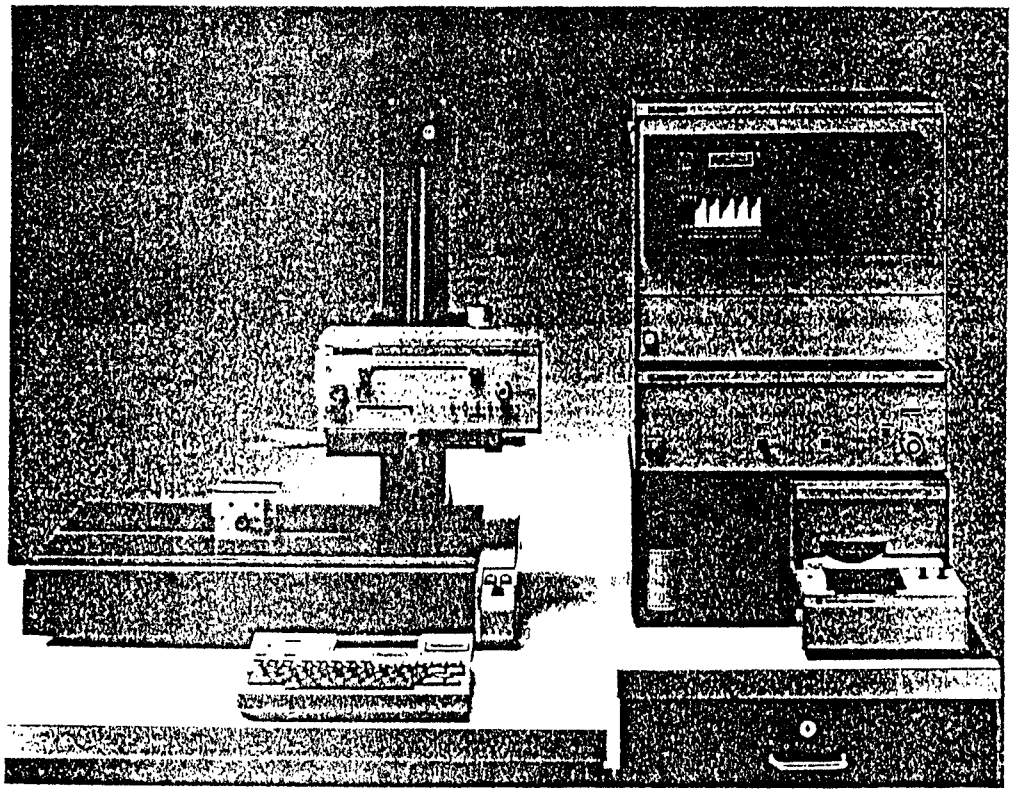

Fig.4.5 A typical Talysurf 6 system

A schematic diagram of a typical stylus instrument is shown in Figure 4.6. Talysurf 6 is a surface texture measuring system of modular design.The processor module

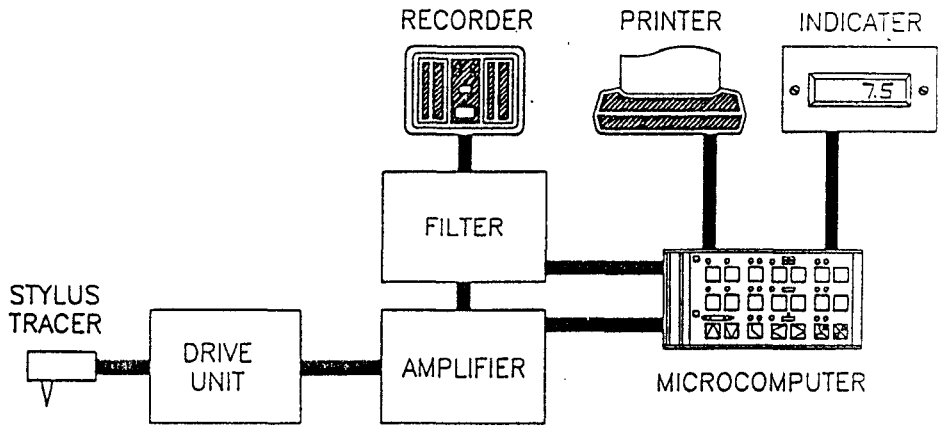

Fig.4.6 Stylus instrumentation

is programmed to provide a selection of roughness, waviness and unfiltered parameters with statistical analysis if required. Data can be output as profile graphs, visual displays of profile form and numerical data, or if necessary a video printer or dot matrix printer can be included and then hard copies can be made of the data visually displayed. The Talysurf 6 is comprised of the following basic parts: a floating tracer point or stylus, of diamond or other durable material, a drive unit, a signal transducer connected to the stylus, an electronic amplifier, a flitter for the amplified signal, a data recorder, and an out device such as a printer.

The stylus moves up and down in a vertical plane, and it is drawn by the tracer along a measuring path. The tip follows the face of the surface. To separate the roughness from the waviness in the surface profile, the stylus mechanism can be combined with a skid. The skid proceeds across the sample surface simultaneously with the stylus, and provides a reference elevation for the peaks and valleys traveled. In this manner lower frequency waviness is filtered, and the output indicates only the higher frequencies.

4.4 Experimental Procedure

Prior to milling, the first step was to ensure that everything, i.e. the milling machine and the specimens, was clean. The milling machine was found to be in relatively good running order,and the table movement, in each direction was checked out.

The type of cutter selected was a standard end mill cutter bit. Normally, the type of mill chosen is governed by the condition of the job. Smaller cutters cost less, but larger cutters are better to obtain the desired surface speed. Ideally, the cutter should be large enough to span the entire work surface such that the job can be done with single pass. However, the difficulty encountered in removing material from the steel specimen in this investigation warranted the use of a smaller cutter, requiring multiple passes.

Direction of rotation in conjunction with direction of feed was considered. In conventional milling, the direction of feed is opposite to the direction of rotation. The disadvantage of this traditional method is that there is always a certain amount of rubbing before the tooth takes hold, and the finished surface shows a series of small scallops. Faster cutting rates and a better finish can be obtained when the feed is in the same direction as the cutter rotation. The added advantage is that the pressure of the cut tends to hold the work down on the table. Due to the restricted movement of the milling machine available for this investigation, the cutting direction was opposite the feed

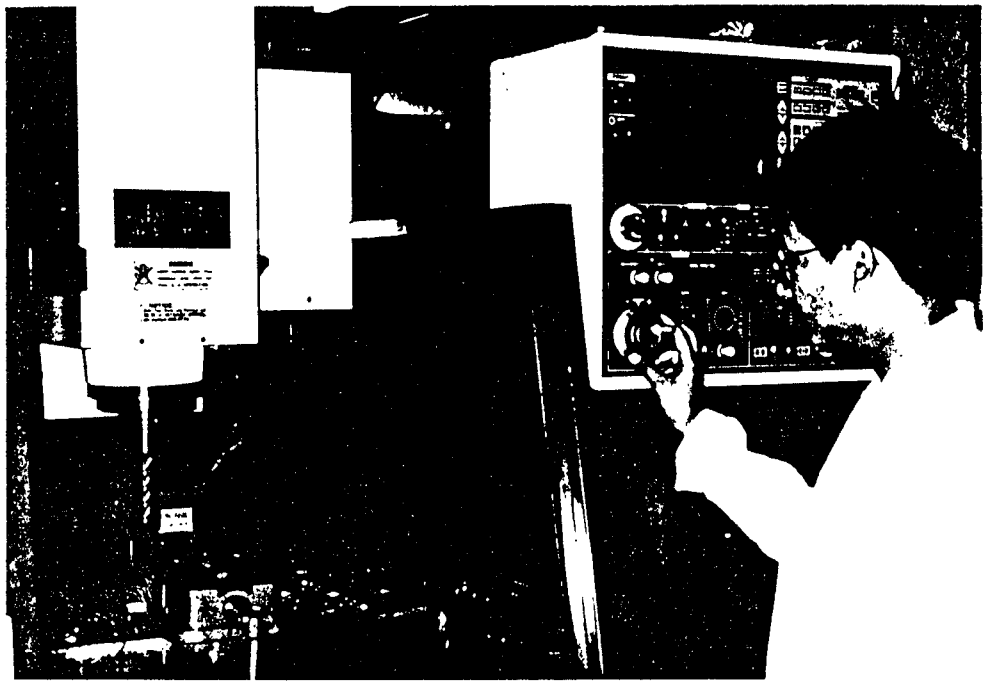

Fig.4.7 (a) Experimental setup

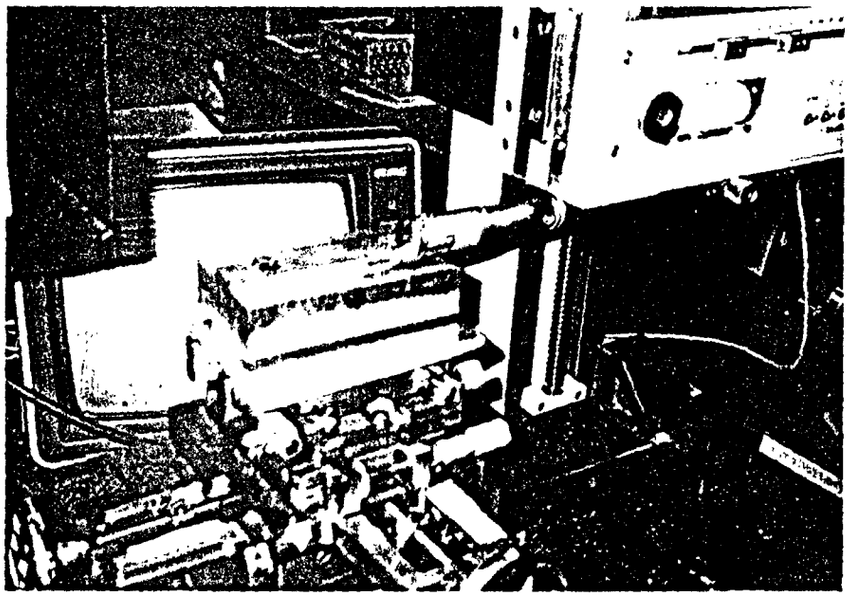

Fig.4.7 (b) Experimental setup

direction, which resulted in some scalloping on the material surfaces.

When mounting the cutter, the overarm was adjusted so the cutter was as close as possible to the work as possible. As all three materials were to be machined simultaneously under like conditions, the specimens were clamped securely together and mounted to the table as a single unit.

4.4.1 Experiment of Ideal Case

For ideal case the data we give in the simulation and experiment are:

Radius of Cutter	R	(0.375 in.) 9.525mm
Number of Flutes	Nt	4

Helix Angle	α_{hx}	30 degree
Feed Per Revolution	fr	3.3358 mm/rev.
Axial Depth of Cut	Z	(1 in.) 25.4mm
Runout	ρ	0 mm

We measure the profiles along the axial depth of cut (Z). There are ten profiles in each case, that is, we divide the axial depth of cut (Z) by ten. Z from Z=1(at the free end) to Z=10(at the fix end). The profiles on the X-Y plane along each Z direction as follows:

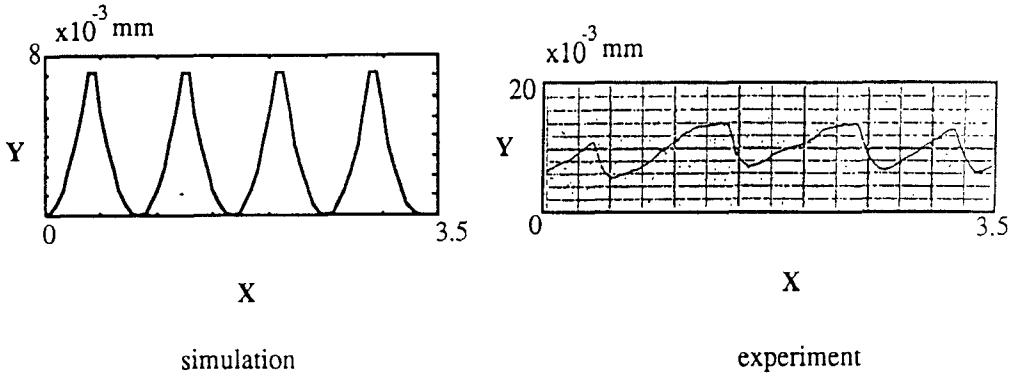

Fig.4.8 The profile of end milling surface in one cutter revolution at Z=1

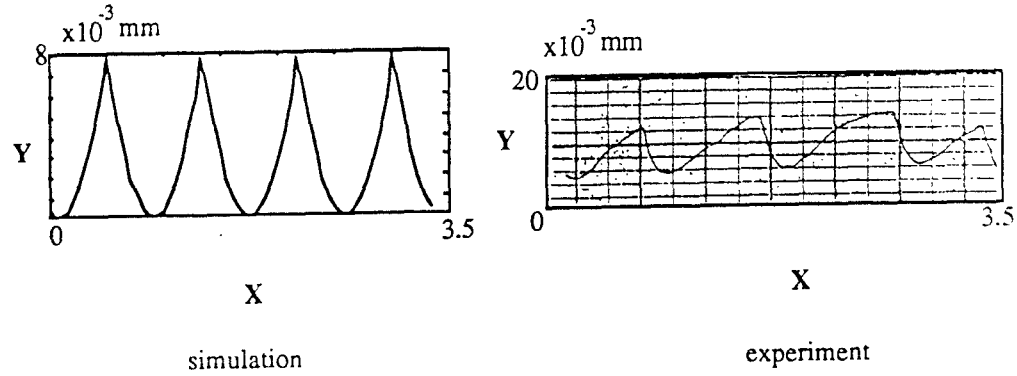

Fig.4.9 The profile of end milling surface in one cutter revolution at Z=2

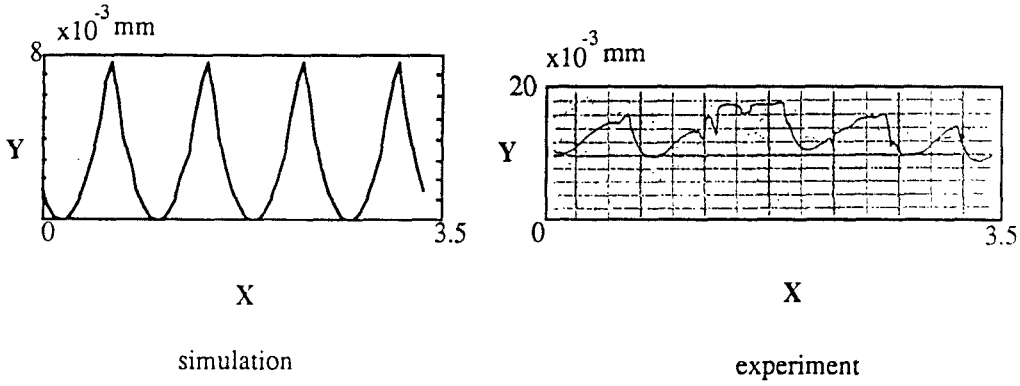

Fig.4.10 The profile of end milling surface in one cutter revolution at Z=3

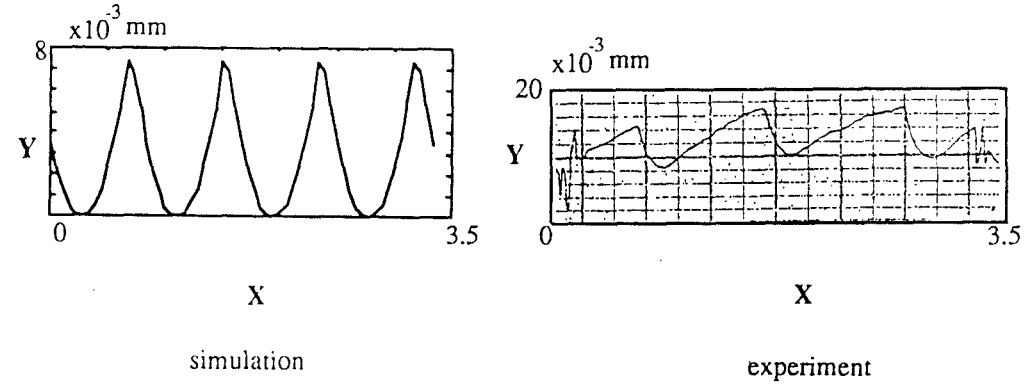

Fig.4.11 The profile of end milling surface in one cutter revolution at Z=4

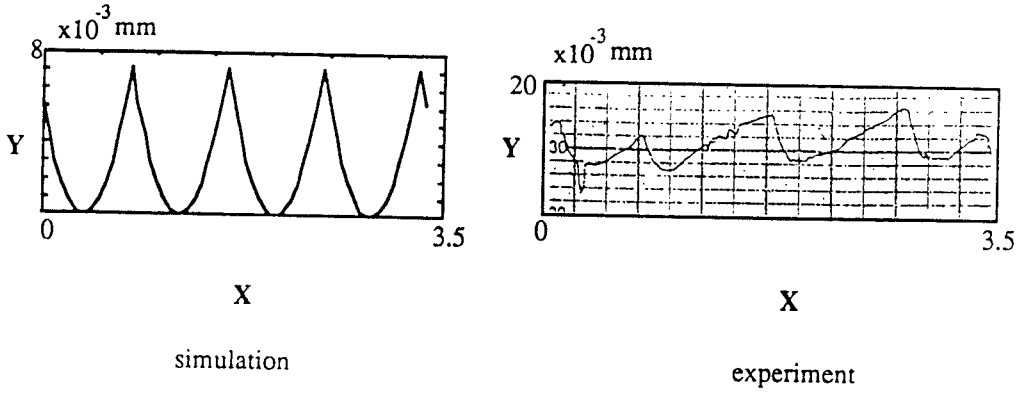

Fig.4.12 The profile of end milling surface in one cutter revolution at Z=5

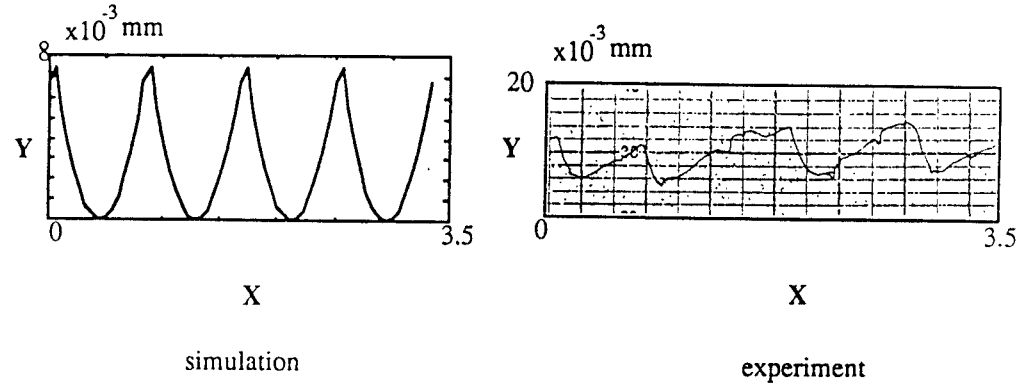

Fig.4.13 The profile of end milling surface in one cutter revolution at Z=6

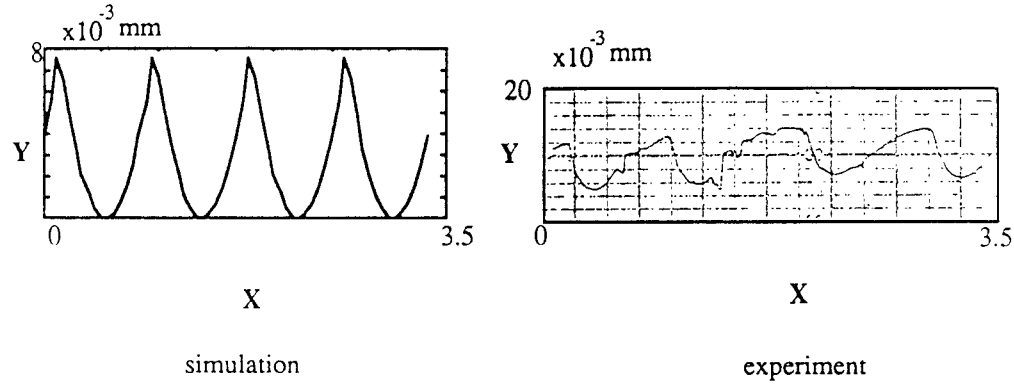

Fig.4.14 The profile of end milling surface in one cutter revolution at Z=7

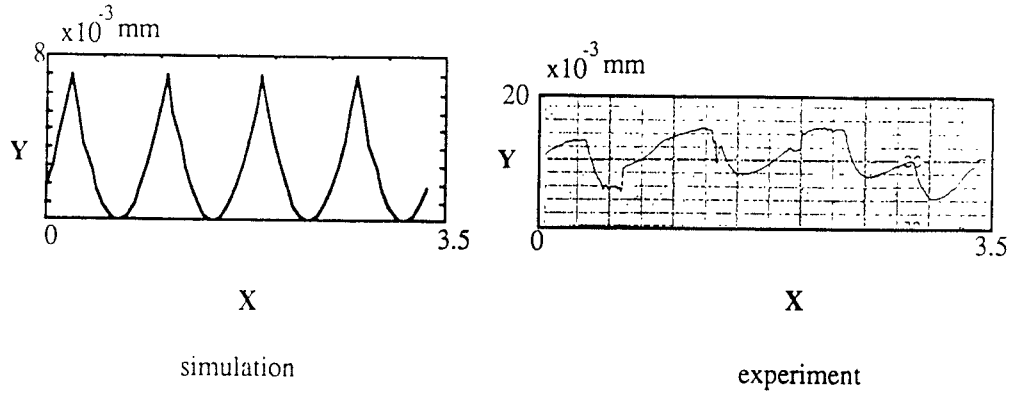

Fig.4.15 The profile of end milling surface in one cutter revolution at Z=8

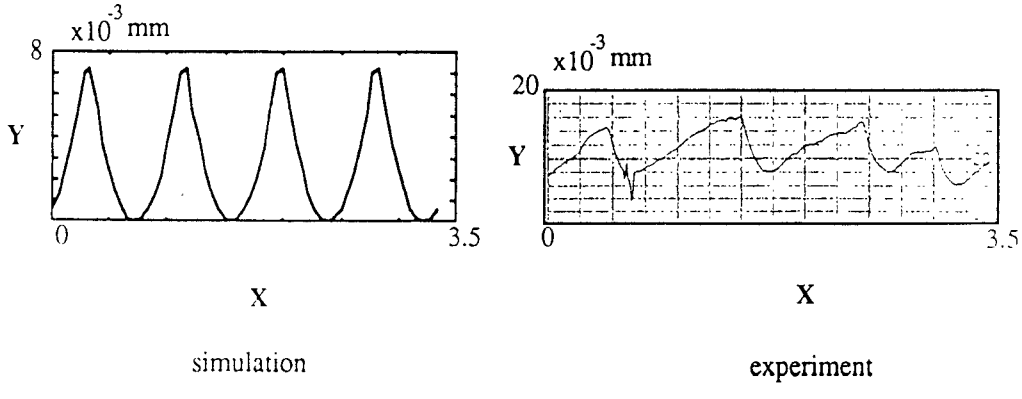

Fig.4.16 The profile of end milling surface in one cutter revolution at Z=9

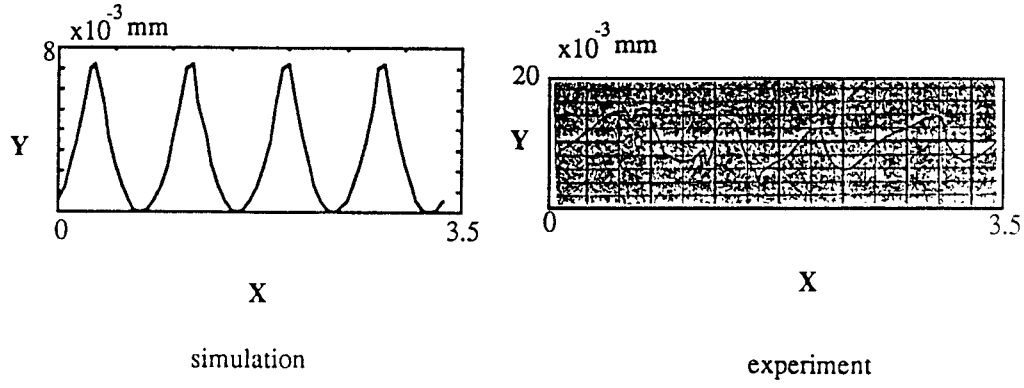

Fig.4.17 The profile of end milling surface in one cutter revolution at Z=10

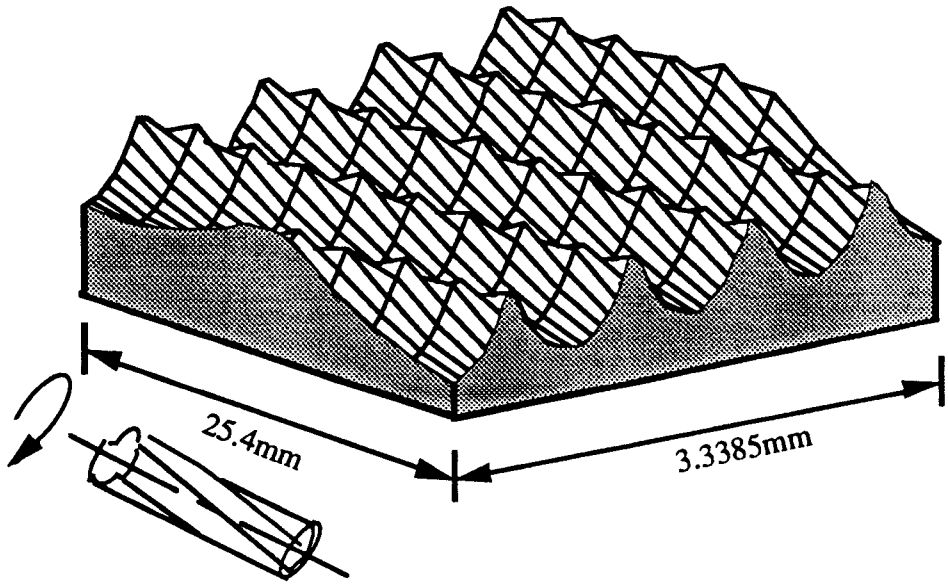

(a) in one cutter revolution

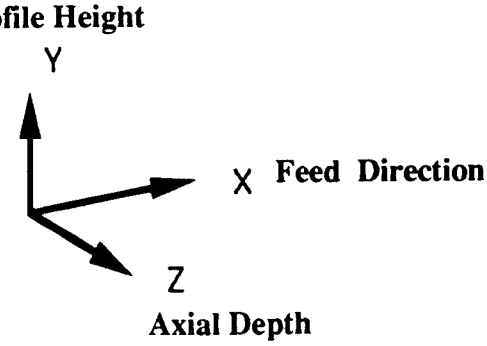

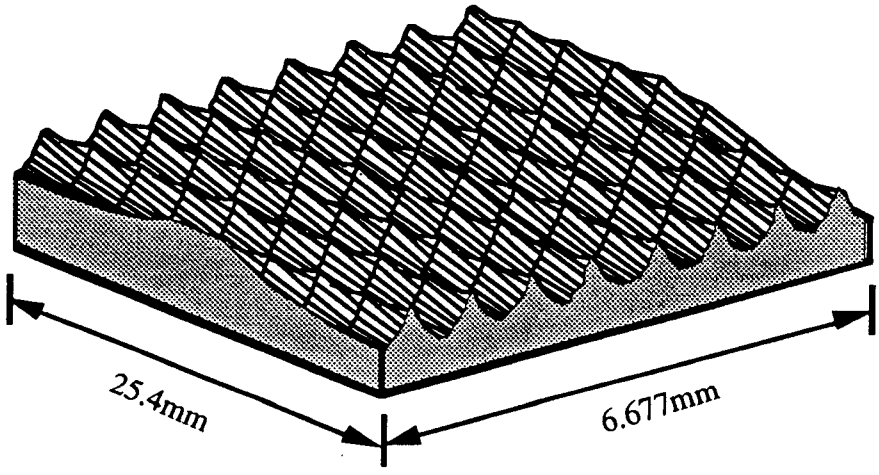

(b) in two cutter revolutions

Fig.4.18 The 3-D geometry of end milled surface from simulation in an ideal case

Ra and PTV value obtained by simulation	Ra and PTV value obtained from experiment
Ra	Ra
2.2 μm	2.3μm
PTV	PTV
7.2 μm	7.8μm

4.4.2 Experiment of Runout Case

For ideal case the data we give in the simulation and experiment are:

Radius of Cutter	R	(0.375 in.) 9.525mm
Number of Flutes	Nt	4
Helix Angle	α_{hx}	30 degree
Feed Per Revolution	fr	3.3358 mm/rev.
Axial Depth of Cut	Z	(1 in.) 25.4mm
Runout	ρ	0.1968mm

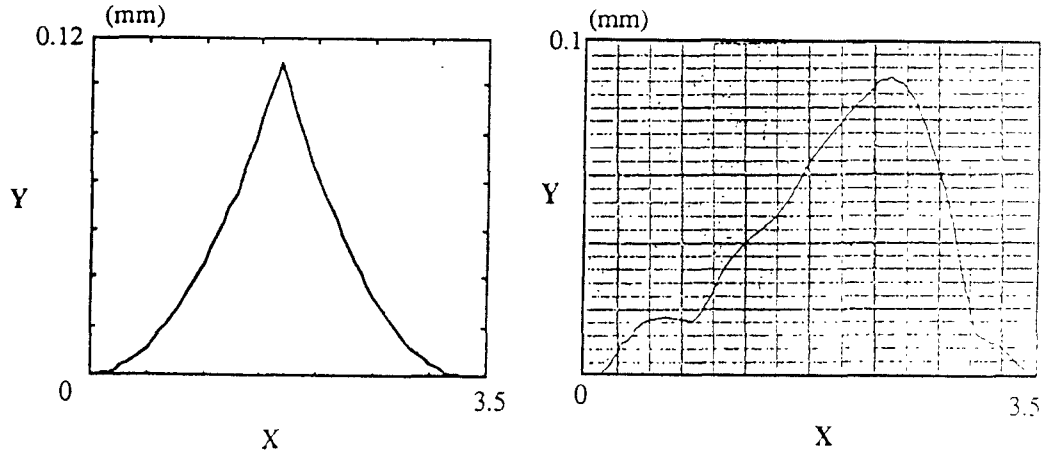

simulation experiment

Fig. 4.20 The profile of end milling surface in one cutter revolution at Z=1

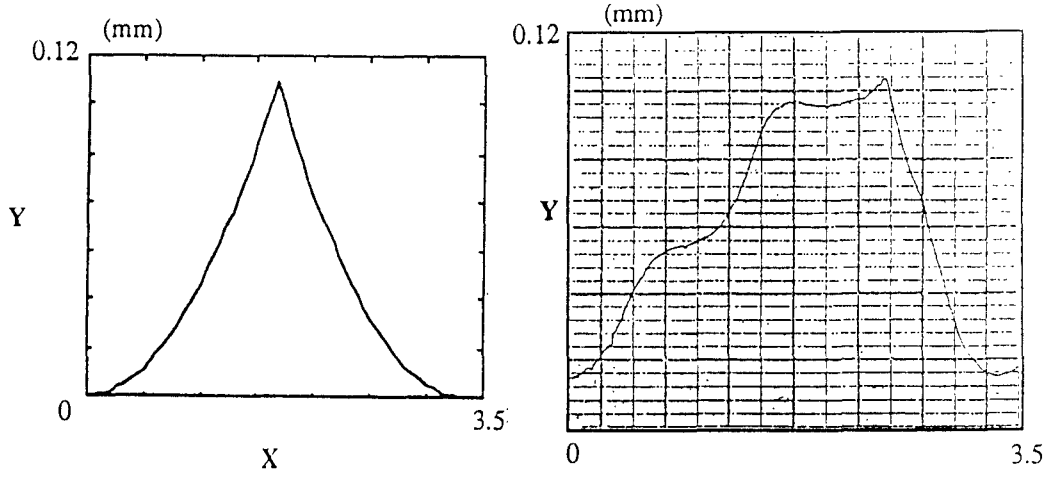

simulation experiment

Fig. 4.21 The profile of end milling surface in one cutter revolution at Z=2

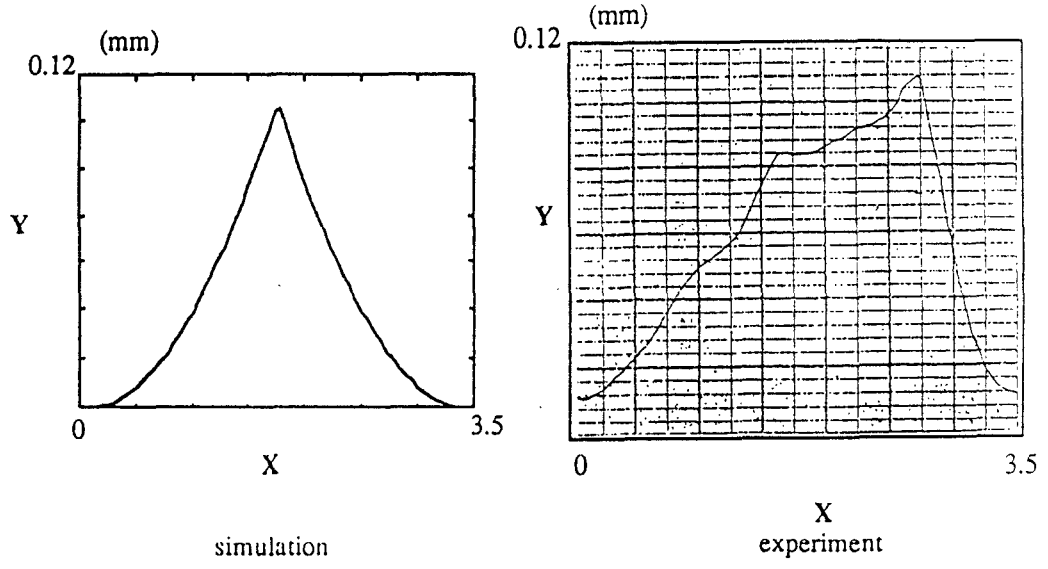

Fig. 4.22 The profile of end milling surface in one cutter revolution at Z=3

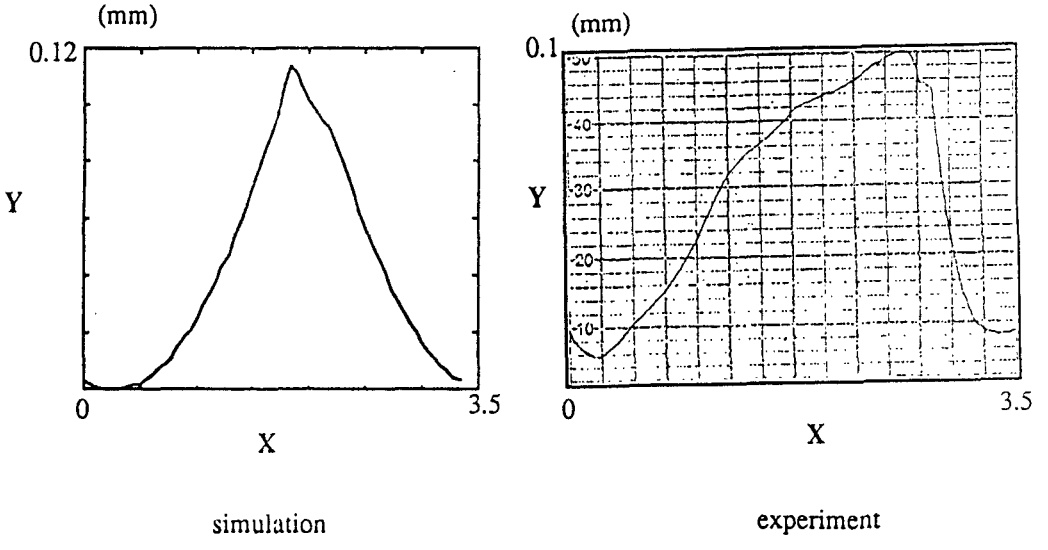

Fig. 4.23 The profile of end milling surface in one cutter revolution at Z=4

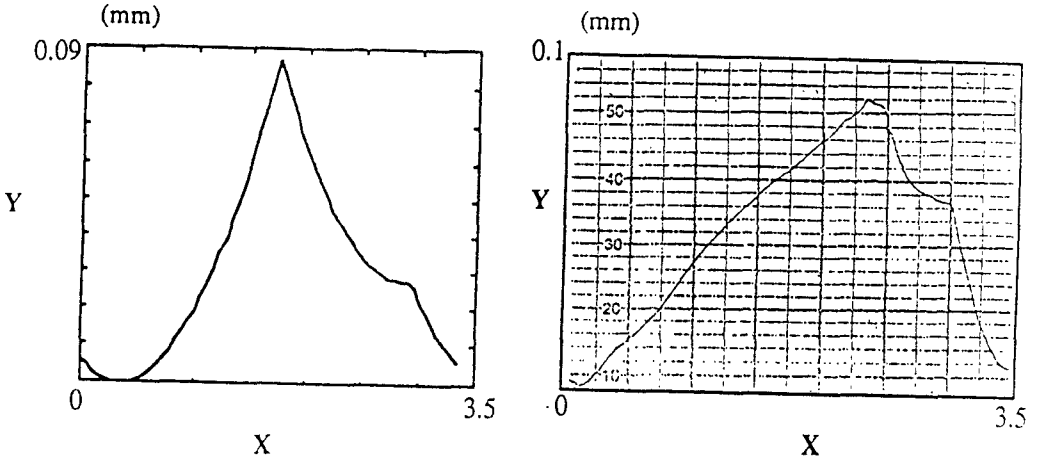

simulation experiment

Fig. 4.24 The profile of end milling surface in one cutter revolution at Z=5

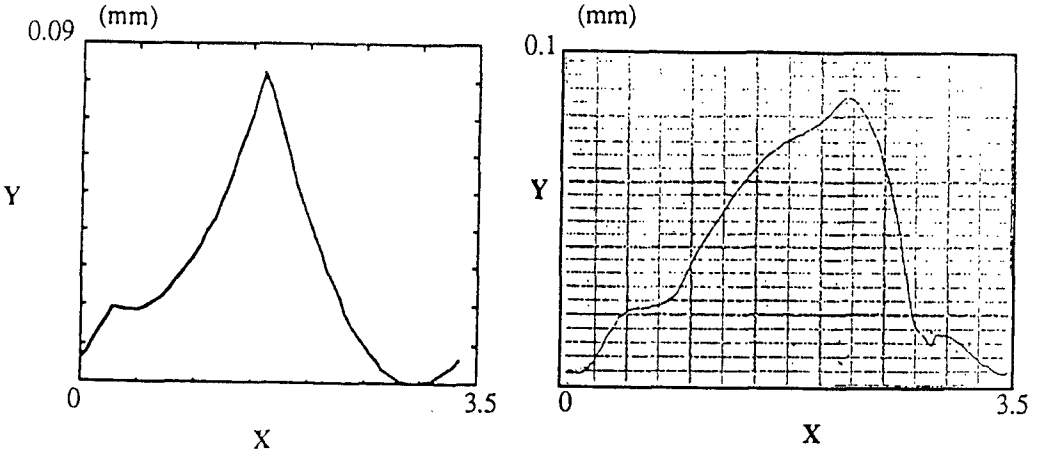

simulation experiment

Fig. 4.25 The profile of end milling surface in one cutter revolution at Z=6

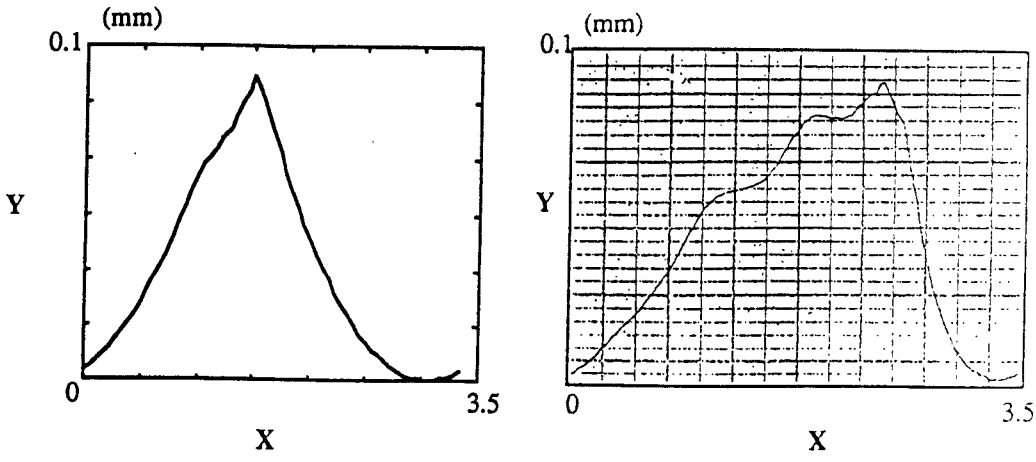

simulation experiment

Fig.4.26 The profile of end milling surface in one cutter revolution at Z=7

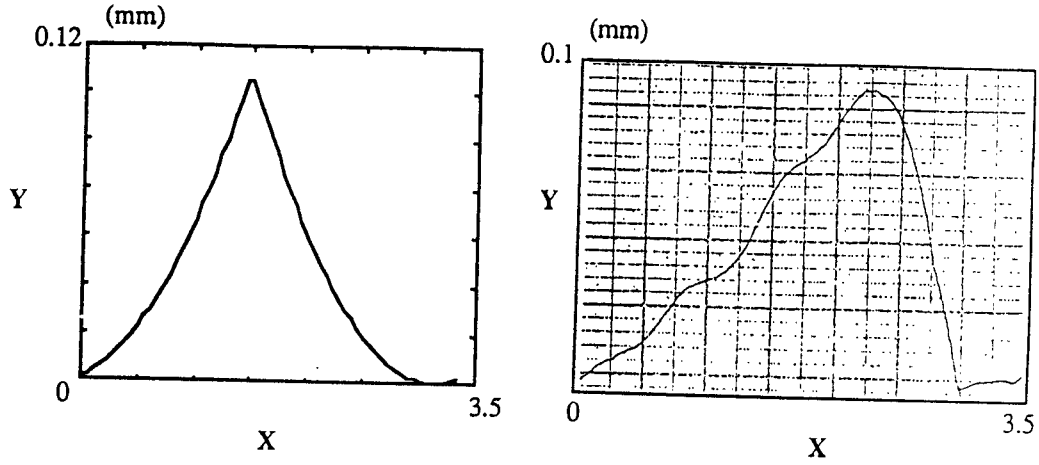

simulation experiment

Fig. 4.27 The profile of end milling surface in one cutter revolution at Z=8

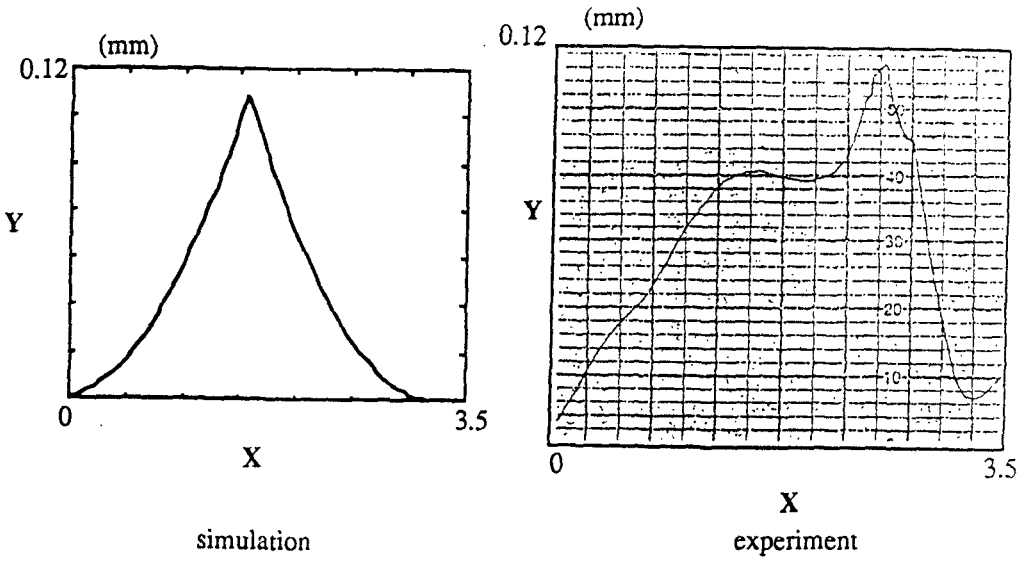

Fig.4.28 The profile of end milling surface in one cutter revolution at Z=9

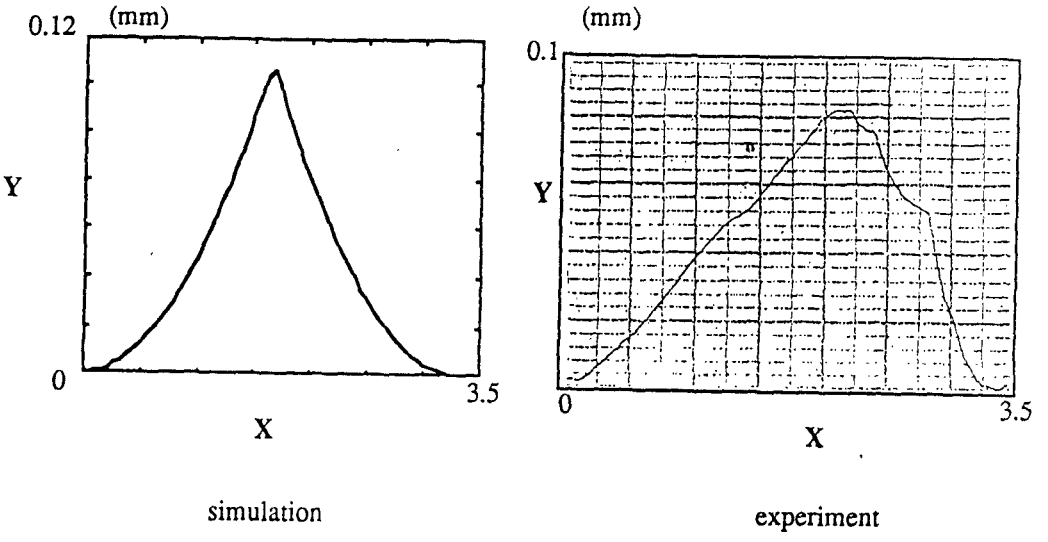

Fig.4.29 The profile of end milling surface in one cutter revolution at Z=10

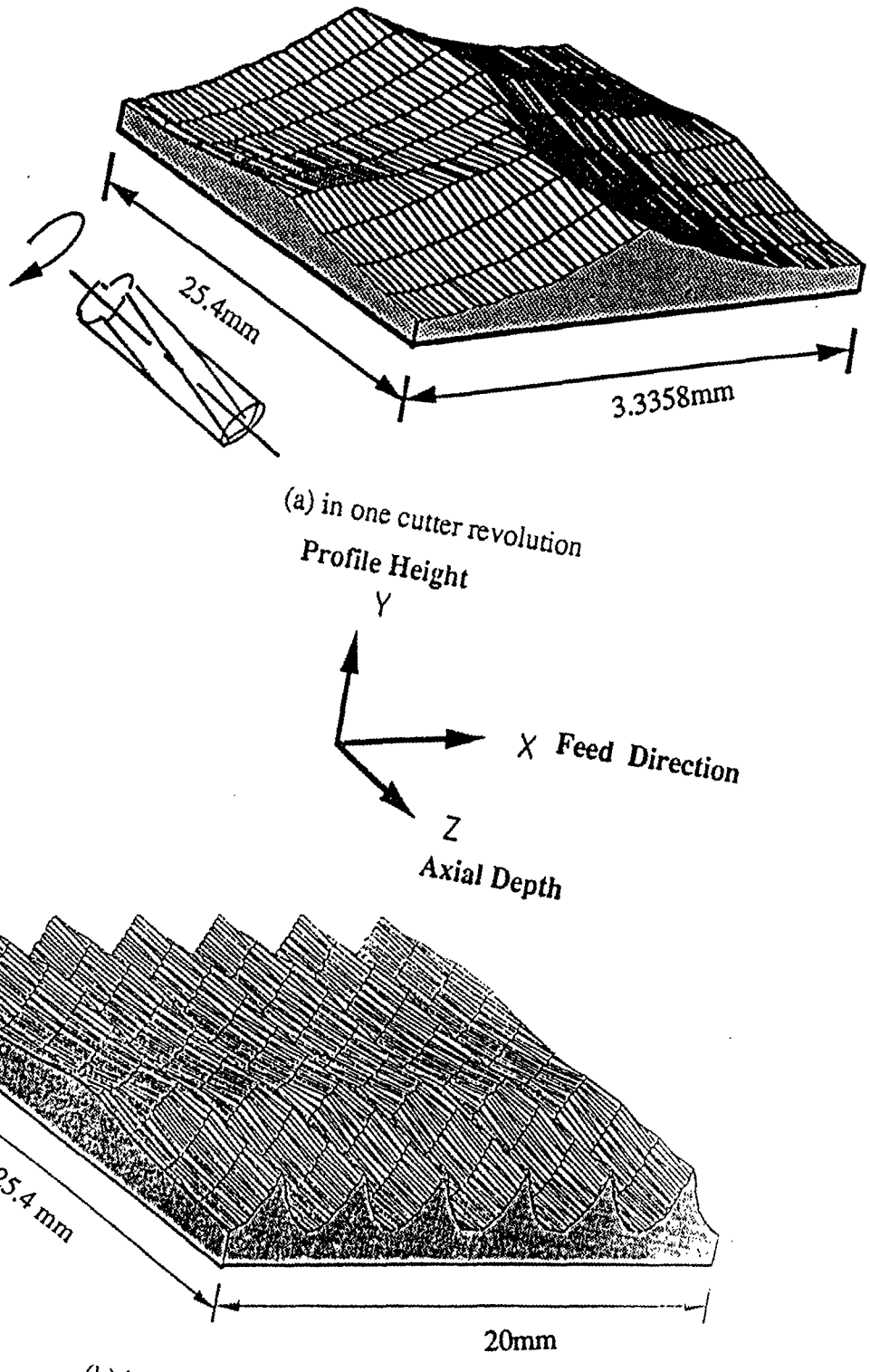

(a) in one cutter revolution

(b) in six cutter revolutions

Fig.4.30 The 3-D geometry of end milled surface from simulation in a runout case

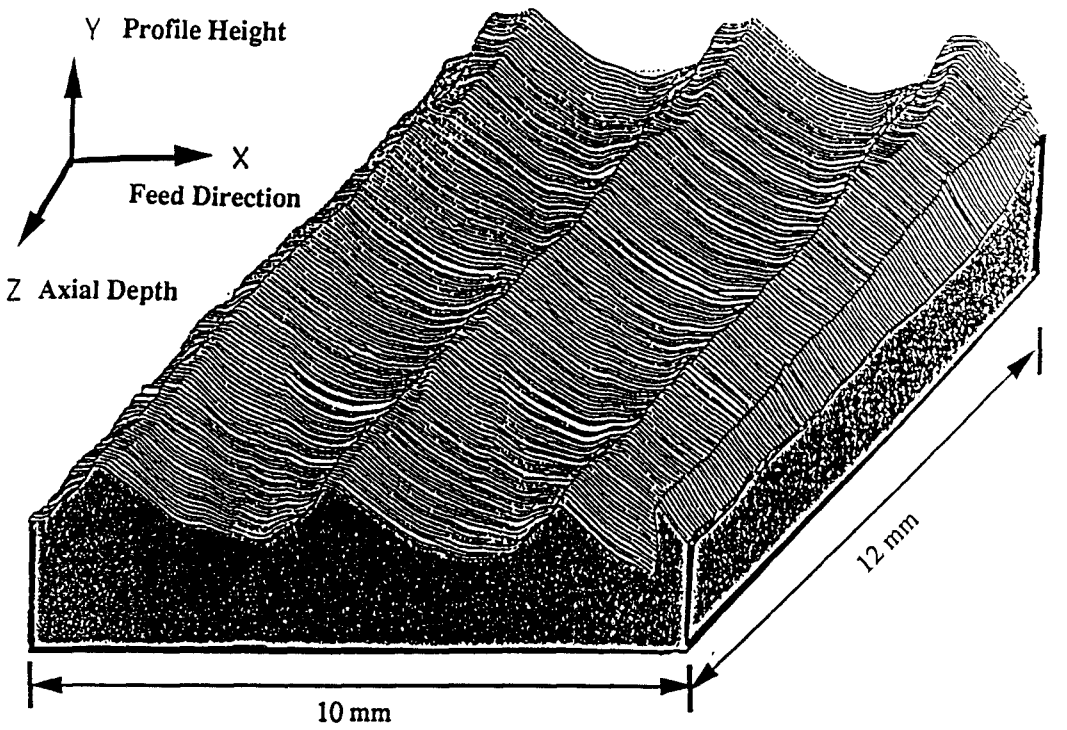

Fig.4.31 The 3-D geometry of end milled surface from experiment in a runout case

Ra and PTV value obtained by simulation	Ra and PTV value obtained from experiment
Ra	Ra
27.2 μm	23.8μm
PTV	PTV
70.5 μm	81μm

4.4.3 Experiment of Deflection and Vibration Case

For the deflection and vibration case the data we give in the simulation and experiment are:

Radius of Cutters	R	(0.375 in.) 9.525mm
Number of Flutes	Nt	4
Helix Angle	α_{hx}	30 degree
Feed Per Revolution	fr	1.668 mm/rev.
Axial Depth of Cut	Z	(1 in.) 25.4 mm

Runout	ρ	0.007 mm
Locating Angle	λ	0 degree
Modules of Elasticity for the Tool	E	207e3 MPa(Nt/mm^2)
Moment of Inertia for the Tool	I	6465 mm^4
EI		1.338255e9 Nt/mm^2
Tool Length	l	108 mm
Width of Workpiece(cut)	a	(1 in.) 25.4 mm
Loading Force Per Unit Length	k_a	50Nt/mm^2
Depth of Cut	u_0	0.254 mm
Tool Mass	m	3.15 kg

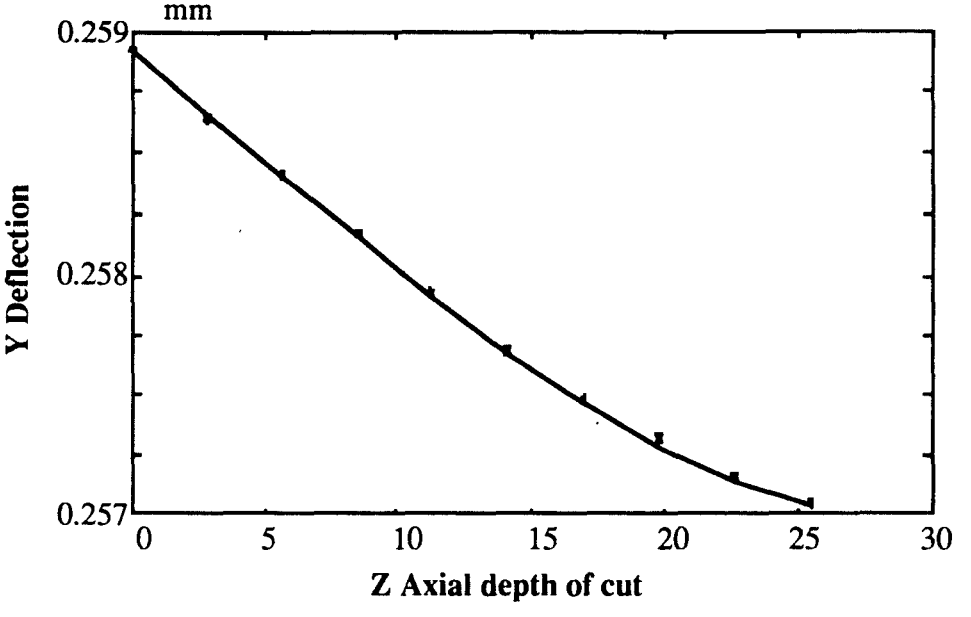

Fig. 4.32 Static deflection along the axial depth of cut Z

We adjust k values in each section of Z(from Z=1 to Z=10) according to the static deflection from the calculation (see Fig. 4.32), and get:

k_{11}=2.9980e7(N/m), k_{21}=2.9990e7(N/m), k_{31}=3.000e7(N/m), k_{41}=3.001e7(N/m), k_{51}=3.003e7(N/m), k_{61}=3.007e7(N/m), k_{71}=3.010e7(N/m), k_{81}=3.012e7(N/m), k_{91}=3.014e7(N/m), k_{101}=3.016e7(N/m),

k_{12}=2.4680e7(N/m), k_{22}=2.4710e7(N/m), k_{32}=2.4735e7(N/m), k_{42}=2.4760e7(N/m), k_{52}=2.4780e7(N/m), k_{62}=2.4790e7(N/m), k_{72}=2.4800e7(N/m), k_{82}=2.4810e7(N/m), k_{92}=2.4820e7(N/m), k_{102}=2.4830e7(N/m),

according to the m, ζ, and k values, we can get the c values in each section of Z and vibration profiles are established (see Fig. 4.33). The c values in each section of Z are:

c_{11}=950(N-sec/m), c_{21}=980(N-sec/m), c_{31}=1015(N-sec/m), c_{41}=1040(N-sec/m), c_{51}=1070(N-sec/m), c_{61}=1105(N-sec/m), c_{71}=1135(N-sec/m), c_{81}=1160(N-sec/m), c_{91}=1200(N-sec/m), c_{101}=1230(N-sec/m)

c_{12}=648(N-sec/m), c_{22}=606(N-sec/m), c_{32}=557(N-sec/m), c_{42}=522(N-sec/m), c_{52}=480(N-sec/m), c_{62}=431(N-sec/m), c_{72}=389(N-sec/m), c_{82}=354(N-sec/m), c_{92}=298(N-sec/m), c_{102}=256(N-sec/m),

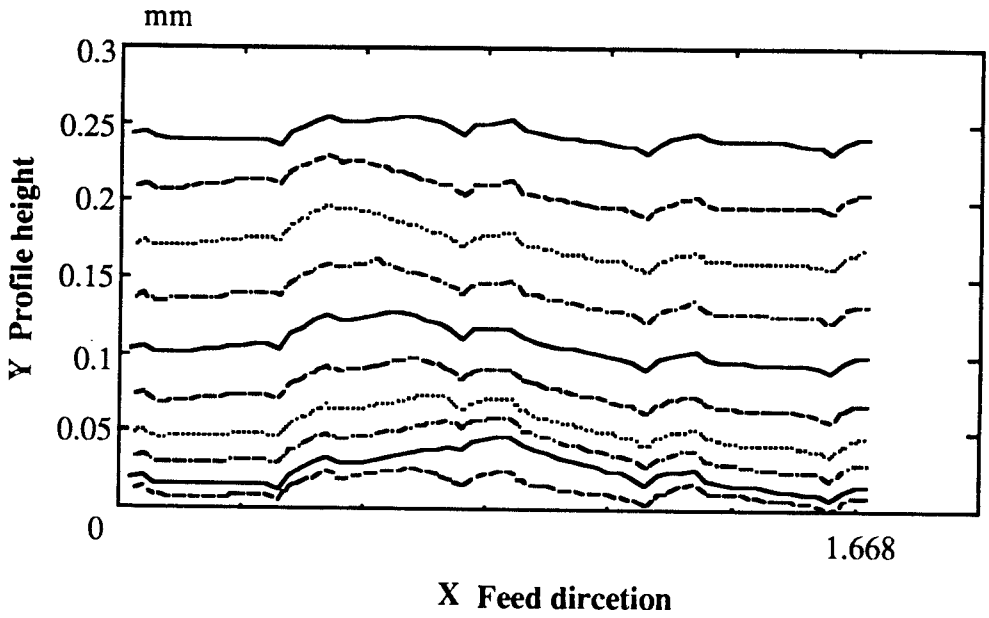

Fig.4.33 The profiles of end milling surface in a cutter revolution in each section of Z

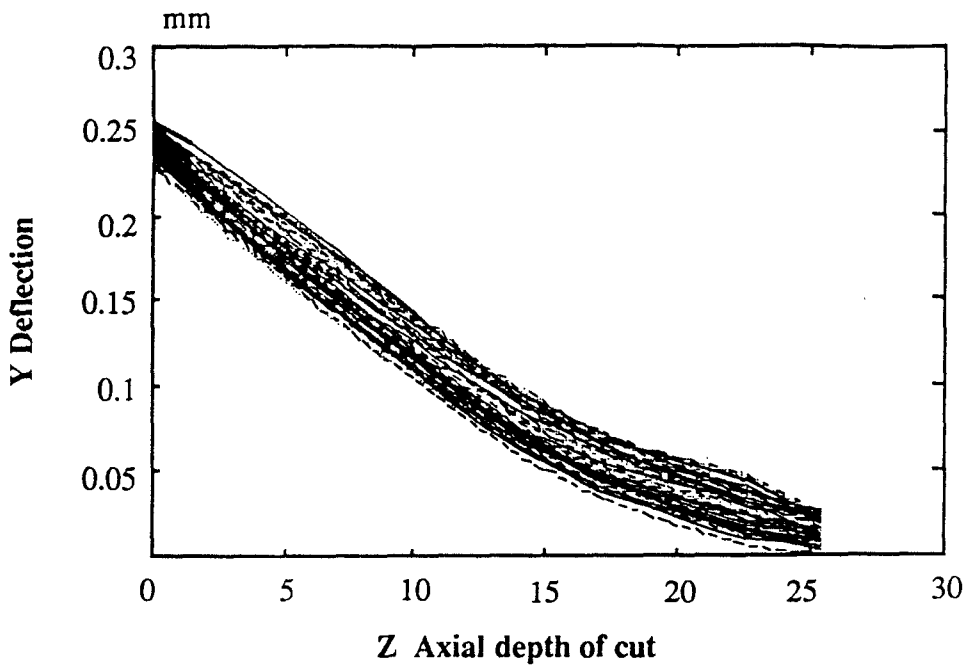

Fig.4.34 The profiles of end milling surface in a cutter revolution along axial depth of cut

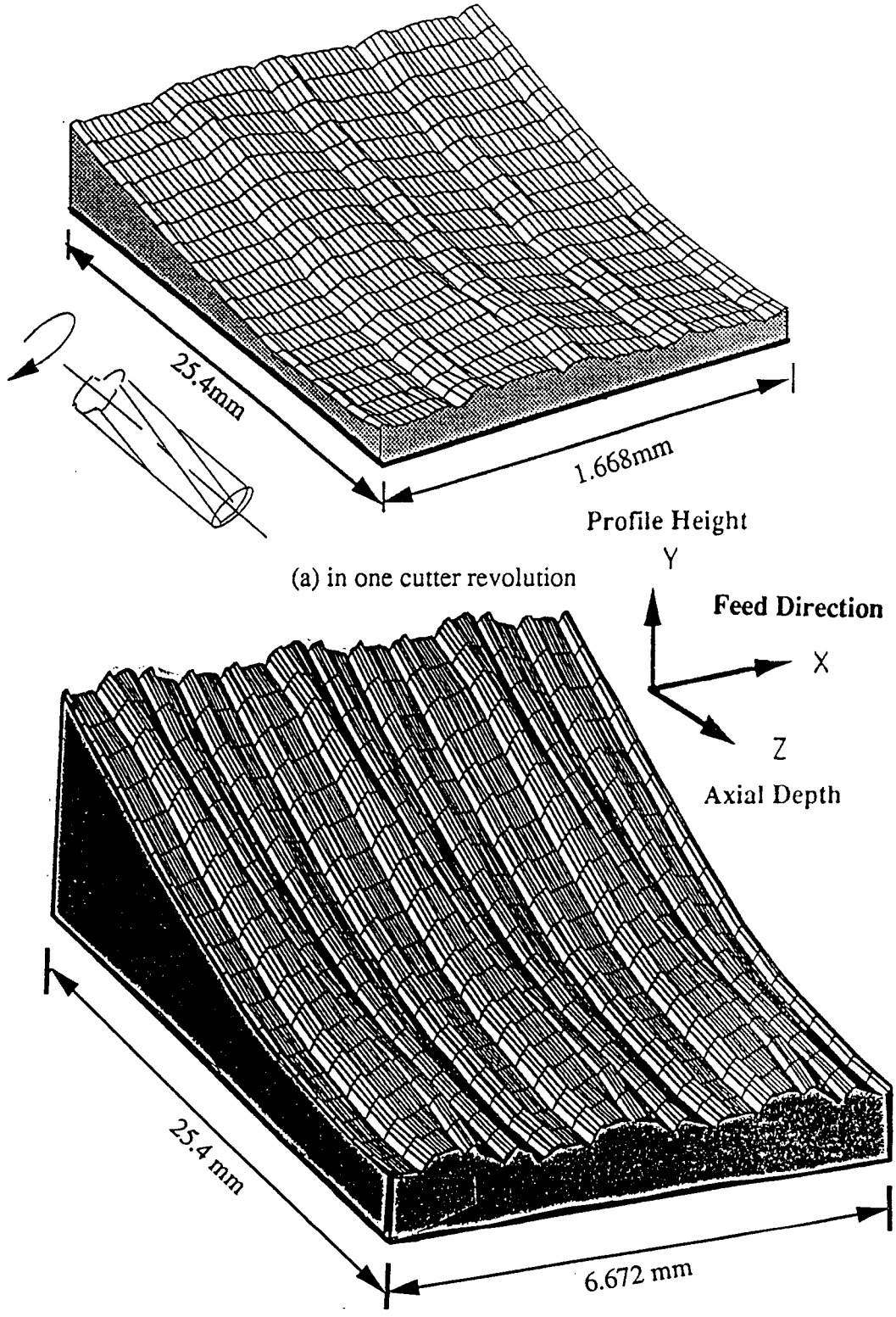

(a) in one cutter revolution

(b) in four cutter revolutions

Fig.4.35 The 3-D geometry of end milled surface from simulation in a vibration case

Ten profiles for vibration case from the experiment are:

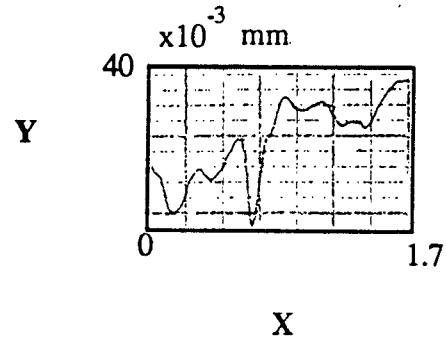

Z=1

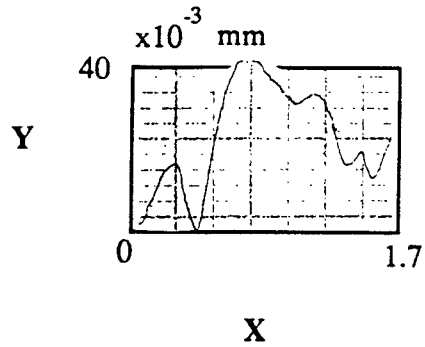

Z=2

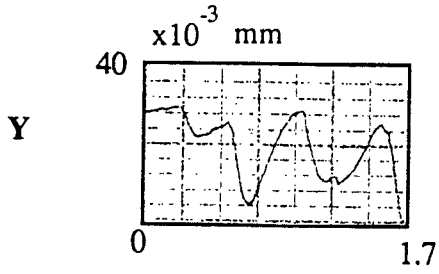

Z=3

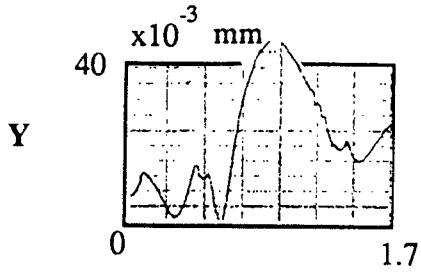

Z=4

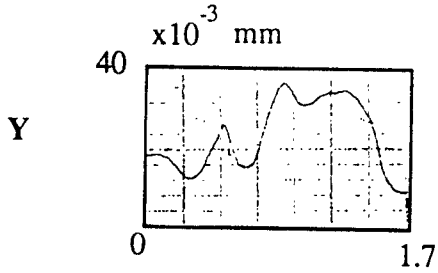

Z=5

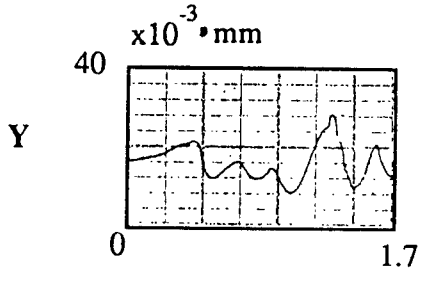

Z=6

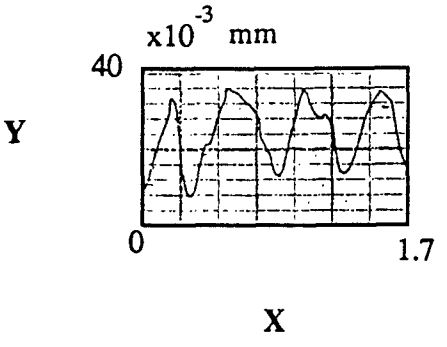

Z=7

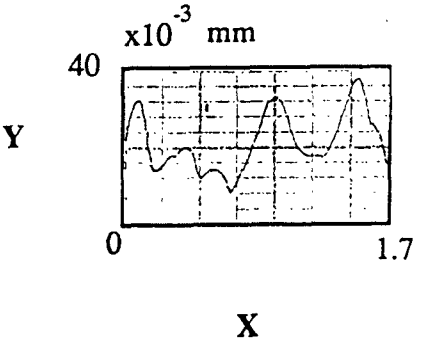

Z=8

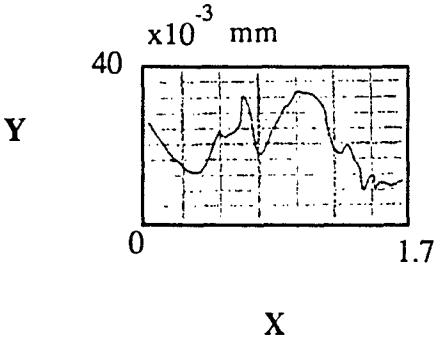

Z=9

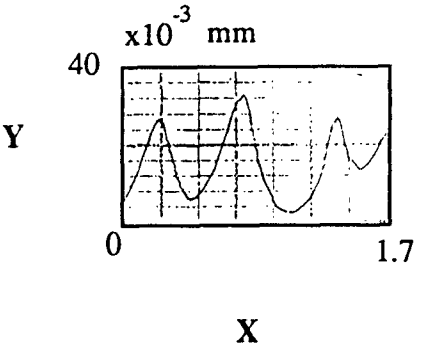

Z=10

Fig.4.36 The profiles of end milling surface in a cutter revolution from Z=1 to Z=10

Ra and PTV value obtained by simulation	Ra and PTV value obtained from experiment
Ra	Ra
8.2 μm	7.72μm
PTV	PTV
20.1 μm	25.3μm

CHAPTER 5 DISCUSSION OF RESULTS

The following sections in this chapter discuss the methodology of experimental design and the results obtained through computer simulations.

5.1 Introduction to Factorial Experimental Design

In our engineering life, experiments are frequently performed to measure the effects of one or more variables on a response. The factorial design, based on the principle of orthogonal array, is very useful for this purpose. These designs are economic and easy to use and can provide a great deal of valuable information. There are of important for a number of reasons.

1. They require relatively few runs per factor studied; and although they are unable to explore fully a wide region in the factor space, they can indicate major trends and so determine a promising direction for further experimentation.
2. When a more thorough local exploration is needed, they can be suitably augmented to form composite designs.
3. In this chapter we see that they form the basis for two level fractional factorial designs. these fractional designs are often of great value at an early stage of an investigation, when it is frequently good practice to use a preliminary experimental effort to look at a large number of factors superficially rather than a small number (which may or may not include the important ones) thoroughly.
4. These designs and the corresponding fractional designs may be used as building blocks so that the degree of complexity of the finally constructed design can be match the sophistication of the problem.
5. The interpretation of the observations produced by the designs can proceed largely by using common sense and elementary arithmetic.

In all these applications, the designs fit naturally into the sequential strategy discussed in this chapter, which is an essential feature of the scientific process.

When planning an experiment, it is necessary to consider variety of variables, or factors. A factorial experiment involves simultaneously more than one factor each at two or more levels. In most cases the number of levels of each factors in experiment is the same. These experiments provide an opportunity to study not only the individual effects of each factor but also their interactions. Sometime experiments are conducted with factors at two levels is namely a " - " sign for value or the absence of a factor and a " + " sign for the high value or presence of a factor.

In general to perform a general factorial design, an investigator selects a fixed number of levels for each of a number of variables (factors) and then runs experiments with all possible combinations. In some cases if the number of factors are large, fractional factorial designs are performed to reduce the total number of experiments that need to be conducted. A display of levels to be run in a design is called a design matrix.

The main effects for each of the factors can be obtained by the difference between two averages

$$\text{Main effect} = (y+) - (y-)$$

where (y+) is the averaged response for the high level of the variables and (y-) is the averaged response for the low level. The signs for the interactive effects can be directly obtained by multiplying the signs of their respective factors. There effects can be manipulated by the same formula used in calculating main effects. The variation between runs can be used to estimated the error level in the experiments. Using the information of the error level, it is possible to obtain those effects that are not significant from statistical point of view and an empirical model for the process can be determined.

5.2 Factorial Design Using Orthogonal Array

The experiments are designed with emphases on main effects. Past engineering experience should be used for selection of characteristics in order to keep the interactions as low as possible.

In fact, experiments are frequently performed to measure the effects of one or more variables on a response. Factorial designs using orthogonal array are extremely useful for this purpose, especially two-level fractional design. These designs are economic and easy to use and can provide a great deal of valuable information.

5.3 Identification of Process Parameters

In order to perform a factorial experiment on the surface roughness of the milling process it is necessary to identify all the factors that are related to the surface texture formation. The objective of this experiment is to determine the effects that the process parameters have in producing the surface roughness and their contribution towards surface topography generation. It is necessary to find out the key factors that cause the roughness of surface, so that they can be controlled within limits or more accurately to stabilize the process.

The parameters related to the generation of surface roughness (Ra, PTV) can be many. For the factorial experiments performed in this thesis work, the factors selected are:

1. Helix angle
2. Runout
3. Feedrate

Regarding the performance measurement or system response, we may choose deflection of the cutting tool or vibration of the cutting force produced during machining.

5.4 Factorial Experimental Design

5.4.1 2^3 Factorial Design

Among the parameters listed above, the following three factors are used in this thesis investigation, they are helix angle, runout, and feedrate for a 2^3 factorial design. The objective of this study is to understand how these factors will effect on the achievement of a possible ideal surface.

In order to achieve a possibly ideal surface, we need to know how these three factors are related to the surface generation.

We have proposed a method to initiate the investigation.

1. Select two levers for each of the three factors.

Helix angle:	10^0	30^0
runout:	0.01 mm	0.05 mm
feedrate:	0.5 mm/rev.	1 mm/rev.

2. Prepare eight tests, the table on the this page shows the matrix of the experimental design.
3. Perform the eight tests and record the Roughness Average values (Ra) at each test. The 8 responses are listed in the Table 5.1.

TABLE 5.1 Data from a 2^3 factorial design (Ra)

test condition number	helix angle degree **H**	runout (mm) **R**	feedrate (mm) **F**	Ra (μm) **Y**	estimated variance at each set of conditions S^2**Ra** (μm)
		a. Original units of variables			
1	10	0.01	0.5	0.35	0.005148
2	30	0.01	0.5	0.38	0.003364
3	10	0.05	0.5	0.37	0.003249
4	30	0.05	0.5	0.38	0.003364
5	10	0.01	1	1.0	0.027556
6	30	0.01	1	1.4	0.088804
7	10	0.05	1	1.4	0.075625
8	30	0.05	1	1.5	0.0529
		b. Coded units of varibles			
1	-	-	-	0.35	
2	+	-	-	0.38	
3	-	+	-	0.37	
4	+	+	-	0.38	
5	-	-	+	1.0	
6	+	-	+	1.4	
7	-	+	+	1.4	
8	+	+	+	1.5	

helix angle (0)		runout(mm)		feedrate(mm)	
-	+	-	+	-	+
10	30	0.01	0.05	0.5	1.0

4. Perform the eight tests the Peak To Valley (PTV) at each test. The responses are also listed in Table 5.2.

TABLE 5.2 Data from a 2^3 factorial design(PTV)

test condition number	helix angle degree H	runout (mm) R	feedrate (mm) F	PTV (μm) Y	estimated variance at each set of conditions S^2_{PTV}(μm)
		a. Original units of variables			
1	10	0.01	0.5	0.44	0.004624
2	30	0.01	0.5	0.47	0.002916
3	10	0.05	0.5	0.70	0.002704
4	30	0.05	0.5	0.69	0.002809
5	10	0.01	1	1.4	0.008649
6	30	0.01	1	1.7	0.077284
7	10	0.05	1	1.8	0.069169
8	30	0.05	1	1.9	0.0441
		b. Coded units of varibles			
1	-	-	-	0.44	
2	+	-	-	0.47	
3	-	+	-	0.70	
4	+	+	-	0.68	
5	-	-	+	1.4	
6	+	-	+	1.7	
7	-	+	+	1.8	
8	+	+	+	1.9	

helix angle (0)		runout(mm)		feedrate(mm)	
-	+	-	+	-	+
10	30	0.01	0.05	0.5	1.0

5. Calculations of main effects.

We grouped the 8 response values into 4 groups, i.e., (y_2,y_1), (y_4,y_3), (y_6,y_5), and(y_8,y_7). Each of the four groups represents a pair of tests which were performed at the same runout and feedrate, but different levels of helix angle.

Therefore, the difference in response between y_2 and y_1 represents the effect of helix angle on the yield when runout is kept at 0.01 mm, and feedrate 0.5 mm/rev is assumed.

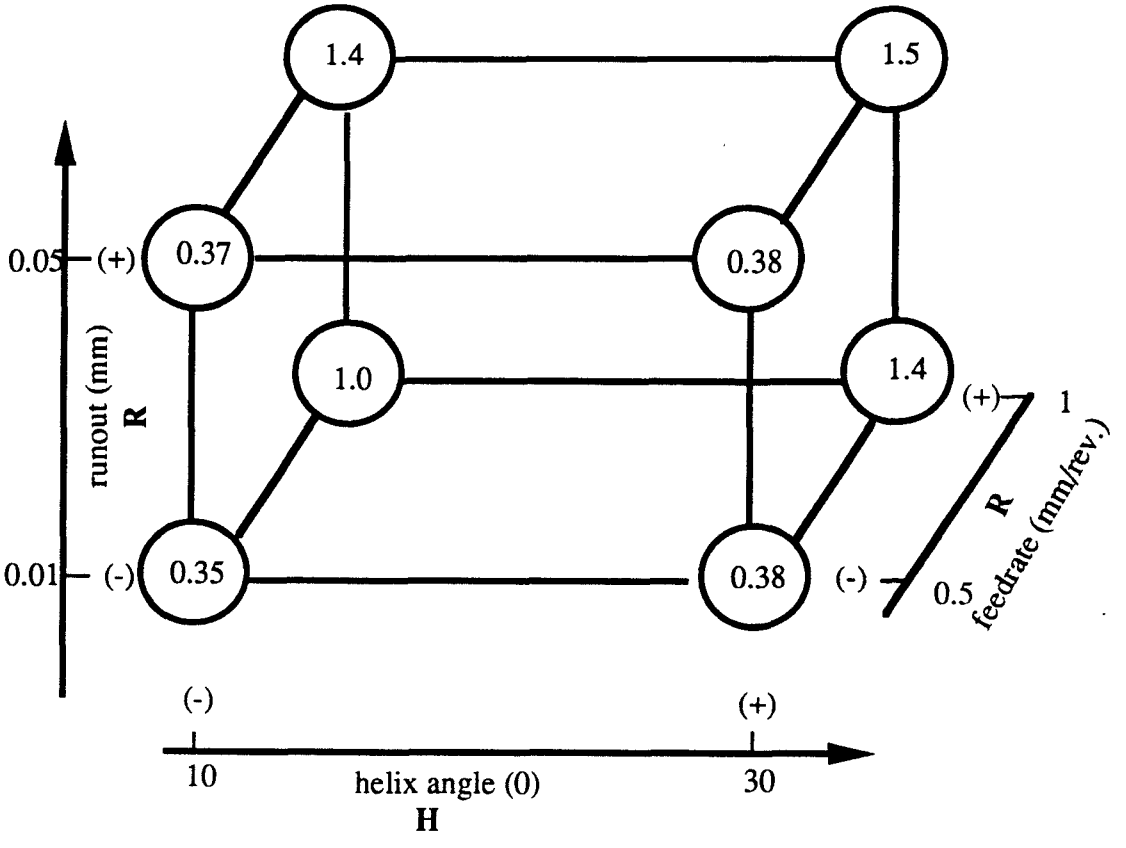

Fig 5.1 Graphical representation of the 2^3 factorial design(Ra)

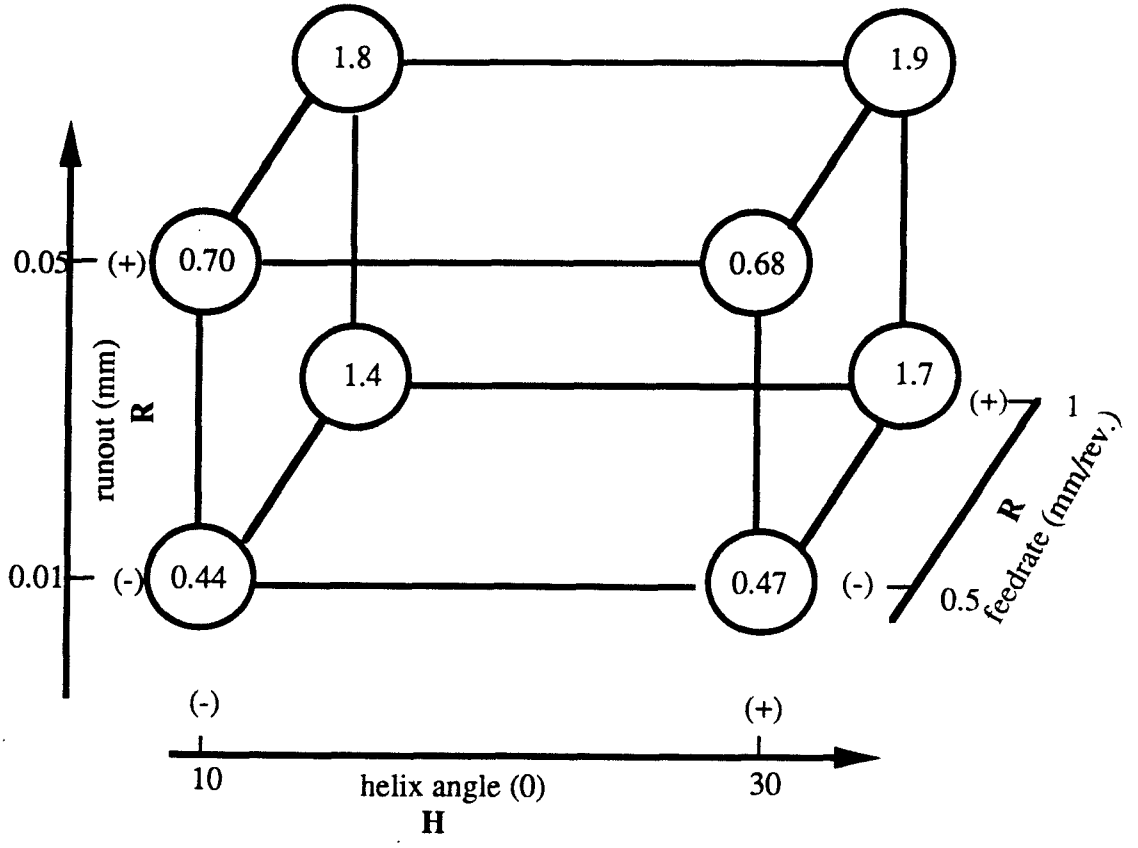

Fig 5.2 Graphical representation of the 2^3 factorial design(PTV)

Evidently, the main effect for each of the three factors can also be seen to be the difference between two averages

Main effect = (y+) - (y-)

where (y+) is the averaged response for plus level of the variable and (y-) is the averaged response for the minus level. So, the three main effects can be evaluateed as follows

helix angle effect (Ra) = (0.38+0.38+1.4+1.5)/4 - (0.35+0.37+1+1.4)/4 = 0.135

runout effect (Ra) = (0.37+0.38+1.4+1.5)/4 - (0.35+0.38+1+1.4)/4 = 0.13

feedrate effect (Ra) = (1+1.4+1.4+1.5)/4 - (0.35+0.38+0.37+0.38) = 0.98

helix angle effect (PTV) = (0.47+0.68+1.7+1.9)/4-(0.44+0.70+1.4+1.8)/4 = 0.1

runout effect (PTV) = (0.70+0.68+1.8+1.9)/4-(0.44+0.47+1.4+1.7)/4 = 0.27

feedrate effect (PTV) = (1.4+1.7+1.8+1.9)/4-(0.44+0.47+0.70+0.68)/4 = 1.13

The average of these measures (for example) is called the main effect of helix angle and is denoted by H. It measures the average effect of helix angle over all conditions of the other variables.

6. Calculating of interaction effects

A measure of nonlinearity or interaction between helix angle and feedrate is supplied by the difference between the average helix angle effect with feedrate (0.5 mm) and the average helix angle effect with feedrate (1 mm/rev.). By convention, half the difference is called the helix angle by feedrate interaction.or, in symbols, the $H \times F$ interaction.

when feedrate (1 mm/rev.) is used

$$y_8 - y_7 \text{ (Ra)} = 0.1$$

$$y_6 - y_5 \text{ (Ra)} = 0.4$$

average helix angle effect =(0.1+0.4)/2=0.25

when feedrate (0.5 mm/rev.) is used

$$y_4 - y_3 \text{ (Ra)} = 0.01$$

$$y_2 - y_1 \text{ (Ra)} = 0.03$$

average helix angle effect =(0.01+0.03)/2= 0.02

the difference = 0.25-0.02= 0.23. Consequently, $H \times F$ interaction= 1/2 difference=(0.25-0.02)/2 = 0.115 = $\frac{y_1 + y_3 + y_6 + y_8}{4} - \frac{y_2 + y_4 + y_5 + y_7}{4}$

In a similar manner, the $H \times R$ interaction and the $R \times F$ interaction can be calculated

$$R \times F = \frac{y_1 + y_2 + y_7 + y_8}{4} - \frac{y_3 + y_4 + y_5 + y_6}{4}$$

$$H \times R = \frac{y_1 + y_4 + y_5 + y_8}{4} - \frac{y_2 + y_3 + y_6 + y_7}{4}$$

$H \times F$ interaction (Ra)=(0.35+0.37+1.4+1.5)/4 - (0.38+0.38+1 +1.4)/4= 0.115

$H \times R$ interaction (Ra)=(0.35+0.38+1+1.5)/4 - (0.38+0.37+1.4+1.4)/4=- 0.08

$R \times F$ interaction (Ra)=(0.35+0.38+1.4+1.5)/4 - (0.37+0.38+1+1.4)/4= 0.12

$H \times F$ interaction (PTV)=(0.44+0.70+1.7+1.9)/4 - (0.47+0.68+1.4+1.8)/4= 0.0962

$H \times R$ interaction (PTV)=(0.44+0.68+1.4+1.9)/4 - (0.47+0.70+1.4+1.8)/4= 0.01325

$R \times F$ interaction (PTV)=(0.44+0.47+1.8+1.9)/4 - (0.70+0.68+1.4+1.7)/4= 0.03

For a three-factor interaction

Consider the helix angle by runout $H \times R$ interaction. Two measures of the $H \times R$ interaction are available from the experiment, one for each feedrate.

$H \times R$ interaction with feedrate (1 mm/rev. +)(Ra):

$$\frac{(y_8 - y_7) - (y_6 - y_5)}{2} = [(1.5\text{-}1.4)\text{-}(1.4\text{-}1)]/2 = -0.15$$

$H \times R$ interaction with feedrate (0.5 mm -)(Ra):

$$\frac{(y_4 - y_3) - (y_2 - y_1)}{2} = [(0.38\text{-}0.37)\text{-}(0.38\text{-}0.35)]/2 = -0.01$$

The difference measures the consistency of the helix angle by runout interaction for the two feedrates. Half this difference is defined as the *three factor interaction* of helix angle, runout, and feedrate, denoted as the $H \times R \times F$ interaction. Thus

$H \times R \times F$ interaction (Ra) = (-0.15+0.01)/2= -0.07

$H \times R \times F$ interaction (PTV) = -0.03825

7. Calculation of the mean. Evidently, the average of the 8 yields represent the general effect contributed by the three factors.

$$\text{Mean (Ra)} = \frac{y_1 + y_2 + y_3 + y_4 + y_5 + y_6 + y_7 + y_8}{8}$$

$$= (0.35+0.38+0.37+0.38+1+1.4+1.4+1.5)/8 = 0.8475$$

$$\text{Mean (PTV)}=\frac{y_1+y_2+y_3+y_4+y_5+y_6+y_7+y_8}{8}$$

$$=(0.44+0.47+0.70+0.68+1.4+1.7+1.8+1.9)/8= 1.1354$$

8. Development of an empirical model

$$y_i = \text{Mean} + \frac{H}{2}X_1 + \frac{R}{2}X_2 + \frac{F}{2}X_3 + \frac{H\times R}{2}X_1X_2 + \frac{H\times F}{2}X_1X_3 + \frac{R\times F}{2}X_2X_3 + \frac{H\times R\times F}{2}X_1X_2X_3$$

For

yi=y1,	X1=-1, X2=-1, X3=-1
yi=y2,	X1=+1, X2=-1, X3=-1
yi=y3,	X1=-1, X2=+1, X3=-1
yi=y4,	X1=+1, X2=+1, X3=-1
yi=y5,	X1=-1, X2=-1, X3=+1
yi=y6,	X1=+1, X2=-1, X3=+1
yi=y7,	X1=-1, X2=+1, X3=+1
yi=y8,	X1=+1, X2=+1, X3=+1

The empirical model for Ra is given by

$y(Ra) = 0.8475 + 0.0675H + 0.065R + 0.49F + 0.0575H\times F - 0.04H\times R + 0.06R\times F - 0.035H\times R\times F$

The empirical model for PTV is given by

$y(PTV)=1.1354+0.05H+0.135R+0.565F+0.0481H\times F+0.0067H\times R+0.01R\times F - 0.019H\times R\times F$

9. A quick method for calculating effects

The calculation performed to obtain the various effects can be characterized by the table of signs shown below.

TABLE 5.3 Signs for calculating effects from the 2^3 factorial design

mean	H	R	F	HR	HF	RF	HRF	PTV averages
+	−	−	−	+	+	+	−	0.44
+	+	−	−	−	−	+	+	0.47
+	−	+	−	−	+	−	+	0.70
+	+	+	−	+	−	−	−	0.68
+	−	−	+	+	−	−	+	1.4
+	+	−	+	−	+	−	−	1.7
+	−	+	+	−	−	+	−	1.8
+	+	+	+	+	+	+	+	1.9

the remaining effect can be obtained in a similar manner. The signs for interactions reveal a remarkable fact: They can be obtained by directly multiplying the signs of their respectively factors. thus the array of signs for the $H \times F$ interaction is obtained by multiplying together the signs for H and F. The method is quite general we note further that each effect is a contrast, and that they are all mutually orthogonal.

5.4.2 Estimation Of Standard Errors for Effects Using Replicated Runs

Variation between runs made at the same experimental conditions is a reflection of the total variability affecting runs made at different experimental conditions. Assume that , in the previous 2^3 factorial design , at each of the 8 experimental conditions, we performed 10 runs.

At each experimental condition, we have a sample including ten runs. The estimated variance for Ra and PTV is given on Tables 5.1 and 5.2, respectively. we obtain s_1^2, s_2^2, s_3^2, ..., s_8^2. The pooled estimate of run variance is

$$S^2 = \frac{s_1^2 + s_2^2 + s_3^2 + s_4^2 + s_5^2 + s_6^2 + s_7^2 + s_8^2}{8}$$

S^2(Ra)=(0.005184+0.003364+0.003249+0.003364+0.027556+0.088804+0.756 25+0.0529)/8= 0.0325

S^2(PTV)=(0.004624+0.002916+0.002704+0.002809+0.008649+0.077285+0.06 9169+0.0441)/8= 0.0265

S(Ra) = 0.18

S(PTV)= 0.163

using this pooled estimate for the run variance, we are able to estimate the variation associated with effects. Each average contains eight observations in the present case. As a result, the variance of each effect is given by

S^2 Ra(effect)=$\frac{1}{4}S^2_{pooled}$=0.0325/4=0.008125, S Ra(effect)= 0.09

S^2PTV(effect)=$\frac{1}{4}S^2_{pooled}$=0.0265/4=0.006625, S PTV(effect)=0.0814

using this information, we are able to identify those effects which are not significant from statistical point of view.

Then, we have the empirical model as follows

The empirical model for Ra:

$$y(Ra) = 0.8475+0.49F$$

The empirical model for PTV:

$$y(PTV) = 1.1354+0.135R+0.565F$$

The physical interpretations of this empirical model are

1. The effect of feedrate (F) is to increase the yield by 0.49 units for Ra and 0.565 units for PTV, and the effect of runout (R) is to increase the yield by about 0.135 units for PTV.

2. The effect of helix angle and all interactions are insignificant for this experiment.
3. The highest yield for (Ra) will be achieved if using high feedrate, and the highest yield (PTV) will be achieved if using high runout + high feedrate.

CHAPTER 6 CONCLUSIONS AND RECOMMENDATIONS

In this chapter, the main conclusions from the present study are summarized. Recommendations for future work are also listed.

6.1 Conclusions

In this thesis study, research focus has been on the mathematical modeling and dynamic analysis of the surface topography generated during an end milling process. A careful experimental verification has been conducted to justify the proposed approach and the developed model that forms a basis of using a computer system to simulate the dynamic generation of machined surfaces during machining. Three conclusions have been drawn from the present study and are listed as follows:

1. The mathematical model developed has shown that the surface texture produced during an end milling process is a combinational result of the kinematic motion of a machine tool, the path of each of the tooth of an end mill, the runout of an end mill setting, static deflection and vibratory motion of the end mill during machining. Without a comprehensive mathematical model to describe the surface topography generation and its implementation on a computer system, it would be, not impossible, but extremely difficult for a NC programmer to predict the machining performance.
2. In order to control the finish quality of machined surfaces, great attention should be given to the reduction of runout. This requirement not only points out the need for process control, but also establishes an important principle for the tolerance design of both the spindle structure of a machine tool and the tool of end mill. This emphasizes the need to push the problem of quality control farther upstream into engineering design, well ahead of the machining process itself.

3. Results from the factorial design of experimentation show that the finish quality will degrade dramatically (a large value of R_a) when using high feedrates. On the other hand, the Peak-to-Valley index is more sensitive to the runout than the Roughness Average index. Under certain conditions, the effect of helix angle on the machining performance seems less significant, especially the interactions between the helix angle and the runout and the interactions between the helix angle and the feedrate setting are not significant.

6.2 Recommendations

Based on the present study, the following recommendations with respect to the future work in this area can be made.

1. The method of surface roughness measurement using a stylus method provides in depth localized data for a given sample. The main disadvantage of this method is that it characterizes small regions that may not represent the entire material surface. It is strongly recommended that a computer-based vision system be used for assessing the finish quality where image processing techniques are used to extract the topographical information from the detected surface pictures.

2. In Chapter 5, a full factorial design was presented for the investigation of system parameters and their effects on the machining performance. When more system parameters are considered, the number of experimental runs increases exponentially. Under such circumstances, it is recommended that a fractional factorial design method be used. The fractional factorial design method requires less number of experimental runs than a corresponding full factorial design. The possibility of having less experimental runs relies on the hope that some system parameters that are not so important concerning the surface topography generation. It is generally true that some system parameters are more important than the others in an initial investigation stage.

3. In this thesis work, the rigidity of workpiece is assumed to be much higher than that of the end mill tool. Thus, the tool vibratory motion is governed solely by the end mill tool. When the rigidity of workpiece is not so high as compared with the rigidity of the end mill tool, the developed model is no longer valid. A new formulation will be needed to take the deflection and vibration of the workpiece during machining into the model development.

Appendix A

The Data of Surface Characterizations From the Experiment for Ideal Case

Rt1	8.0	μm
Rt2	7.5	μm
Rt3	8.0	μm
Rt4	7.3	μm
Rt5	7.8	μm
Ra	2.42	μm
Rq	2.75	μm
Ry	8.0	μm
Rtm	7.7	μm
Rv	5.8	μm
Rp	5.1	μm
Sm	840	μm
LAMQ	467	μm
DELQ	2.1	DEG
Rsk	0.0	
Rku	1.8	
S	264	μm
R3z	0.0	μm
R3m	3.7	μm
R3y	0.0	μm

Z=1

Rt1	7.8	μm
Rt2	8.5	μm
Rt3	8.2	μm
Rt4	8.1	μm
Rt5	8.4	μm
Ra	2.49	μm
Rq	2.84	μm
Ry	8.5	μm
Rtm	8.2	μm
Rv	5.0	μm
Rp	4.8	μm
Sm	843	μm
LAMQ	671	μm
DELQ	1.5	DEG
Rsk	0.1	
Rku	1.8	
S	380	μm
R3z	0.0	μm
R3m	4.1	μm
R3y	0.0	μm

Z=2

Rt1	7.4	μm
Rt2	8.6	μm
Rt3	7.5	μm
Rt4	7.4	μm
Rt5	7.4	μm
Ra	2.16	μm
Rq	2.51	μm
Ry	8.6	μm
Rtm	7.6	μm
Rv	4.5	μm
Rp	4.3	μm
Sm	842	μm
LAMQ	514	μm
DELQ	1.8	DEG
Rsk	0.3	
Rku	1.8	
S	238	μm
R3z	0.0	μm
R3m	3.8	μm
R3y	0.0	μm

Z=3

Rt1	12.7	μm
Rt2	8.3	μm
Rt3	6.9	μm
Rt4	7.8	μm
Rt5	6.7	μm
Ra	2.19	μm
Rq	2.65	μm
Ry	12.7	μm
Rtm	8.5	μm
Rv	10.4	μm
Rp	4.6	μm
Sm	608	μm
LAMQ	234	μm
DELQ	4.1	DEG
Rsk	-0.3	
Rku	3.0	
S	333	μm
R3z	0.0	μm
R3m	3.6	μm
R3y	0.0	μm

Z=4

Rt1	11.5	µm
Rt2	7.4	µm
Rt3	7.1	µm
Rt4	7.8	µm
Rt5	6.9	µm
Ra	2.23	µm
Rq	2.66	µm
Ry	11.5	µm
Rtm	8.1	µm
RV	8.1	µm
RP	5.7	µm
Sm	641	µm
LAMQ	371	µm
DELQ	2.6	DEG
Rsk	0.2	
Rku	2.4	
S	117	µm
R3z	0.6	µm
Rpm	3.8	µm
R3y	4.9	µm

Z=5

Rt1	6.5	µm
Rt2	9.0	µm
Rt3	8.5	µm
Rt4	8.1	µm
Rt5	6.3	µm
Ra	2.22	µm
Rq	2.60	µm
Ry	9.0	µm
Rtm	7.7	µm
RV	5.4	µm
RP	5.0	µm
Sm	536	µm
LAMQ	395	µm
DELQ	2.4	DEG
Rsk	0.2	
Rku	2.0	
S	109	µm
R3z	2.9	µm
Rpm	3.6	µm
R3y	7.1	µm

Z=6

Rt1	6.9	µm
Rt2	8.3	µm
Rt3	7.4	µm
Rt4	7.7	µm
Rt5	6.8	µm
Ra	2.46	µm
Rq	2.76	µm
Ry	8.3	µm
Rtm	7.4	µm
RV	5.0	µm
RP	4.6	µm
Sm	467	µm
LAMQ	352	µm
DELQ	2.8	DEG
Rsk	0.1	
Rku	1.7	
S	117	µm
R3z	2.9	µm
Rpm	3.4	µm
R3y	6.0	µm

Z=7

Rt1	8.4	µm
Rt2	8.5	µm
Rt3	7.1	µm
Rt4	7.6	µm
Rt5	6.0	µm
Ra	2.58	µm
Rq	3.07	µm
Ry	8.5	µm
Rtm	7.5	µm
RV	6.3	µm
RP	4.7	µm
Sm	478	µm
LAMQ	375	µm
DELQ	2.9	DEG
Rsk	-0.0	
Rku	2.0	
S	149	µm
R3z	0.0	µm
Rpm	2.8	µm
R3y	0.0	µm

Z=8

Rt1	6.5	μm
Rt2	11.6	μm
Rt3	8.3	μm
Rt4	7.5	μm
Rt5	5.9	μm
Ra	2.23	μm
Rq	2.63	μm
Ry	11.6	μm
Rtm	7.9	μm
Rv	8.2	μm
Rp	5.1	μm
Sm	923	μm
LAMQ	358	μm
DELQ	2.6	DEG
Rsk	0.1	
Rku	2.1	
S	144	μm
R3z	0.1	μm
Rpm	3.3	μm
R3y	2.3	μm

Z=9

Rt1	14.5	μm
Rt2	6.7	μm
Rt3	7.1	μm
Rt4	6.7	μm
Rt5	5.7	μm
Ra	2.21	μm
Rq	2.66	μm
Ry	14.5	μm
Rtm	8.1	μm
Rv	11.5	μm
Rp	4.5	μm
Sm	486	μm
LAMQ	234	μm
DELQ	4.1	DEG
Rsk	-0.2	
Rku	3.2	
S	135	μm
R3z	0.0	μm
Rpm	3.0	μm
R3y	0.0	μm

Z=10

Appendix B

The Data of Surface Characterizations From the Experiment for Runout Case

Rt1	82	μm
Rt2	79	μm
Rt3	92	μm
Rt4	99	μm
Rt5	78	μm
Ra	25.1	μm
Rq	28.5	μm
Ry	99	μm
Rtm	86	μm
Rv	56	μm
Rp	52	μm
Sm	3408	μm
LAMQ	2163	μm
DELQ	4.7	DEG
Rsk	-0.5	
Rku	1.9	
S	880	μm
R3z	0	μm
Rpm	38	μm
R3y	0	μm

Z=1

Rt1	92	μm
Rt2	85	μm
Rt3	78	μm
Rt4	93	μm
Rt5	83	μm
Ra	26.1	μm
Rq	29.3	μm
Ry	93	μm
Rtm	86	μm
Rv	48	μm
Rp	47	μm
Sm	3355	μm
LAMQ	2331	μm
DELQ	4.5	DEG
Rsk	-0.3	
Rku	1.6	
S	1714	μm
R3z	0	μm
Rpm	42	μm
R3y	0	μm

Z=2

Rt1	88	μm
Rt2	81	μm
Rt3	74	μm
Rt4	86	μm
Rt5	78	μm
Ra	25.2	μm
Rq	28.4	μm
Ry	88	μm
Rtm	82	μm
Rv	48	μm
Rp	40	μm
Sm	3429	μm
LAMQ	2438	μm
DELQ	4.2	DEG
Rsk	-0.3	
Rku	1.6	
S	1516	μm
R3z	0	μm
Rpm	37	μm
R3y	0	μm

Z=3

Rt1	89	μm
Rt2	82	μm
Rt3	80	μm
Rt4	88	μm
Rt5	95	μm
Ra	26.1	μm
Rq	29.3	μm
Ry	95	μm
Rtm	87	μm
Rv	48	μm
Rp	48	μm
Sm	2264	μm
LAMQ	2367	μm
DELQ	4.5	DEG
Rsk	-0.3	
Rku	1.7	
S	1409	μm
R3z	0	μm
Rpm	41	μm
R3y	0	μm

Z=4

Rt1	82	μm
Rt2	74	μm
Rt3	77	μm
Rt4	89	μm
Rt5	82	μm
Ra	24.1	μm
Rq	27.3	μm
Ry	89	μm
Rtm	81	μm
Rv	46	μm
Rp	43	μm
Sm	3337	μm
LAMQ	2266	μm
DELQ	4.3	DEG
Rsk	-0.3	
Rku	1.7	
S	1283	μm
R3z	0	μm
Rpm	39	μm
R3y	0	μm

Z=5

Rt1	79	μm
Rt2	79	μm
Rt3	53	μm
Rt4	80	μm
Rt5	79	μm
Ra	21.7	μm
Rq	24.7	μm
Ry	80	μm
Rtm	74	μm
Rv	45	μm
Rp	44	μm
Sm	3399	μm
LAMQ	2115	μm
DELQ	4.2	DEG
Rsk	-0.3	
Rku	1.8	
S	1084	μm
R3z	0	μm
Rpm	35	μm
R3y	0	μm

Z=6

Rt1	93	μm
Rt2	72	μm
Rt3	71	μm
Rt4	73	μm
Rt5	75	μm
Ra	21.6	μm
Rq	24.4	μm
Ry	93	μm
Rtm	77	μm
Rv	43	μm
Rp	50	μm
Sm	3460	μm
LAMQ	1909	μm
DELQ	4.6	DEG
Rsk	-0.1	
Rku	1.7	
S	808	μm
R3z	0	μm
Rpm	40	μm
R3y	0	μm

Z=7

Rt1	67	μm
Rt2	79	μm
Rt3	83	μm
Rt4	83	μm
Rt5	80	μm
Ra	22.3	μm
Rq	25.7	μm
Ry	83	μm
Rtm	79	μm
Rv	43	μm
Rp	55	μm
Sm	3420	μm
LAMQ	2110	μm
DELQ	4.4	DEG
Rsk	-0.1	
Rku	1.8	
S	1073	μm
R3z	0	μm
Rpm	43	μm
R3y	0	μm

Z=8

Rt1	78	µm
Rt2	81	µm
Rt3	88	µm
Rt4	88	µm
Rt5	66	µm
Ra	24.6	µm
Rq	28.6	µm
Ry	88	µm
Rtm	80	µm
Rv	50	µm
Rp	45	µm
Sm	2541	µm
LAMQ	2359	µm
DELQ	4.4	DEG
Rsk	-0.3	
Rku	1.8	
S	1133	µm
R3z	0	µm
Rpm	41	µm
R3y	0	µm

Z=9

Rt1	80	µm
Rt2	79	µm
Rt3	70	µm
Rt4	81	µm
Rt5	87	µm
Ra	22.8	µm
Rq	26.0	µm
Ry	87	µm
Rtm	79	µm
Rv	47	µm
Rp	41	µm
Sm	3370	µm
LAMQ	2478	µm
DELQ	3.8	DEG
Rsk	-0.4	
Rku	1.8	
S	2150	µm
R3z	0	µm
Rpm	37	µm
R3y	0	µm

Z=10

Appendix c

The Data of Surface Characterizations From the Experiment for Deflection and

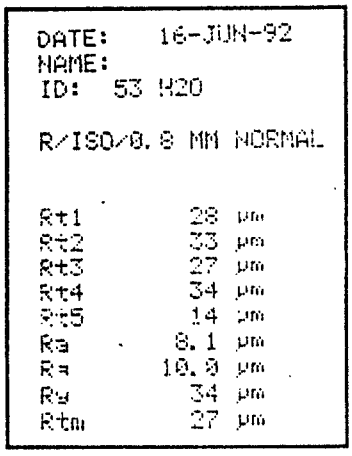

DATE: 16-JUN-92
NAME:
ID: 53 H20

R/ISO/0.8 MM NORMAL

Rt1	28	µm
Rt2	33	µm
Rt3	27	µm
Rt4	34	µm
Rt5	14	µm
Ra	8.1	µm
Rq	10.9	µm
Ry	34	µm
Rtm	27	µm

Z=1

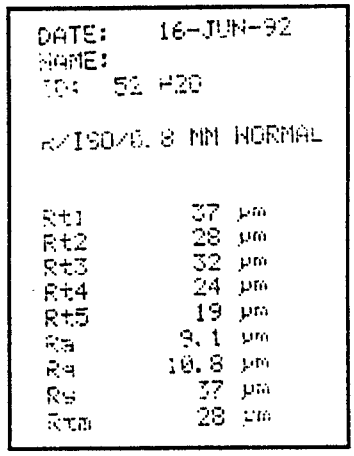

DATE: 16-JUN-92
NAME:
ID: 52 H20

R/ISO/0.8 MM NORMAL

Rt1	37	µm
Rt2	28	µm
Rt3	32	µm
Rt4	24	µm
Rt5	19	µm
Ra	9.1	µm
Rq	10.8	µm
Ry	37	µm
Rtm	28	µm

Z=2

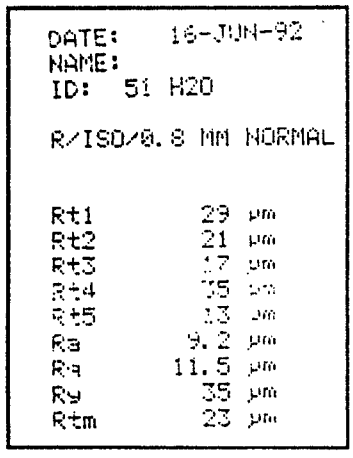

DATE: 16-JUN-92
NAME:
ID: 51 H20

R/ISO/0.8 MM NORMAL

Rt1	29	µm
Rt2	21	µm
Rt3	17	µm
Rt4	35	µm
Rt5	13	µm
Ra	9.2	µm
Rq	11.5	µm
Ry	35	µm
Rtm	23	µm

Z=3

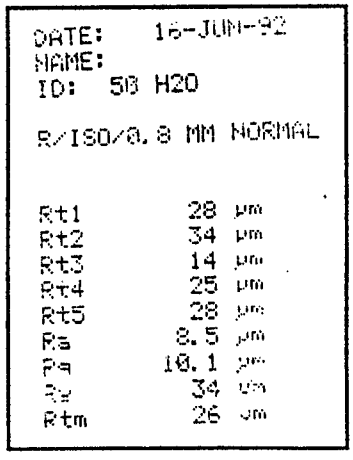

DATE: 16-JUN-92
NAME:
ID: 50 H20

R/ISO/0.8 MM NORMAL

Rt1	28	µm
Rt2	34	µm
Rt3	14	µm
Rt4	25	µm
Rt5	28	µm
Ra	8.5	µm
Rq	10.1	µm
Ry	34	µm
Rtm	26	µm

Z=4

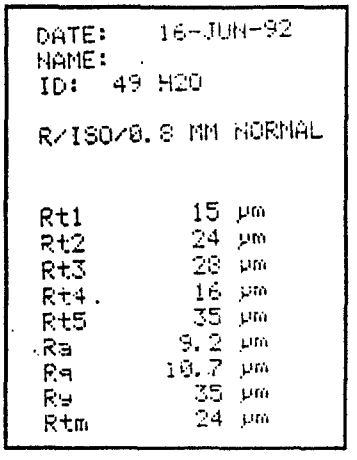

Z=5

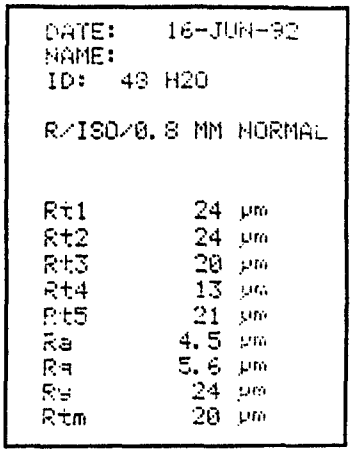

Z=6

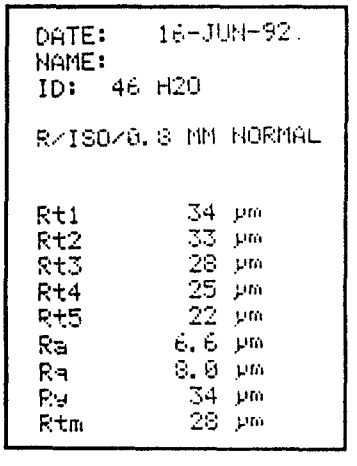

Z=7

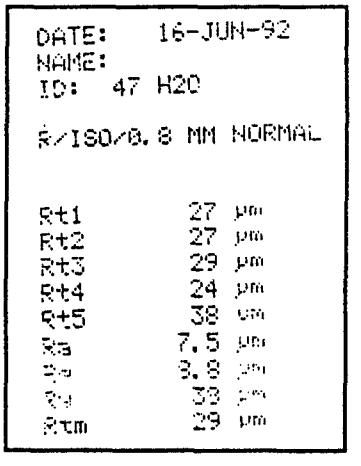

Z=8

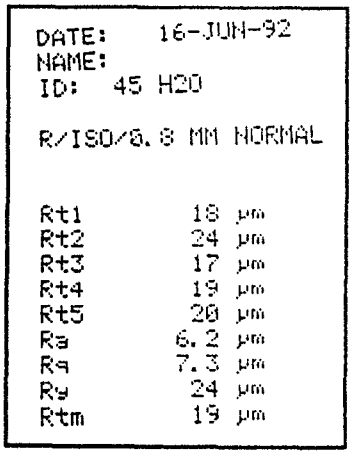

Z=9

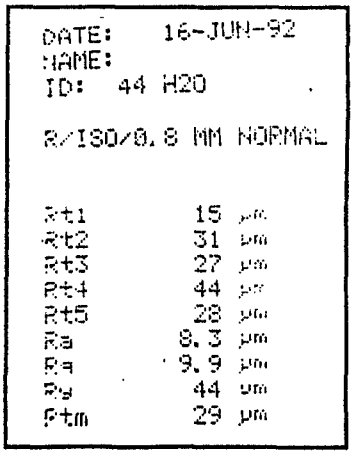

Z=10

Appendix D

Programs for Ideal and Runout Case Surface Generation

```
% p=input('parallel axis runout offset : ');
% l=input('locating angles (degree): ');
% r=input('radius : ');
% n=input('spindle speed : ');
% cl=input('cutter length : ');
% fr=input('feedrate (mm/rev) : ');
% ah=input('helix angle (degree) : ');
% nf=input('number of flute : ');
% cl=input('cutting length : ');

p=0.1968; l=0; ah=30; nf=4; n=300; r=9.525; cl=25.4; fr=3.3358;          % Input data

l=l*pi/180;                                                  % change degree to radius
ah=ah*pi/180;                                                % change to radius

% x, y : coordaintes by flute equation
% xx, yy : collection of x, y by varying z
% x2 : x coordinate
% y2 : y(x, z)

T=3000;                                                  % # of points in a cycle of motion
nx=60; nz=9;                                    % # of points in x, z direction in 3D plot
theta=[0:T-1]*2*pi/T;
x2=[0:nx]*fr/nx;
frf=-fr*0.2;
frr=fr*1.2;
y2=ones(nx+1,nz+1)*(p+r);
z0=1;
z=(z0-1)*cl/nz; a=z*tan(ah)/r;
xx=[]; yy=[];
y=-p*cos(theta+l)-r*cos(theta-a);                                    % phi = 0
```

```
[my, iy]=min(y);
x0=p*sin(theta(iy)+l)+r*sin(theta(iy)-a)+fr*(theta(iy))/(2*pi);
x0=0;
%
for z0=1:nz+1
z0
plot1=ones(nx+1,nf)*(p+r);
xx=[]; yy=[];
z=(z0-1)*cl/nz; a=z*tan(ah)/r;
for i=-nf:3*nf+2
    ii=rem(i,nf)+1;
    if ii<=0; ii=ii+nf; end;
    phi=2*i*pi/nf;
    x=p*sin(theta+phi+l)+r*sin(theta-a)+fr*(theta+phi)/(2*pi);

    y=-p*cos(theta+phi+l)-r*cos(theta-a);
    len=length(x); k=min(find(x>r));
    x=x-x0;
    x=[x(len)-fr x x(1)+fr]; y=[y(len) y y(1)];
    for k=find((x>=frf) & (x<=frr))
        if (y(k)<0 & k<=T+1)
            m=find((x2>=min([x(k) x(k+1)])) & (x2<=max([x(k) x(k+1)]
)));
            for j=m
                if y2(j,z0)>min([y(k) y(k+1)])
                    y0=y(k)+(x2(j)-x(k))*(y(k+1)-y(k))/(x(k+
1)-x(k));
                    if (y0<y2(j,z0)) y2(j,z0)=y0; end;
                end
            end
        end
    end
    xx=[xx; x]; yy=[yy; y];
end   % i loop
plot(x2,y2(:,z0));
    %
```

```
%
%
plot(x2, plot1); shg; grid;
%     disp('press return'); pause;
%     hold on; plot(xx', yy'); hold off;
%     clg
end    % z0
%
% Calculating the surface quality indices
%
% dx=.5/60*1.e3 (micron);
dx=fr/nx*1.e3;
[sr]=surf(y2',dx);
msr=mean(sr);
ssr=std(sr);
ra=msr(1);
ptv=msr(3);
ptv_max=msr(4);
sra=ssr(1);
sptv=ssr(3);
%

mesh(y2,[1 1 0.2])                                          % 3d plot
pause
plot(x2,y2(:,z0)-min(y2(:,z0)));                    % profile of milled surface
pause
plot(xx',yy');                                              % trajectory of each flute

% add title('...'), xlabel('...'), ylabel('...')
% use axis([min_x max_x min_y max_y]) to plot part of figure
```

Appendix E

Programs for Surface Generation with Runout , Tool deflection, and Tool Vibration Case

```
m=5.0;                                                    % Tool mass
u=.0005;                                                  % Depth of cut
c1=[1.0e8 1.2e8 1.4e8 1.6e8 1.8e8 2.0e8 2.2e8 2.4e8 2.6e8 2.8e8]/1.0e5 ;
c2=[2.0e8 2.2e8 2.4e8 2.6e8 2.8e8 3.0e8 3.2e8 3.4e8 3.6e8 3.8e8]/1.0e5 ;
k1=[1.3e8 1.31e8 1.31e8 1.31e8 1.32e8 1.32e8 1.31e8 1.31e8 1.30e8 1.30e8];
k2=[6.1e7 6.11e7 6.12e7 6.14e7 6.14e7 6.15e7 6.18e7 6.19e7 6.21e7 6.22e7];
kc=1000000.;
A=10.;
B=20.;
alpha=40.;
alpha=pi*alpha/180.;
beta=60.;
beta=pi*beta/180.;
nx=60;
fr=0.5;
nf=4;
nz=10;
pp=3;
%
pp=pp+1;
w=2*pi*nf/nx;
c=[1:20];
for i=1:20, c(i)=sin(pi*i/pp)*pp/i;, end;
yyy=ones(nx,nz);
s=[1:nx];
for k=1:nz
 K1p=k1(k)+kc*cos(alpha-beta);
 K2p=k2(k)+kc*sin(alpha-beta);
 R1=kc*cos(alpha-beta);
 R2=kc*sin(alpha-beta);
 d1=(R2-K1p)*kc*u/(R1*R2-K1p*K2p);
```

```
 d2=(R1-K2p)*kc*u/(R1*R2-K1p*K2p);
 d=A^2+B^2;
 d=d^0.5;
 MM=zeros(4);
 for i=1:20
  MM(1,1)=K1p-m*(i*w)^2;
  MM(1,2)=c1(k)*i*w;
  MM(1,3)=R1;
  MM(2,1)=-c1(k)*w*i;
  MM(2,2)=K1p-m*(i*w)^2;
  MM(2,4)=R1;
  MM(3,1)=R2;
  MM(3,3)=K2p-m*(i*w)^2;
  MM(3,4)=c2(k)*w*i;
  MM(4,2)=R2;
  MM(4,3)=-c2(k)*i*w;
  MM(4,4)=K2p-m*(i*w)^2;
  b=[A B A B]*c(i);
  x=MM\b';
  q1=x(1)*cos(i*w*s)+x(2)*sin(i*w*s);
  q2=x(3)*cos(i*w*s)+x(4)*sin(i*w*s);
  j=q1*cos(alpha)+q2*sin(alpha);
  yyy(:,k)=yyy(:,k)+j';
 end;
 yyy(:,k)=yyy(:,k)+(d1*cos(alpha)+d2*sin(alpha))*3;
end;
yyy=[yyy ; yyy(nx,:)];
% p=input('parallel axis runout offset : ');
% l=input('locating angles (degree): ');
% r=input('radius : ');
% n=input('spindle speed : ');
% cl=input('cutter length : ');
% fr=input('feedrate (mm/rev) : ');
% ah=input('helix angle (degree) : ');
% nf=input('number of flute : ');
% cl=input('cutting length : ');
```

```
% tl=input('tool length : ');
% EI=input('E*I : ');
% w=input('force per length : ');

p=0.05; l=45; ah=10; nf=4; n=600; r=20; cl=20; fr=0.5;tl=70;EI=10e7;        %Input data

w=50;

l=l*pi/180;                                                    % change degree to radius
ah=ah*pi/180;                                                  % change to radius

% x, y : coordaintes by flute equation
% xx, yy : collection of x, y by varying z
% x2 : x coordinate
% y2 : y(x, z)

T=3000;                                                % # of points in a cycle of motion
nx=60; nz=9;                                  % # of points in x, z direction in 3D plot
theta=[0:T-1]*2*pi/T;
x2=[0:nx]*fr/nx;
frf=-fr*0.2;
frr=fr*1.2;
y2=ones(nx+1,nz+1)*(p+r);
z0=1;
z=(z0-1)*cl/nz; a=z*tan(ah)/r;
xx=[]; yy=[];
y=-p*cos(theta+l)-r*cos(theta-a);                                  % phi = 0
[my, iy]=min(y);
x0=p*sin(theta(iy)+l)+r*sin(theta(iy)-a)+fr*(theta(iy))/(2*pi);
x0=0;
%
for z0=1:nz+1
z0
plot1=ones(nx+1,nf)*(p+r);
xx=[]; yy=[];
z=(z0-1)*cl/nz; a=z*tan(ah)/r;
```

```
for i=-nf:3*nf+2
      ii=rem(i,nf)+1;
      if ii<=0; ii=ii+nf; end;
      phi=2*i*pi/nf;
      x=p*sin(theta+phi+l)+r*sin(theta-a)+fr*(theta+phi)/(2*pi);
      y=-p*cos(theta+phi+l)-r*cos(theta-a);
      len=length(x); k=min(find(x>r));
      x=x-x0;
      x=[x(len)-fr x x(1)+fr]; y=[y(len) y y(1)];
      for k=find((x>=frf) & (x<=frr))
          if (y(k)<0 & k<=T+1)
              m=find((x2>=min([x(k) x(k+1)])) & (x2<=max([x(k) x(k+1)]
)));
              for j=m
                  if y2(j,z0)>min([y(k) y(k+1)])
                      y0=y(k)+(x2(j)-x(k))*(y(k+1)-y(k))/(x(k+
1)-x(k));
                      if (y0<y2(j,z0)) y2(j,z0)=y0; end;
                  end
              end
          end
      end
      xx=[xx; x]; yy=[yy; y];
end    % i loop
plot(x2,y2(:,z0));
      plot(x2, plot1); shg; grid;
    clg
end    % z0
zz=0:cl/nz:cl;
dy=w*(zz-cl).^4/24+cl*w*zz.^3/6-w*cl*cl*zz.^2/4+w*cl*l*(cl-tl)*zz/2...
  +cl*w*tl^3/3-w*cl^2*tl^2/4;
dy=dy/EI;

for i=1:nx+1,
     y2(i,:)=y2(i,:)+dy;
end;
```

```
y3=y2+1000*yyy;
y=y3(:,1);
y_average=sum(y3)/length(y3);
ra = sum(abs(y3-ones(nx+1,1)*y_average))/length(y3);
rr=ra ;
ra = sum(ra)/length(ra)
sra = rr - ra;
sra = sra.^2;
sra = sum(sra)^0.5/length(sra)
dd=4;
len=(nx+1)/dd;
for i=1:nz+1
    y0=[];
    for i=1:dd
        y0=[y0  y((i-1)*len+1:i*len+1)];
    end
    ptv(i)=sum(max(y0)-min(y0))/dd;
    ptv_max(i)=max(max(y0)-min(y0));

end;
sptv = ptv;
ptv=max(ptv)
sptv = sptv - ptv;
sptv = sptv.^2;
sptv = sum(sptv)^0.5/length(sptv)
ptv_max=max(ptv_max)



mesh(y2,[1 1 0.2])                                  % 3d plot
pause
plot(x2,y2(:,z0)-min(y2(:,z0)));                    % profile of milled surface
pause
plot(xx',yy');                                      % trajectory of each flute
```

```
xxx=[1:nx+1]*fr/(nx+1);
ff=y3(:,1)-min(y3(:,1));                                  % profile virbration
plot(xxx',y3)
gg=yyy(:,1)-min(yyy(:,1)); %
xxx=[1:nx+1]/n/(nx+1);
plot(xxx',gg)
tx1=y3(:,1);
txn=y3(:,nz+1);
mid=([y3 txn]+[tx1 y3])/2 ;for i=1:nz
 midd(:,i)=mid(:,i+1);
end;
y4=ones(nx+1,2*nz+1);
y4(:,1)=y3(:,1);
for i=1:nz
 y4(:,2*i)=midd(:,i);
 y4(:,2*i+1)=y3(:,i+1);
end;
% mesh(y4) 17points3d
sx=[1:2*nz+1]-1;
sx=sx*cl/2/nz;
sx=sx';
plot(sx,y4(1,:)-min(y4(1,:)))                             % the profile of x=0
plot(sx,y4-min(min(y4)))                                  % the profile of x=0 to 0.5
```

References

1. "Accuracy of Milled Surfaces--Effect of Cutter Diameter, Number of Teeth, Runout, and Feed,"Metal Cuttings," Vol. 9/1,1961, P. 2.
2. Babin, T., J. Lee, J. Sutherland, and S. Kapoor, "A model for End Milled Surface Topography,"Proceedings of NAMRC 13," 1985.
3. Babin, T., J. Sutherland, and S. Kapoor, "On the Geometry of End Milled Surfaces,"Proceedings of NAMRC 14, 1986, PP. 168-176.
4. Devor, R., W. Kline, and W. Zdeblick, "A Mechanistic Model for the Force System in End Milling with Application to Machining Airframe Structures,"Proceedings of NAMRC 8, 1980, pp. 297-303.
5. D. J. Whitehouse, "SurfacA Link Between Manufacture and Function," Proc. Instin. Mech. Engrs., Vol. 192, 1978, pp. 179-188.
6. Fujii, Y.H. Iwabe, and M. Suzuki, "Effect of Dynamic Behavior of End Mill in Machining on Work Accuracy,"Bulletin of Japan Socity of Precision Engineering, Vol. 13/1, 1979, p. 20.
7. Fu, H., R. Devor, and S. Kapoor, "The Optimal Design of Tooth Spacing in face Milling Via A Dynamic Force Model,"Proceedings of NAMRC 12, 1984, pp.291-297.
8. John William Sutherland, "A Dynamic Model of the Cutting Force System In the End Milling Process," Ph.D. Thesis, University of Illinois at Urbana-Champaign, 1987.
9. Kline, W.,and R. Devor, "The effect of Runout on Cutting Geometry and Forces in End Milling,"Int. J. Mach. Tool Des. Res., Vol. 23, No. 2/3, 1983, pp. 123-140.
10. Kline, W., R. Devor, and I. Shareef, "The Prediction of Surfsace Accuracy in End Milling," Journal of Engineering for Industry, Trans. ASME, Vol. 104, 1983, pp. 272-278.

11. M. E. Martellotti, "An Analysis of the Milling Process," Trans. ASME, Vol. 63, 1941, pp. 677-700.

12. M.E. Martellotti, "An analysis of the Milling Process, Part II--Down Milling," Trans. ASME, Vol. 67, 1945, pp. 233-251.

13. Merritt, H., "Theory of Self-Exicted Machine-Tool Chatter, Contribution to Machine-Tool Chatter Research-1,"Journal of Engineering for Industry, Trans. ASME, Vol. 87, 1965, pp. 447-454.

14. P. E. Gygax, "Experimental full cut milling Dynamic,", 1980,Ann.CIRP 29, 61

15. R. E. Devor, and J. W. Sutherland, "An Improved Method for Cutting Force and Surface Error Prediction in Flexible End Milling Systems," Submitted to the J. Eng. Ind., Trans. ASME.

16. Sridhar, R., R. Horn, and G. Long, "A General Formulation of the Milling Process Eqution, Contribution to machine Tool Chatter Research-5,"Journal of Engineering for Industry, Trans. ASME, Vol. 90, 1968, pp. 317-324.

17. Tlustry, J., "Dynamic of High-Speed Milling,"Journal of Engeering for Industry, Tran.ASME, Vol. 108, 1986, pp. 59-67.

18. Tlustry, J., and M. Elbestawi, "Analysis of Transients in an Adaptive Control Servomechanism for Milling with Constant Force,"Journal of Engineering for Industry, Trans. ASME, Vol. 99, 1977, pp. 766-772.

19. Tlusty, J., and F. Ismail, "Basic Non-Linearity in Machining Chatter,"Annals of the CIRP, Vol. 30/1, pp. 299-304.

20. T. G. King and T. A. Spedding, "Towards a Rotational Surface Profile Characterization System," Precision Engineering, Vol. 5, No. 4, 1983, pp. 153-160.

21. W. A. Kline, R. E. Devor, and J. Lindberg, "The Prediction of Cutting Forces in End Milling with Application to Cornering Cuts," Int. J. Mach. Tool Des. Res., Vol. 22, No. 1, 1982, pp. 7-22

22. W. A. Kline, "The prediction of cutting forces and Surface Accuracy for the End Milling Process," Ph.D. Thesis.1982, University of Illinois at Urbana-Champaign.